AD-A062 842 WOODS HOLE OCEANOGRAPHIC INSTITUTION MASS F/G 8/3
A STUDY OF THE VELOCITY STRUCTURE IN A MARINE BOUNDARY LAYER - --ETC(U)
DEC 78 J S TOCHKO N00014-74-C-0262
UNCLASSIFIED WHOI-78-90 NL

1 OF 3
AD
A062842

UNCLASSIFIED 12/78

SECURITY CLASSIFICATION OF THIS PAGE (When Data Entered)

REPORT DOCUMENTATION PAGE	READ INSTRUCTIONS BEFORE COMPLETING FORM
1. REPORT NUMBER: WHOI-78-90 (14)	2. GOVT ACCESSION NO.
	3. RECIPIENT'S CATALOG NUMBER (9)
4. TITLE (and Subtitle): A STUDY OF THE VELOCITY STRUCTURE IN A MARINE BOUNDARY LAYER - INSTRUMENTATION AND OBSERVATIONS. (6)	5. TYPE OF REPORT & PERIOD COVERED: Technical ≠ Rept. 17
	6. PERFORMING ORG. REPORT NUMBER
7. AUTHOR(s): John S. Tochko (10)	8. CONTRACT OR GRANT NUMBER(s): N00014-74-C-0262 (13) NSF-OCE-76-10523
9. PERFORMING ORGANIZATION NAME AND ADDRESS: Woods Hole Oceanographic Institution, Woods Hole, MA 02543	10. PROGRAM ELEMENT, PROJECT, TASK AREA & WORK UNIT NUMBERS: NR 083-004
11. CONTROLLING OFFICE NAME AND ADDRESS: NORDA, National Space Technology Laboratory, Bay St. Louis, MS 39529 (11)	12. REPORT DATE: Dec[illegible] 1978
	13. NUMBER OF PAGES: 190
14. MONITORING AGENCY NAME & ADDRESS (if different from Controlling Office) (12) 193p.	15. SECURITY CLASS. (of this report): Unclassified
	15a. DECLASSIFICATION/DOWNGRADING SCHEDULE

16. DISTRIBUTION STATEMENT (of this Report)

Approved for public release; distribution unlimited.

17. DISTRIBUTION STATEMENT (of the abstract entered in Block 20, if different from Report)

18. SUPPLEMENTARY NOTES

19. KEY WORDS (Continue on reverse side if necessary and identify by block number)

1. Benthic Boundary Layer Flow
2. Acoustic Current Meter
3. Reynolds Stress Measurement

20. ABSTRACT (Continue on reverse side if necessary and identify by block number)

Refer to previous two pages for abstract of dissertation.

A

DD FORM 1 JAN 73 1473 EDITION OF 1 NOV 65 IS OBSOLETE S/N 0102-014-6601

UNCLASSIFIED 12/78

SECURITY CLASSIFICATION OF THIS PAGE (When Data Entered)

381 000

WHOI-78-90

A STUDY OF THE VELOCITY STRUCTURE IN A MARINE BOUNDARY LAYER - INSTRUMENTATION AND OBSERVATIONS

by

John S. Tochko

WOODS HOLE OCEANOGRAPHIC INSTITUTION
Woods Hole, Massachusetts 02543

December 1978

DOCTORAL DISSERTATION

Prepared for the Office of Naval Research under Contract N00014-74-C-0262; NR 083-004 and for the National Science Foundation under Grant OCE 76-10523.

Approved for Distribution:

Earl E. Hays, Chairman
Department of Ocean Engineering

Robert W. Morse
Dean of Graduate Studies

B

A STUDY OF THE VELOCITY STRUCTURE IN A MARINE BOUNDARY LAYER - INSTRUMENTATION AND OBSERVATIONS

by

JOHN STEVEN TOCHKO

B.E., The Cooper Union School of Engineering
(1972)

SUBMITTED IN PARTIAL FULFILLMENT OF THE
REQUIREMENTS FOR THE DEGREE OF
DOCTOR OF PHILOSOPHY

at the

MASSACHUSETTS INSTITUTE OF TECHNOLOGY

and the

WOODS HOLE OCEANOGRAPHIC INSTITUTION

February 1978

Signature of Author: John S. Tochko
Joint Program in Oceanographic Engineering,
Massachusetts Institute of Technology-Woods Hole
Oceanographic Institution, February 1978

Certified by: Albert J. Williams 3rd
Thesis Supervisor

Accepted by: Earl E. Hays
Chairman, Joint Committee on Oceanographic
Engineering, Massachusetts Institute of Technology-
Woods Hole Oceanographic Institution

C

A STUDY OF THE VELOCITY STRUCTURE IN A MARINE BOUNDARY LAYER

- INSTRUMENTATION AND MEASUREMENTS

by

John Steven Tochko

Submitted to the Department of Ocean Engineering in partial fulfillment of the requirements for the degree of Doctor of Philosophy.

ABSTRACT

The design and operation of a unique flow measuring instrument for bottom boundary layer studies in the marine environment is documented. The effectiveness of the instrument in acquiring data with which models of near bottom flows in the ocean can be tested is demonstrated by the results of a field experiment in Vineyard Sound.

The instrument uses four sensors which measure the mean and fluctuating parts of the three components of the velocity vector at four heights above the sea bed. The sensors employ the acoustic travel time difference technique, and are designed to minimize sensor-induced flow disturbances. *BASS*, an acronym for *Benthic Acoustic Stress Sensor*, has a resolution of .033 cm/sec per least bit, a range of ±62 cm/sec, noise of .07 cm/sec in 10 sec, and an estimated accuracy of ±.5 cm/sec, referred to an in situ zero point. A complete set of velocity measurements is made every .750 seconds, each measurement being the vector component averaged over 15 cm. The data is internally recorded on digital cassette tape. Eight hours of continuous data can be recorded.

BASS was deployed in a tidal flow in Vineyard Sound at a depth of 10 m where a time series of u, v, and w velocities at 26 cm, 46 cm, 96 cm, and 210 cm above the bottom was recorded. The mean velocity was determined by fitting each 6 hour series with a sixth order polynomial and the deviations from the polynomial, the fluctuating velocity components, were correlated to produce Reynolds stress profiles. The stress series shows very few negative stress events while the dominant positive events have an average duration of 5 seconds and exceed 30 dynes/cm^2.

Zero offset was removed from the mean by assuming a log profile at maximum ebb. Deviations from a log profile developed when the current dropped below 40% of maximum, i.e., when the flow could no longer be considered steady. A break in the Reynolds stress profile at 1 m suggested a larger length scale than the 1 cm bottom roughness was present in the flow. A value of u_* was determined by using the quadratic drag law (u_* = 1.56 cm/sec), the log profile method (u_* = 1.60 cm/sec), and the

eddy correlation method (u_* = 1.91 cm/sec). Integral length scales of 5 m cross-stream, and 2.5 m vertically were identified by correlation calculations. Two length scales were present in the downstream direction, 5 m within 1 meter of the wall and 8 m further from the wall.

Thesis Supervisor: Albert J. Williams 3rd
Title: Associate Scientist

ACKNOWLEDGEMENTS

Dr. Albert J. Williams 3rd helped me in many ways during the course of this work. He not only guided my academic progress, but also came to my rescue when I had technical difficulties with the instrumentation or with my automobile. I am grateful to him for the key role he played in getting BASS off the drawing board and into the ocean.

The technicians and engineers of the Ocean Engineering Instrument Section provided sound technical advice in the design and construction phases of this project.

Dr. Brad Butman of the U.S. Coast and Geodetic Survey provided the mounting frame for the instrument.

Tim Fofonoff and Jacob Ladderman helped with the preparations for the field experiment.

Woods Hole divers, Dr. William Grant and Matthew Greer provided valuable field observations and photographs. I thank Dr. Grant for his critical reviews of the early drafts of the text.

Captain Roy Campbell and the crew of the M.V. Whitefoot made the field deployment procedure work faultlessly.

Dr. Robert Spindel generously allowed me the use of his project's computer for the data analysis.

Karen Pires prepared early drafts of the text, and was assisted by Judith De Santi in typing the final manuscript.

I thank my thisis committee, Dr. G.T. Csanady, Dr. W.L. Harris, Sr., Dr. C.D. Hollister and Dr. O.S. Madsen for their advice and critical

review of the thesis. Dr. I.N. McCave also provided valuable criticism.

Finally I thank my friends Matt Greer, Chris Myles, George Rodenbusch, and James R. Sullivan for their encouragement and help during the course of this thesis. The Woods Hole Oceanographic Institution Education Program patiently supported my work. Support from the National Science Foundation is also acknowledged.

TABLE OF CONTENTS

TABLE OF CONTENTS (cont.) Page No.

LIST OF FIGURES AND TABLES

PREFACE

This thesis documents the development of instrumentation to measure benthic boundary layer flow and its test in a tidal channel in Vineyard Sound. An understanding of the characteristics of bottom boundary layer flows is necessary in order to determine the attributes this instrument must possess to perform its designated task. For this reason, and because this thesis may be read by scientists interested in near bottom flow measurements who are not fluid dynamicists, there is a basic discussion of the scaling parameters of turbulent boundary layers.

The results of the field test are presented as a unique data set in which the three components of the velocity vector at four levels above the seabed were sampled simultaneously with the data being obtained from sensors having an averaging volume with a characteristic dimension of 15 cm. The data are presented and interpreted as a demonstration of the potential of the instrument rather than as a contribution to the understanding of turbulent estuarine boundary layers. The contribution of this thesis is neither the data set nor its interpretation, but rather the proven capability of the instrumentation to make superior measurements from which models can be tested and our knowledge of marine boundary layer flows increased.

The quality of the measurements from this instrument approaches that previously obtainable only from flume studies. The instrument was tested in the sea rather than in a flume for the practical reasons

of economics and availability. Large flumes (deeper than two meters) are generally expensive and unavailable while a nearby natural flow was readily accessible. The individual sensors were tested in a small tow tank, but the real test of the system was its deployment in the ocean. The reason for studying a boundary layer in nature rather than applying laboratory results to natural flows lies in the observation that not enough is known yet about the forcing functions and dynamically important features of natural flows to model them entirely on laboratory measurements. The data collected primarily for the validation of the instrument also shows promise in increasing our understanding of shallow tidal flows under the conditions of the field test.

Finally, the selection of material included in this thesis can best be understood in the context of the events which lead to its completion. In January 1975, I gained familiarity with the instrumentation possibilities of an acoustic shearmeter by assisting in its construction and testing while also learning more about turbulent flows and helping to produce research proposals to develop instrumentation for mearuring deep-sea boundary layer flows. Funding developed in 1976 and I began construction of my prototype designs. The complete instrument was ready for testing in August 1977, and was deployed in Vineyard Sound where the flow is reasonably simple. The data set from this deployment was subjected to computer analysis until early December. Along the way, a suite of programs was generated for data editing, plotting, and analysis, which resulted in plots of many measures of this turbulent flow. Besides valididating the measurement technique, the results were applied

to a simple model of a boundary layer flow which was later expanded to include the effects of unsteadiness and multiple length scales. Additional models and analysis schemes have been brought to my attention through my attempts to interpret the data set. These must however remain the target for future work.

CHAPTER 1

INTRODUCTION

The thrust of the research documented in this thesis has been directed toward achieving two goals: the first is to provide ocean scientists with a unique tool capable of making detailed measurements of the velocity structure in a marine boundary layer, and the second goal is to demonstrate the ability of this instrument to obtain significantly better measurements than can be obtained with existing instruments so that our understanding of boundary layer flow processes can be increased. The motivation behind this stems from the need expressed by investigators in many ocean-related disciplines for engineering data associated with the transport processes in near bottom flows. The dynamics of the flow in the immediate vicinity of the sea bed govern the fluxes of heat, momentum, chemical species, and sediment, and also play a dominant role in the formation and alteration of sediment bedforms. A detailed engineering investigation of the flow parameters in a geophysical boundary layer is necessary to gain insight into such varied problems as the interchange of thermal and kinetic energy between the bottom waters and the sediments, the transport of these sediments, the refraction of acoustic signals, and the operating conditions for engineering projects, oceanographic experiments, contained sea-bed waste disposal and deep sea mining. The interaction of the stresses at the boundary with the interior flow is an important phenomena to understand in order to model the dynamics of the global flow of the interior of the ocean.

Most boundary layer research has been performed in wind tunnels, flumes and in the atmosphere. The relatively few field measurements made in the ocean have used sensors which lacked the ability to simultaneously produce time series of the three components of the velocity vector at various distances from the bottom. Deep sea experiments using visual and mechanical measuring techniques have given only coarse estimates of the flow conditions on the bottom.

The first part of this study presents a summary of the important scales and velocity relationships in turbulent boundary layers, describes methods of investigating the parameters in such a flow in the marine environment, and then traces the design and development of a new instrument capable of supplying velocity data crucial to the understanding of marine boundary layer processes. The instrument represents the state of the art in making velocity fluctuation measurements in the sea with adequate resolution so that the fluctuating components of the velocity can be separated from the mean flow. In the second part of this study, the results of field work in a near shore boundary layer using the instrument are presented. The analysis of the data set from this field study demonstrates the unique capabilities of this tool for making inroads into the study of marine boundary layers. Clearly, advances in our understanding of geophysical boundary layers depend on the ability to make measurements of the type described in this last section.

1.1 Turbulent Boundary Layer Scales

One of the difficulties in investigating turbulent boundary layers is the presence of a multiplicity of length scales. It is the purpose of this section to summarize the various scaling parameters in a steady, horizontally homogeneous, unstratified, turbulent boundary layer. In the ocean all of the above assumptions are generally violated as a whole or individually. However, the simple model developed from such a discussion provides a useful foundation to help understand what characteristics a velocity sensor must have in order to make successful measurements in marine boundary layers. It also helps in understanding the limitations involved in making boundary layer measurements.

Most of the large scale boundary layer flows in nature such as in estuaries, in the atmosphere, and near the ocean bottom are turbulent and time dependent. The characteristically high Reynolds numbers associated with such flows are a consequence of their large length scales. The early work on high Reynolds number boundary layers was performed in fluid mechanics laboratories. The discussion to follow is based on these laboratory studies. A detailed treatment of turbulent boundary layers can be found in standard texts such as Schlichting (1968) or Tennekes and Lumley (1972), or in classical works such as Clauser (1956).

One way of treating the problem of multiple length scales is to consider the scaling parameters of the flow starting at the solid boundary and continuing upwards to the free surface.

At the solid boundary, an assumption must be made about the geometry of the wall. Assuming for the moment a flat, mirror-smooth surface, the no slip boundary condition requires the existence of a region near the solid wall where viscosity must play a role. Physically, the flow is retarded near the wall and this fluid-solid interaction manifests itself as a shear stress on the boundary. This bottom shear stress, τ_b, may be used to define the friction velocity, u_*, defined as,

$$u_* \equiv \left(\frac{\tau_b}{\rho}\right)^{1/2} \qquad (1.1)$$

where ρ is the fluid density. The friction velocity is not a directly observable quantity, but rather a characteristic scaling parameter in turbulent flows with the units of velocity.

An estimate of the length scale over which viscous effects are important is obtained from the ratio of the kinematic viscosity, $\nu(cm^2/sec)$, to the friction velocity, $u_*(cm/sec)$, that is,

$$\frac{\nu}{u_*} = L_\nu \qquad (1.2)$$

The shear stress in the fluid is of a viscous nature over a distance L_ν from the boundary, and so the bottom stress can be written:

$$\tau_b = \rho \nu \left.\frac{dU}{dz}\right|_{z=0} \qquad (1.3)$$

where U is the horizontal velocity and z is the vertical distance

coordinate up from the bottom. Substituting the definition of u_* given by Eq. (1.1) and integrating the above expression, a linear velocity distribution results:

$$\frac{U}{u_*} = \frac{u_* z}{\nu} \qquad (1.4)$$

Experimentally, it has been found that this relationship holds over a region which has a thickness on the order of $5\nu/u_*$ (Schlichting, 1968). This region in which viscosity dominates is called the viscous sublayer.

Relaxing the assumption of a smooth boundary, and introducing roughness elements of a characteristic length, k_b, on the solid wall can cause dramatic changes in the flow near the wall. When $k_b < 5\nu/u_*$, the flow is termed hydrodynamically smooth. If the scale of the roughness elements approaches the characteristic dimension of the viscous sublayer; that is, if $k_b > 5\nu/u_*$, then the sublayer cannot form because it is broken up by the turbulence shed from the roughness elements. The flow is said to be in a transitional regime between hydrodynamically smooth and rough flow when $5 < u_* k_b/\nu < 70$. Completely rough turbulent flow exists when $u_* k_b/\nu > 70$; $u_* k_b/\nu$ is often called the roughness Reynolds number (Nikuradse, 1933) and is seen to be the ratio of sublayer thickness to the roughness height.

For practical situations in the ocean, ν/u_* is usually much smaller than the bottom roughness scale, and so a viscous sublayer would not be expected; however even in the case of $\nu/u_* > k_b$,

the sublayer thickness would be on the order of millimeters which would indeed be a challenge to the observationalist.

In the case of a rough boundary for which $\nu/u_* \gg k_b$, the length scale in the wall region is k_b. As the distance from the wall is increased, the effects of the boundary become less pronounced, and eventually the flow is unaffected by the wall's presence. Ultimately rotational or stratification effects become dominant and determines the thickness of the layer. At this distance the scaling length is the thickness of the boundary layer itself. Typically this boundary layer thickness, δ, is arbitrarily defined as the point where the mean horizontal velocity is 98% of the free stream velocity.

Three scaling lengths have now been identified, ν/u_*, k_b, and δ. The boundary layer thickness is many times larger than the roughness length or sublayer thickness, and since the range of separation of the two scales is so great, there is a region away from the boundary where k_b is too small to be dynamically important and δ is too large to have any effect. This level where the vertical separation from the boundary, z, satisfies both $z/k_b \gg 1$ and $z/\delta \ll 1$ is called the inertial sublayer. The scaling parameter for length in the inertial sublayer is simply z, the distance from the boundary. This region is characterized by the absence of significant viscous effects, and the shear stresses are due to the turbulent velocity fluctuations. These turbulent stresses will be discussed in detail later in this chapter, but at present it should be mentioned that these stresses scale as u_*^2, and that they are approximately

constant in the inertial sublayer as can be shown from the equations of motion (see for example the discussion in Tennekes and Lumley (1972) pp. 149-153). Many experiments carried out in flumes, wind tunnels, and pipes have shown that in the inertial sublayer the velocity distribution is logarithmic. These types of observations formed the impetus for the work of von Karman and Prandtl. Theodore von Karman in 1930 first derived the logarithmic profile for hydrodynamically smooth flow using a similarity argument. Prandtl subsequently developed the logarithmic velocity distribution for hydrodynamically rough conditions using a mixing length approach.

Assuming a layer of constant stress, the variation of mean velocity with height can be expressed in terms of the scaling parameters of the inertial sublayer; u_* is the relevant velocity scale and z the length scale:

$$\frac{dU}{dz} = \frac{cu_*}{z}$$

where c is a constant. This expression integrates to

$$\frac{U}{u_*} = c_0 \ln z + c_1 \qquad (1.5)$$

where c_0 and c_1 must be determined experimentally. The constant, c_0, is usually written $\frac{1}{\kappa}$, κ being von Karman's constant which is approximately equal to 0.4 for clear water. Suspended material in the flow tends to decrease the value of κ, and values as small as .26 have been reported (Raudkivi, 1967).

The empirically determined constant, c, is related to the roughness of the boundary, and the logarithmic velocity profile is usually written in a form that reflects this

$$\frac{U}{u_*} = \frac{1}{\kappa} \ln \frac{z}{z_o} \qquad (1.6)$$

where z_0 is a parameter reflecting the roughness height for the boundary. Over a rough boundary z_0 has been shown by experiments to be dependent on the characteristic dimension of the roughness elements, k_b, by the relation

$$z_o = \frac{k_b}{N}$$

where N depends on the roughness Reynolds number of the flow and k_b is the equivalent sand grain roughness (Nikuradse, 1933). For completely rough turbulent flow N is equal to 30; while for transitional flows it has a value near 22.

The above model of the logarithmic boundary layer profile has been derived for steady unstratified flow which is free of suspended matter and is horizontally homogeneous. If these assumptions are violated, deviations from logarithmic behavior would be expected. Stratification could put a lid on the log layer and shorten its vertical extent; while suspended material would decrease κ and thus alter the slope of the log profile.

Two other length scales in the boundary layer should be mentioned since they would be important depending on [illegible]cuation

under analysis. The smallest scale of eddies which should exist represents the scale at which the eddies are dissipated by viscosity. In the inertial sublayer this length scale, known as the Kolmogorov fine scale, is given by

$$L_\kappa = \left[\left(\frac{\nu}{u_*}\right)^3 \kappa z\right]^{1/4} \qquad (1.7)$$

where z is the vertical distance from the boundary (Tennekes and Lumley, 1972).

On a much larger scale, oceanic and atmospheric flows feel the effects of the earth's rotation. The scaling velocity can still be taken as u_* but the length scale must take the Coriolis parameter, $f(\sec^{-1})$, into account. The thickness of this layer, called the Ekman layer, would then be on the order of u_*/f. Wimbush and Munk (1971) estimate the Ekman layer height to be $\kappa u_*/f$. If the Coriolis force is indeed felt, as in the case of an ocean basin with great horizontal extent, then theory shows (for example Tennekes and Lumley, 1972) that the velocity vector will deflect towards the right with increasing distance from the bottom in response to the Coriolis force. Monin and Obukhov (1954) indicate the height of the constant stress layer as

$$\delta_{\tau=\text{constant}} = \frac{.2u_*^2}{U_\infty f}$$

where U_∞ is the free stream velocity.

In tidal flows and for boundary layers under waves, the radian wave frequency, ω, scales the boundary layer thickness as,

$$\delta \sim \frac{\kappa u_*}{\omega}$$

where κ is von Karman's constant and $\omega = 2\pi/T$, T being the period of the oscillation. These flows have been investigated by Kajiura (1964), Grant and Madsen (1977), and Smith (1977).

Table 1.1 (in part from Wimbush, 1976) and Figure 1.1 illustrate order of magnitude estimates of the various layer thicknesses in three flow regimes in the ocean.

Note the critical dependence on u_* in the calculations leading to Table 1.1. The next section (1.2) will describe the methods used to obtain u_*. The above discussion on the structure of the boundary layer is based largely on measurements executed under laboratory conditions in which the mean flow was fully developed, stationary, neutrally stable and horizontally homogeneous.

In the ocean the mean flow is constantly changing and, depending on location, the fluctuations can be over time scales ranging from seconds to months. The in situ measurements of Heathershaw (1974) and Gordon (1974) have demonstrated that turbulent fluctuations occur intermittently near the boundary and hence the transport processes in the boundary layer require careful time series analysis. This concept of intermittency must be kept in mind when dealing with the dynamics of the boundary. Intermittency as it relates to the present study will be treated in a later section (1.2.4).

TABLE 1.1: Boundary Layer Scales (in part from Wimbush, 1976)

Regime	Quiescent Ocean Basin	Rise, Slope, Shelf	Intense Currents
Mean velocity U_∞	10^{-2} m/sec	10^{-1} m/sec	1 m/sec
Friction velocity $u_* \sim \frac{U_\infty}{10}$	10^{-3} m/sec	10^{-2} m/sec	10^{-1} m/sec
Thickness of sublayer $\delta_\nu \sim 5\frac{\nu}{u_*}$	8×10^{-3} m	8×10^{-4} m	8×10^{-5} m
Thickness of constant stress layer $\delta_{\tau=c}$	2×10^{-1} m	2 m	20 m
Reynolds stress $\tau(z) \sim \rho u_*^2$	10^{-3} dyn/cm^2	10^{-1} dyn/cm^2	10 dyn/cm^2
Thickness of logarithmic layer $\delta_L \sim \frac{.1u_*}{f}$	1 m	10 m	100 m
Thickness of Ekman layer δ_E	4 m	40 m	400 m
Kolmogorov fine scale at $\delta_{\tau=c}$	4×10^{-3} m	1.5×10^{-3} m	4×10^{-4} m

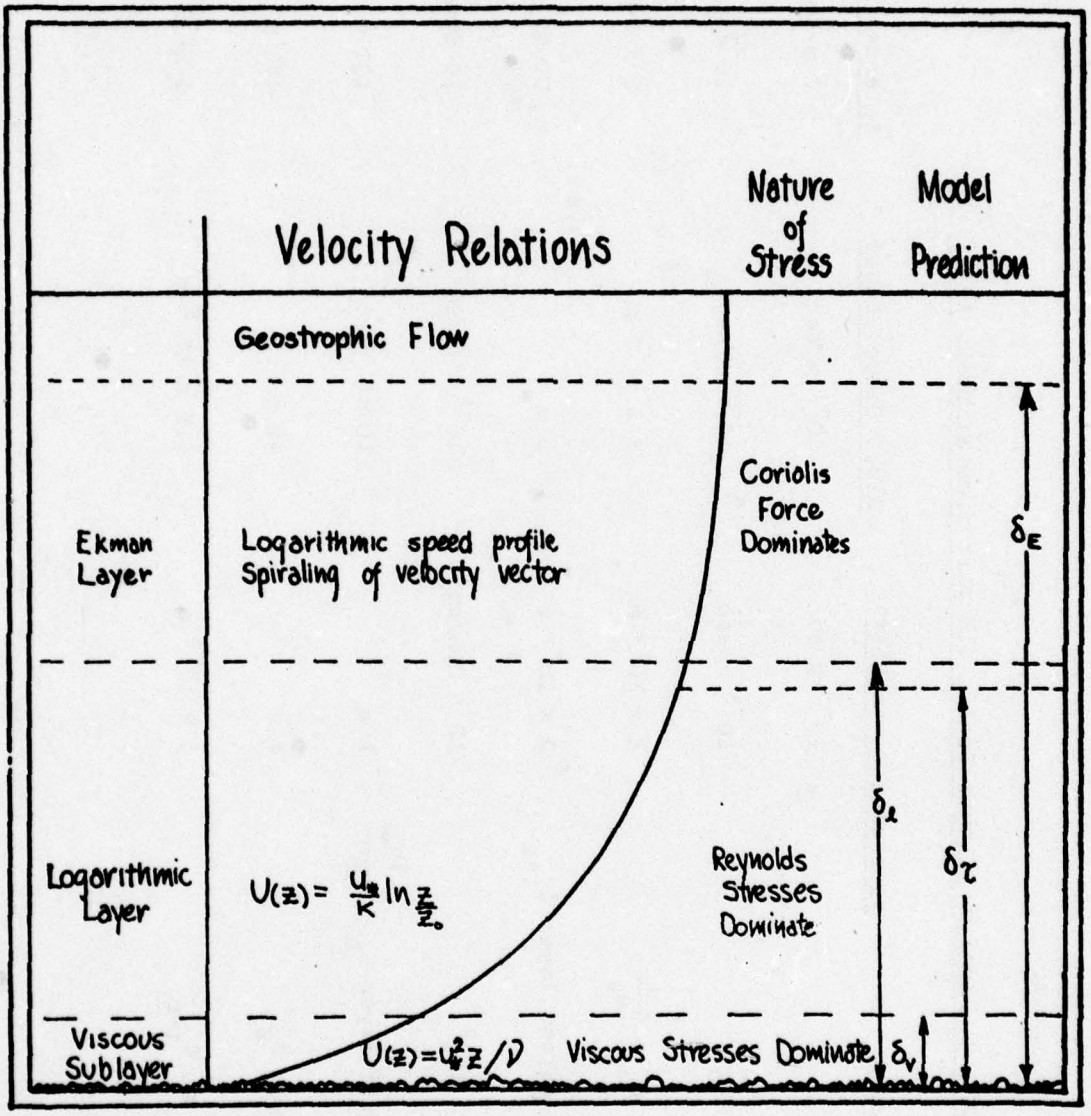
Velocity Relations
Nature of Stress
Model Prediction
Geostrophic Flow
Ekman Layer
Logarithmic speed profile
Spiraling of velocity vector
Coriolis Force Dominates
δ_E
δ_l
δ_τ
Logarithmic Layer
$U(z) = \frac{u_*}{k} \ln \frac{z}{z_0}$
Reynolds Stresses Dominate
Viscous Sublayer
$U(z) = u_*^2 z / \nu$
Viscous Stresses Dominate
δ_ν

Figure 1.1

The field research undertaken to demonstrate capabilities of the instrumentation system developed for this thesis was performed in a shallow water ($\sim$ 10 m) tidal current. The question raised is: What can the type of data from this instrument say about how well current boundary layer models describe unsteady flow in shallow water? It is expected that the value of u_* will be a time varying function which should reflect the state of the tide (Kajiura, 1964). Since the bottom stress is proportional to the friction velocity, this has important implications for sediment transport in tidal currents.

In contrast to the deep ocean, the flow in a shallow tidal channel will exhibit no veering of the velocity vector since the sides of the channel will prohibit the effect of the Coriolis force from being significant to the dynamics of the flow. The driving force in shallow water in the case investigated is the pressure gradient due to the tide since no wind was present; and under quasi-steady conditions, a linear shear stress distribution will result ranging from zero at the free surface in the absence of wind to a maximum at the sediment-water interface.

Although the hydraulic forcing for the shallow water channel is different from that of the deep ocean, a constant stress layer near the bottom is expected which in turn would result in a logarithmic velocity profile when the flow is fully developed. In the absence of stratification, the logarithmic profile might be expected to exist throughout the water column except close to the free surface; however, it is more probable that in an actual experiment, the density structure

or the topography will dictate the height of the logarithmic layer.

It is anticipated that the flow will be intermittent and that analyses of the velocity fluctuations will reveal events responsible for large amounts of momentum transport, and that these events will have a multiplicity of scales.

Keeping the foregoing model and these expected results in mind, a discussion of previous experiments and methods of analysis is in order.

1.2 Background to Methods of Investigation and Previous Work

In this section, the methods which have been used to investigate the structure of the boundary layer in the marine environment are discussed. The target of these investigations predominately has been an appropriate value for the bottom shear stress, τ_b. Inherent in the analyses are important results with regard to length and time scales in the boundary layer.

1.2.1 Quadratic Drag Law

Classically, the determination of the shear stress at the bottom boundary in channel flow is made by measuring the mean horizontal velocity over the bottom and then invoking a quadratic drag law of the form:

$$\tau_b = C_f \rho \frac{U^2}{2} \qquad (1.8)$$

where τ_b = bottom shear stress

c_f = drag coefficient

ρ = fluid density

U = mean horizontal velocity

Implicit in this approach are the assumptions of steady flow and no density stratification. The empirical constant, c_f, can be determined with the flow similitude approach of using historical flume data obtained at the same roughness Reynolds number. As an example, in Vineyard Sound there is a tidal current of $\sim$ 30 cm/sec at a level 100 cm above the gravel bottom (.5 - 1.0 cm dia. pebbles). Following the approach mentioned above and using data from the text-book of Daily and Harleman (1966), one obtains a frictional coefficient of 5.0×10^{-3} for the site in Vineyard Sound. Interestingly in 1959 Bowden, Fairbairn and Hughes (1958) made near bottom velocity measure-ments in a tidal current (U $\sim$ 30 cm/sec) off Red Wharf Bay in North Wales. At that location the bed was composed of firm sand and shingle. By using the logarithmic profile technique (to be discussed in the next section), they obtained a value of $c_f = 7.0 \times 10^{-3}$ as defined by Eq. 1.8 for conditions similar to those described for Vineyard Sound. Their reference velocity was 1 meter.

Although the quadratic drag law oversimplifies the dynamics of the flow, it does lend itself to situations where horizontal velocity data is available from only one sensor near the bottom. It must be remembered that the drag coefficient is a function of Reynolds number and roughness, and that although it is constant when the boundary

layer is fully developed, it can vary considerably during periods when the flow is non-steady (Kajiura, 1964). Once a proper parameterization of the flow is made, future measurements can be simpler because the effects of roughness and turbulence can be treated through the drag coefficient.

1.2.2 Logarithmic Profile Method

> "The logarithmic velocity profile in the inertial sublayer is one of the major landmarks in turbulence theory. With analytical tools of a rather general nature a very specific result has been obtained, even though the equations of motion cannot be solved in general."
>
> (Tennekes and Lumley, 1972)

In section 1.1 the logarithmic profile in the inertial sublayer was derived, and can be written as

$$U(z) = \frac{u_*}{\kappa} \ln \frac{z}{z_0}$$

A plot of U versus the Naperian logarithm of z should yield straight lines whose slopes will give u_*/κ, and whose intercept with the U axis will yield z_0. A value of u_* can thus be found if a value for κ is assumed. It is taken to be 0.4 which is the clear water value.

Sverdrup (et al., 1942) has pointed out that measurements of velocity at two levels are necessary to obtain values of z_0 and u_* and measurements at three or more levels are required to validate the equation in the oceans. The first attempt at this was performed by Revelle and Fleming using a pendulum current meter at the entrance

of San Diego Harbor in 1937 (Sverdrup, et al., 1942). Measurements in the lower two meters in a tidal current of about 25 cm/sec showed good agreement with the log profile; frictional stress of 6 dynes/cm^2 were computed along with a bottom roughness of 2 cm.

Another pioneering study, this one more detailed, was made by Mosby in 1946, and again in 1949 (Mosby, 1946; Mosby 1949). Figure 1.2 is reproduced from his first paper. It shows mean velocity profiles during a five hour experiment in a strong tidal current north of Bergen, Norway. He found that for half hour averages of velocity the profile deviated from logarithmic but longer averages on the order of hours "may very well be interpreted by the usual logarithmic law" (Mosby, 1946). In Mosby's work is seen the surfacing of the time averaging problem which is to plague hydrodynamists, meteorologists and oceanographers in the decades to come.

Lesser (1951) also measured near bottom (< 2 m) mean velocities over differing bottom types and also found a good agreement to the log profile after suitable averaging similar to Mosby. More recently Wimbush and Munk (1970) report a logarithmic profile to a height of two meters above the bottom of the Pacific ($U \sim 5$ cm/sec). Sternberg (1970) on the other hand found that in the San Clemente Basin "many of the velocity profiles were not logarithmic thus precluding the analysis procedure." Quantitatively he estimates logarithmic profiles occurred between 22 and 57 percent of the time for his experiments off the California coast. Two possible causes for this could be unsteadiness in the boundary layer driving force, or multiple

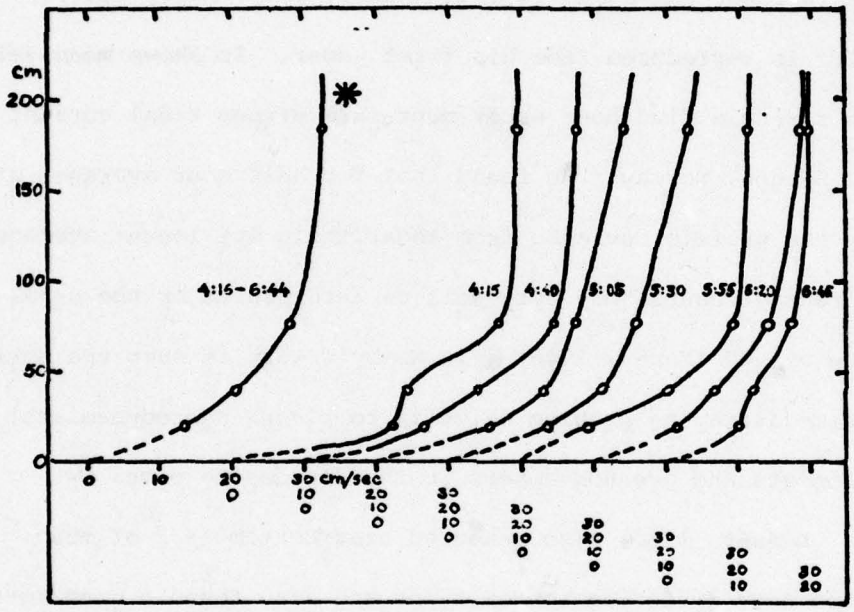

Mean Velocity Profiles (after Mosby, 1946)
25 minute averages
* is a 2½ hour average

Figure 1.2

roughness length scales as suggested by the work of Smith and McLean (1977). Their work shows that for a bed geometry exhibiting multiple roughness scales a series of logarithmic layers is expected. These layers are stacked vertically with each successive layer corresponding to an increasingly large length scale feature on the boundary. With these multiple scales, a simple mixing length argument based on only one length scale for the flow breaks down. Thus, it is not surprising that observation of a continuous logarithmic profile is elusive in regions where differing bottom length scales exist.

In contrast to this, various field investigations and a multitude of laboratory studies indicate that the logarithmic velocity distribution is a permanent feature in steady turbulent boundary layers, as in a laboratory flume or the atmosphere. The effects of the unsteadiness of the flow, the density structure, and the bottom topography must all be considered when attempting to fit oceanic observations to a steady, equilibrium boundary layer model.

1.2.3 Reynolds Stresses and Eddy Correlations

In this thesis a lower case letter with a tilde denotes the instantaneous value of a quantity; an upper case letter denotes a time averaged mean quantity; and a lower case letter represents the fluctuating component. Using this notation, the Reynolds decomposition of the time varying quantity, $\tilde{u}$, is defined as,

$$\tilde{u} = U + u$$

Figure 1.3 illustrates the coordinate system used throughout this thesis.

Proceeding from the equations of motion for an incompressible, viscous fluid, and using the continuity equation, one obtains the Navier-Stokes equations which then can be subjected to a Reynold's decomposition to give the steady state Reynolds momentum equation in tensor notation:

$$\rho U_j \frac{\partial U_i}{\partial x_j} = \frac{\partial}{\partial x_j}\left[-P\delta_{ij} + \frac{\mu}{2}\frac{\partial U}{\partial x_j} - \rho\overline{u_i u_j}\right] + F_i \qquad (1.9)$$

Mean Convection = pressure gradient + viscous stress + Reynolds stress + Body Forces

The overbar signifies a time average and

U_i, U_j = mean velocity components

u_i, u_j = fluctuating velocity components

ρ = density of the fluid

μ = molecular viscosity

P = time averaged pressure

i, j = coordinate indices 1 = x, 2 = y, 3 = z

F_i = body forces ($F_1 = F_2 = 0$, $F_3 = -\rho g$)

The vertical flux of momentum acts as an effective resistance to motion and an effective shear stress. Turbulent fluxes of momentum are known as Reynolds stresses.

Symbolically, the Reynolds stress tensor can be written as

$$\tau_{ij} = -\rho\overline{u_i u_j}$$

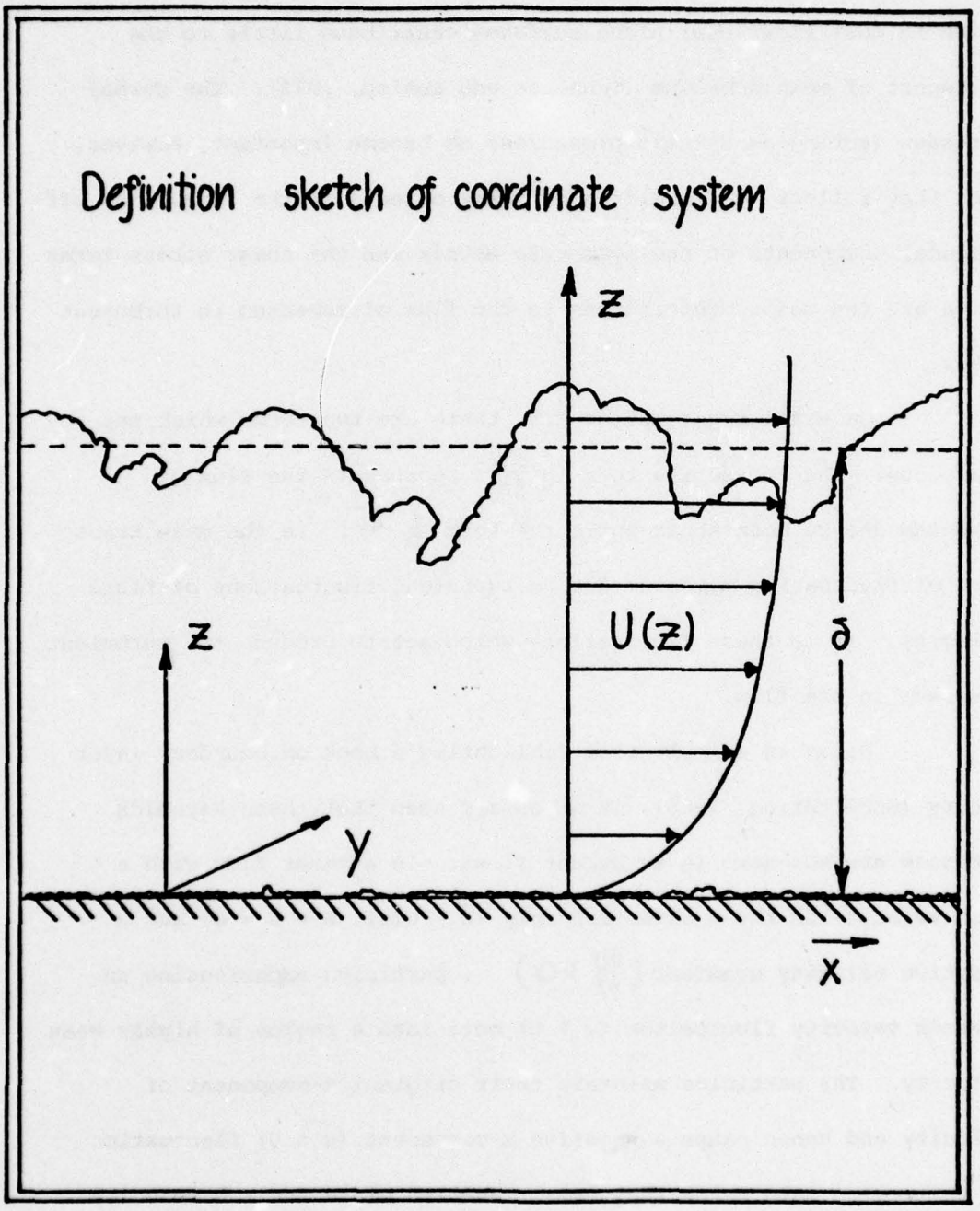

Figure 1.3

Along the diagonals are normal stresses ($\rho\overline{u^2}$, $\rho\overline{v^2}$, $\rho\overline{w^2}$) which in most flows over plane surfaces contribute little to the transport of mean momentum (Tennekes and Lumley, 1972). The normal stresses (acting as dynamic pressures) do become important, however, when they reflect the form drag of large objects in the flow. The off-diagonal components of the symmetric matrix are the shear stress terms which are the major contributors to the flux of momentum in turbulent flows.

On examining equation 1.9, there are two terms which are analogous. The convective term $U_j \frac{\partial U_i}{\partial x_j}$ represents the flux of momentum due to mean shear while the term $\frac{\partial}{\partial x} \overline{u_i u_j}$ is the mean transport of fluctuating momentum due to turbulent fluctuations of fluid velocity. It is these fluctuations which act to produce the turbulent stresses in the flow.

Using an example from Schlichting's book on boundary layer theory (Schlichting, 1968), it is easily seen that these Reynolds stresses are non-zero in turbulent flows. In a shear flow with a mean velocity in the x direction only ($U = U(z)$, $W = V = 0$) and a positive velocity gradient ($\frac{\partial U}{\partial z} > 0$) , particles experiencing an upwards velocity fluctuation ($w > 0$) move into a region of higher mean velocity. The particles maintain their original x-component of velocity and hence cause a negative x-component ($u < 0$) fluctuation in the region into which they have travelled since their U velocity is less than the local value of U. Alternatively, particles moving downwards ($w < 0$) cause a positive u fluctuation by the same mechanism.

Thus, most of the time a negative value of w is associated with a positive value of u while a positive w fluctuation is associated with a negative horizontal velocity fluctuation, and this leads to a Reynolds stress $(-\rho\overline{uw})$ which when time averaged is not only non-zero but positive.

In the Reynolds stress or eddy correlation method of determining the bottom shear stress, the basic assumption is that the stress is constant in the inertial sublayer. The value of the stress at the boundary is approximately equal to the shear stress in the fluid at small distances from the boundary. This opens up the possibility that a single sensor capable of measuring the velocity fluctuations in the inertial sublayer can give a value of bottom shear stress. Over a smooth boundary the shear stress in the constant stress region is constant to about 10% (Heathershaw, 1976), and thus the use of a single sensor may work in this instance. Over rough boundaries, however, there is a possibility of multiple roughness scales with each scale controlling a separate constant stress layer (Smith and McLean, 1977). This possibility would cast doubt onto the validity of single point fluctuation measurements to determine the bottom stress.

In a flow with velocity shear, turbulence can arise and sustain itself. Experimental evidence suggests that the initial onset of turbulence is due to the sudden breakdown of laminar flow in localized regions (Schlichting, 1968). The breakdowns occur because disturbances, such as roughness elements or pressure

perturbations, cause instabilities in the laminar flow. Once formed, the localized regions of turbulence can grow and sustain themselves by extracting energy from the mean shear. The turbulent fluctuations produce apparent stresses against which the mean flow does work, and thus there can be considerable flux of momentum between different points in the flow.

Present day concepts of turbulence have been molded from velocity fluctuation measurements made in the laboratory, mainly made with hot wire anemometers. The technique is unsuitable for use in the ocean due to difficulties in maintaining a stably operating hot wire for long periods of time, and it was not until 1956 that the first attempt was made to measure directly the horizontal and verical fluctuations of velocity in the sea. *This work was done by Bowden* and Fairbairn (1956) in a tidal current in North Wales using a 2 axis electromagnetic current meter (depth = 12 - 22 m; U = 25 - 50 cm/sec), and values of Reynolds stress ranged from 2 to 4 dynes/cm^2 which corresponded to an average coefficient of correlation as defined by

$$r_{uw} = \frac{[\overline{uw}]}{[\overline{u^2}]^{1/2}[\overline{w^2}]^{1/2}} \approx -0.4 \qquad (1.10)$$

It was also observed that the u component contained more energy in fluctuations of longer period than did the w component and it was suggested that the major contributions to the shearing stress would come from frequencies between 0.01 Hz and 0.25 Hz (periods of 4 to 100 sec).

Bowden performed a similar experiment a few years later and reports (Bowden, 1962) from spectral computations that the peak values of the energy spectra occur at wavenumbers of $.04 \times 10^{-4}$ m^{-1}, $.25$ m^{-1}, and $.70$ m^{-1} for the u, v, and w velocity fluctuations respectively. This indicates phenomena having wavelengths of 25 m, 4 m, and 1.4 m in the x, y, and z directions.

In the same paper (Bowden, 1962), the integral scales of the flow are also calculated. These integral scales reflect the average size of eddies in three dimensions and are obtained by multiplying the integral of the autocorrelation function by the mean advection velocity, that is, the autocorrelation function for a record of horizontal velocity u(t) which is T seconds long is defined as,

$$R_u(\tau) = \frac{\int_0^T u(t)\,u(t-\tau)\,dt}{\int_0^T u^2(t)\,dt} \qquad (1.11)$$

and thus,

$$L_u = U\int_0^T R(\tau)\,d\tau \qquad (1.12)$$

Bowden's results were L_u = 3.6 m, L_v = 1.6 m and L_w = 1.3 m for streamwise, cross-stream, and vertical directions respectively.

Figure 1.4 shows mean autocorrelation curves for u and w at 75 cm and 150 cm above the bottom computed for a 21 minute time series (reproduced from Bowden and Fairbairn, 1956). The salient feature in the figure is the differing rates at which $R_u(\tau)$ and $R_w(\tau)$ decrease with increasing lag. Since the curves for 150 cm

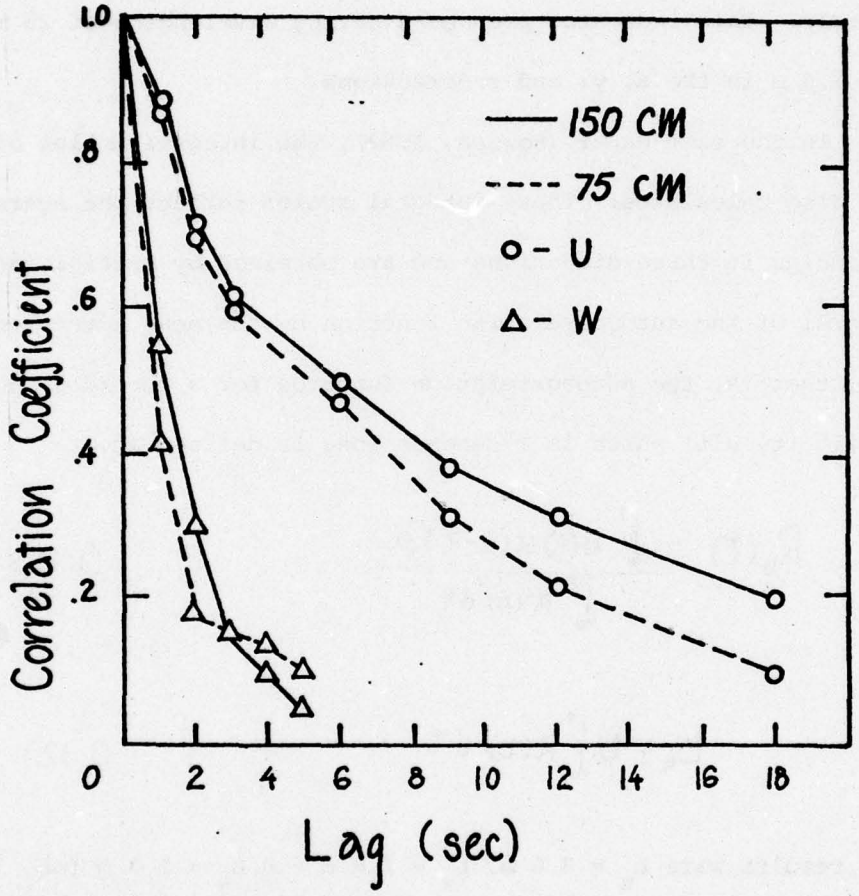

Mean Autocorrelation Curves for u and w at 150 and 75 cm above the bottom (after Bowden and Fairbairn (1956))

Figure 1.4

lie above those for 75 cm, it seems suggestive that fluctuations of longer periods become more important at increasing distances above the bottom. The data in the figure seems to indicate this for the u-component only.

Using the same technique as Bowden and working also in the Irish Sea, Heathershaw (in McCave, 1976) measured horizontal and vertical fluctuations and computed Reynold's stresses by the eddy correlation technique. He found that turbulent energy production occurs a wavenumbers in the range $3 \times 10^{-4} < k < 3 \times 10^{-2}$ cm^{-1}; and that the dissipation scale was well separated from the production scale and corresponded to wavenumbers between 10^{-3} cm^{-1} and 10 cm^{-1}. It was also observed that peak values of the Reynolds stress sometimes attained magnitudes which were 10 - 30 times the mean stress. These high stress events occurred intermittently with average durations between 5 and 20 sec.

The instruments of Bowden (1962) and Heathershaw (1976) measured only two components of the flow. The first attempt at measuring the three components of velocity fluctuations in a marine environment was performed in 1967 by Seitz in the Patuxent Estuary which empties into Chesapeake Bay (Seitz, 1971). By lowering a three axis acoustic Doppler shift current meter on a tower, data was obtained of the velocity fluctuations at various depths in the estuary. The primary concern of the Seitz study was to investigate the energy spectra of the three components of velocity fluctuations; however, bottom shear stresses were also computed using the constant stress

layer assumption, that is,

$$\tau_b = -\rho \overline{uw}$$

Figure 1.5 (reproduced from Seitz, 1971) shows the variation of the square root of bottom stress with mean horizontal velocity. Twice the square of the slope of the line in Figure 1.5 gives the coefficient, c_f, in the quadratic drag equation,

$$\tau_b = \frac{c_f \rho U^2}{2}$$

thus empirically linking the bottom stress to the horizontal velocity through a measurement of the Reynolds stress. For the line in Figure 1.5 the drag coefficient is 2.8×10^{-3}.

Gordon and his colleagues (Gordon and Dohne, 1973; Gordon, 1975; Gordon and Witting, 1976) have also made velocity fluctuation measurements in an estuary emptying into Chesapeake Bay. The theme of the research has been to show the dependence of the structure of turbulent stresses on the phase of the estuarine tide. The most recent model (Gordon, 1975a) suggests that the influence of the longitudinal pressure gradient in a tidal flow is tied to the Reynolds stress in such a way that the Reynolds stresses are greater for a decelerating flow than for an accelerating flow. This might be explained by an increase in pressure fluctuations due to the adverse pressure gradient on the decelerating tide which in turn caused increased instability in the flow leading to a greater level of turbulent fluctuations. Figure 1.6 (reproduced from Gordon,

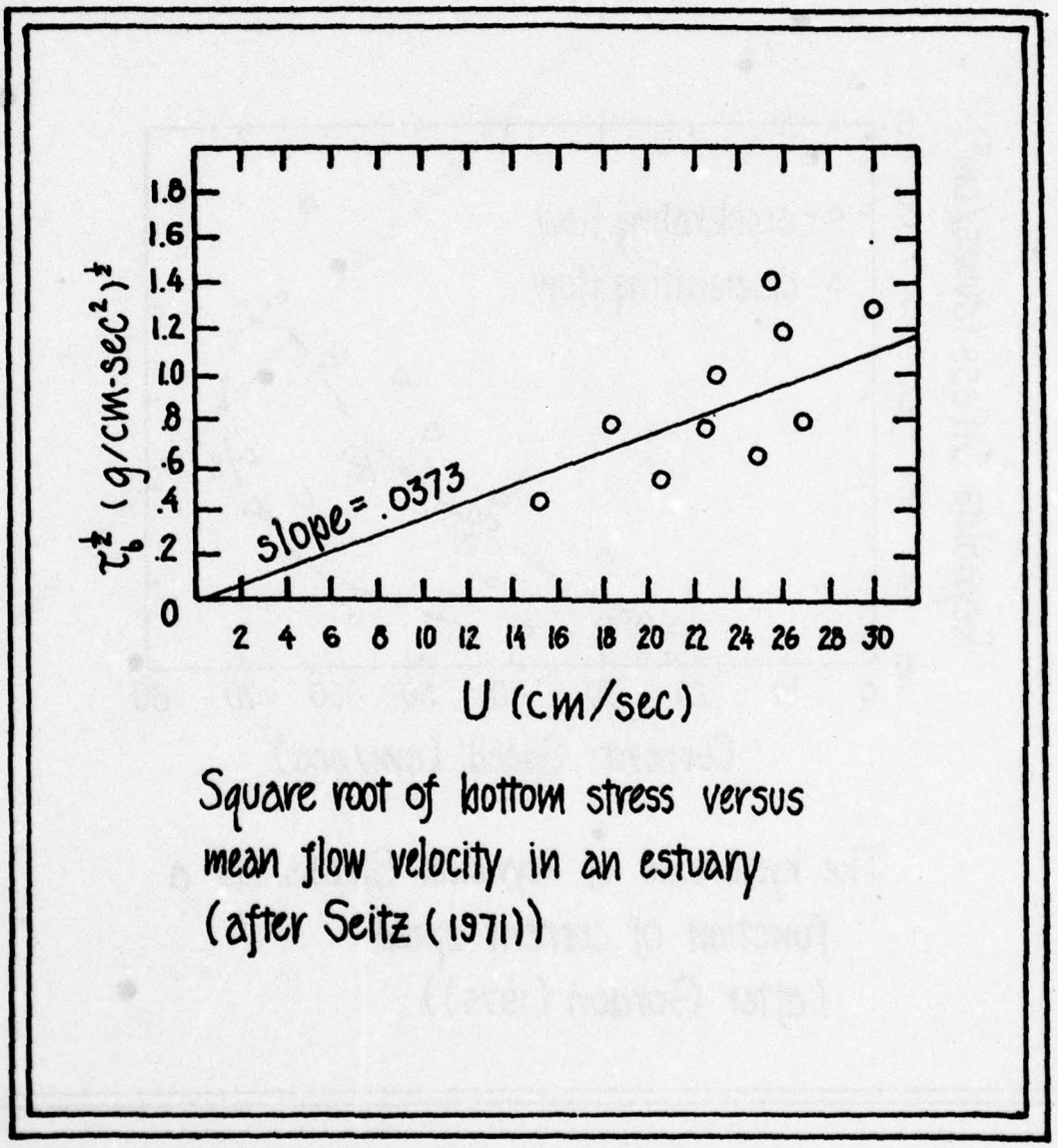

Square root of bottom stress versus mean flow velocity in an estuary (after Seitz (1971))

Figure 1.5

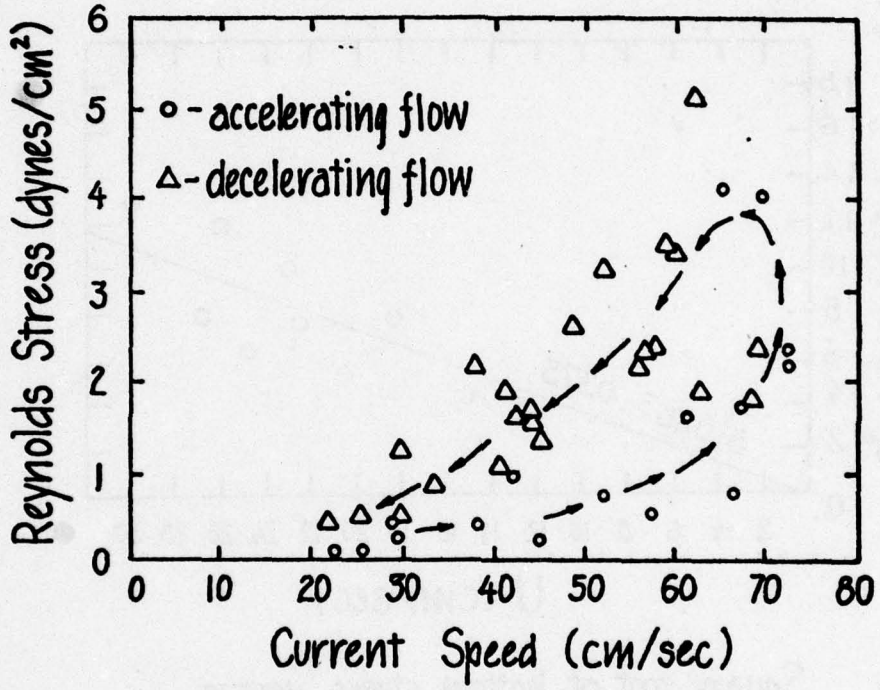

The hysteresis of Reynolds Stress as a function of current speed (after Gordon (1975))

Figure 1.6

1975a) shows this "hysteresis effect"; the implied result being that for the same current speed more sediment is likely to be transported during periods of decreasing tidal velocity than during times of increasing velocity. Recently measurements in Eastern Long Island Sound (Everdale, 1976; Bohlen, 1977) show no evidence of this asymmetric behavior of velocity fluctuations and Bohlen points out that the distribution of shear stresses in the water column and the transport of sediment along the bottom are the resultant of not only the horizontal pressure distribution as reflected by the phase of the tide, but also of local boundary layer characteristics namely, basin configuration, local hydrographic conditions, and boundary roughness. This suggests that Gordon's modelling might be an oversimplified approach. Data from the Irish Sea presented by Bowden et al. (Bowden, Fairbairn and Hughes, 1959) also show no dependence of shear stress on the acceleration of the flow. There is an important difference between Gordon's experiments and those of Bowden and Bohlen which is that Gordon worked in a confined channel while the measurements in the Irish Sea and Eastern Long Island Sound were made in a relatively open basin. The data set is incomplete in both topographical configurations and more measurements of Reynolds stress are required.

Just as the longitudinal pressure gradient effects the character of the Reynolds stresses, so too does it impress itself on the level of intermittency in the flow. Both Gordon (1974) and Heathershaw (1974) have made observations of turbulent events in natural flows; the details of this important momentum transferring mechanism are the subject of the next section.

1.2.4 Intermittency

The eddy correlation technique is accurate and provides results in close agreement with other methods (see for example Miyake et al., 1970); however, a difficulty does arise in that a poor choice of the time averaging interval in calculating the Reynolds stress will give erroneous results. The turbulent boundary layer is not a conveyor belt carrying a homogeneous and isotropic field of turbulence downstream; it is rather a process fraught with intermittent momentum transporting events. Due regard must be placed on the relationship between the mean frequency of these events and the sampling and averaging scheme used to obtain Reynolds stresses.

Many experiments have been performed to graphically illustrate intermittency in the viscous sublayer, and at that scale the intermittency of high stress events is known as bursting. Laboratory observations and the general concepts of the process are found in Townsend (1958) and Grant (1958), but it was not until the late 1960's that the experiments of Kline and his colleagues (Kline et al., 1967) focused attention on the importance and implications of intermittency in turbulent boundary layers. Additional light was shed by the flow visualization studies carried out by Corino and Brodkey (1969), Kim et al. (1971) and others. These researches graphically revealed the presence of well-organized motions in the viscous sublayer and gave indications of the temporal and spatial extent of the features.

Basically, the bursting process consists of two types of events. In the first type, streaks of slowly moving fluid close to the solid boundary are lifted as sudden violent jets or ejections into the faster moving overlying fluid. In the other mode, often called sweeping or inrushing, there is a diffuse inrush of high speed fluid toward the wall in effect tossing the low speed fluid away from the boundary. Figure 1.7 illustrates the two cases. These motions are three dimensional and appear to occur at random; they behave in a manner similar to the sinuous movements of snow flurries across the surface of a frozen pond or roadway. Being highly coherent, bursts and sweeps both represent large contributions to the Reynolds stress (Grass, 1971). Wallace, et al. (1972) and Willmarth and Lu (1972) have verified in open channel laboratory studies that the largest contribution to Reynolds stress and turbulent energy occurs during the bursting or ejection phase and much of the remainder of the turbulent stress can be attributed to the inrush or sweep phase.

In terms of the discussion in the foregoing section on the effects of pressure gradients, Kline, et al. (1967) found that adverse pressure gradients (corresponding to a decelerating flow) make bursting more frequent whereas a favorable pressure gradient reduces the bursting rate. In highly accelerated flows, the bursting was found to cease entirely, and this was attributed to relaminarization of the flow.

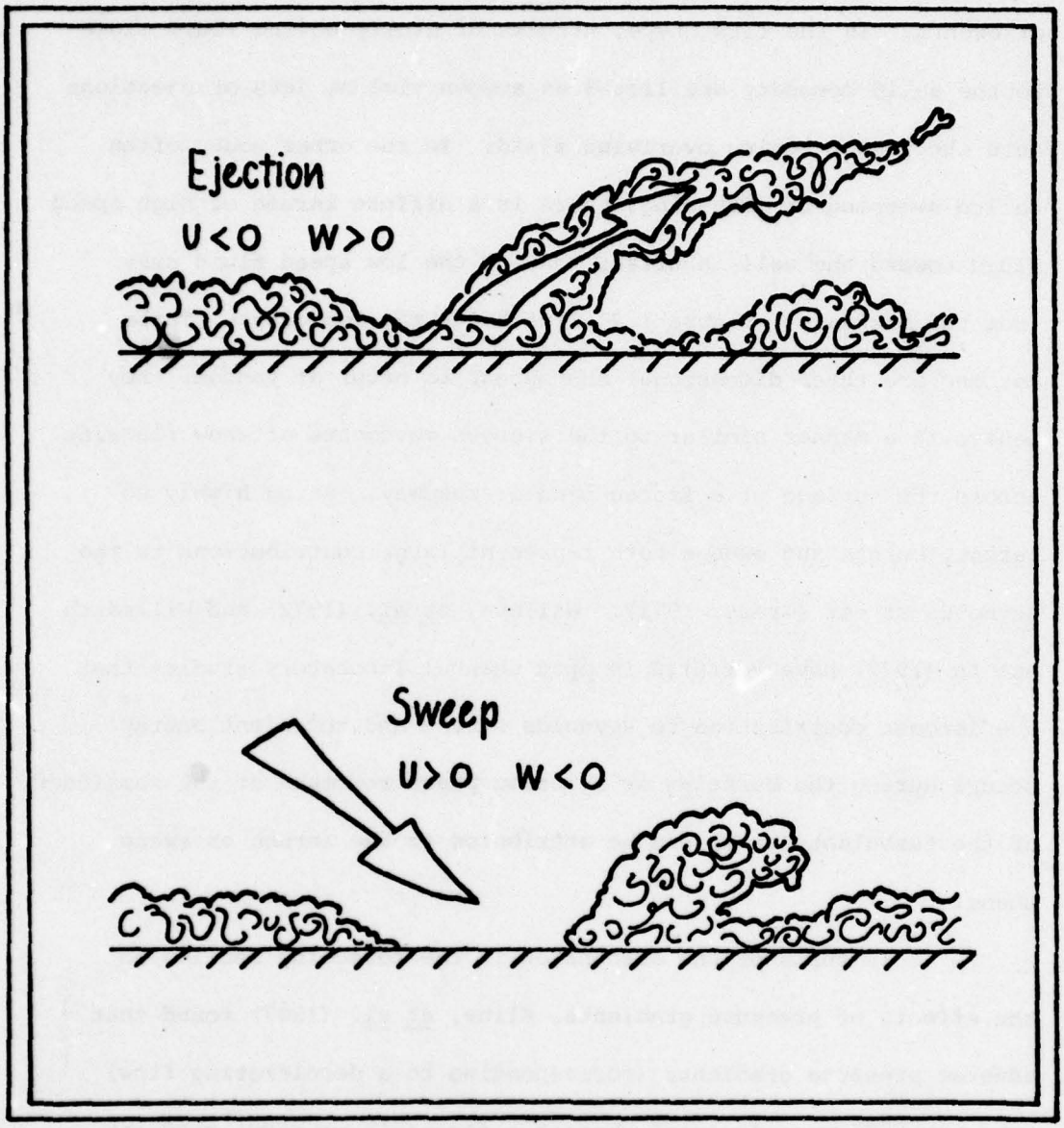

Figure 1.7

Strickly speaking, the term "bursting" should only be applied in discussions of intermittency in the viscous sublayer since many of the models for the dynamics of the bursting process are specific to the sublayer region (for example, see Landau, 1975).

In the ocean the viscous sublayer is expected to be extremely thin ($\sim$ 1 cm) if it exists at all. This is due to the large scale of the flow as reflected in the high Reynolds number. Yet, as in all turbulent flows, intermittency will be present, and features similar to sweeps and ejections might exist even in the absence of a viscous sublayer. It is not clear that the mechanism responsible for the intermittency will be the same. The events will be scaled differently from those occurring in sublayer bursting, but their dynamics might be similar.

Both Gordon (1974, 1975a) and Heathershaw (1974, 1976) have observed the phenomena of ejections and sweeps in natural flows, and the correspondence between adverse pressure gradient and increased intermittency has been shown to exist in a geophysical flow (Gordon and Witting, 1977). Gordon and Witting (1977) also report that the ejections and sweeps observed in the Choptank River had average durations of 7 seconds and the average period between large momentum transporting events was on the order of 45 seconds. Heathershaw (1976) discusses similar results for the Irish Sea.

Perhaps one of the more important aspects of Gordon's results is the picture it prompted him to paint of the marine boundary layer: "The overall turbulent motions...may be treated as

a dual population, consisting of large scale, dynamically active, coherent structures superimposed on a passive background of relatively small scale isotropic turbulence that contributes little or nothing to the vertical transport of momentum." Gordon and Witting, (1977).

This sounds like a good model, but it also points out that perhaps the dual population is precipitated by some characteristic topography in the estuary rather than being a general feature of turbulence in high Reynolds number channel flow.

1.3 Previous Instrumentation

The motivation for developing the new instrumentation described in this thesis stems from inadequacies of currently available instrumentation in providing data which meets the specifications for detailed investigations of turbulent boundary layers.

In considering the discussion on length scales at the beginning of this chapter, one of these specifications is to resolve the smallest length scale of dynamical importance to the flow. In the case of shallow marine boundary layers, this length can be estimated to be on the order of tens of centimeters. (It should be emphasized here that this scale does not include wave boundary layers where the boundary layer itself is only of the order 5 to 10 centimeters.) To calculate the complete Reynolds stress tensor, an instrument must be able to measure the three components of the velocity vector, and permit the separation of the fluctuating components from the mean flow. Besides sampling the flow in time, it is important to sample

it in space as well; this allows variation of the velocity structure with distance from the boundary to be seen. A minimal requirement here is three or more sensors at various levels above the bottom. If measurements are to be made routinely, then the instrument must be able to operate by itself and record data internally in order to minimize the complexities and expense of surface ship support.

The requirements mentioned above are basic demands to be placed on instrumentation used for boundary layer studies in the sea. They are included as part of this section on previous instrumentation to point out the motivation for the instrumentation system described in the next chapter which also includes a detailed discussion of sensor requirements.

What follows is a compilation of the instrumentation schemes which have been employed to study marine boundary layer dynamics. Rather than listing in the text every experimenter who has lowered a current meter close to the bottom, Table 1.2 has been constructed to give a chronology of boundary layer research in the sea. The text highlights the major advances in the field. At the same time some of the shortcomings inherent in the particular instruments are pointed out. These shortcomings provided valuable insights that were used in the development of the instrumentation described in this thesis.

Revelle and Fleming (Sverdrup, et.al., 1942) used three Nansen Pendulum current meters mounted on a tripod to obtain near bottom current profiles in the lower 2 m of the boundary layer in order to extend logarithmic profile observations into the sea. A more ambitious

TABLE 1.2

Summary of Marine Boundary Layer Studies

Legend

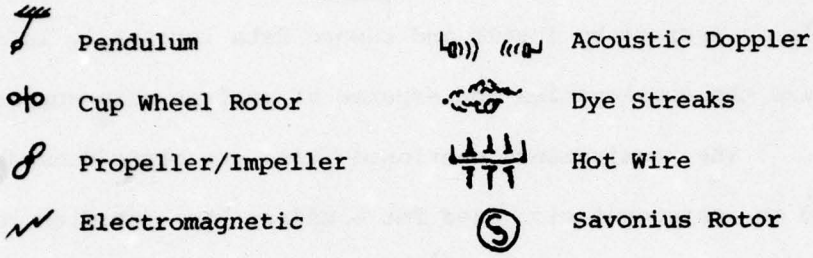

Investigator	Sensor	Depth (m)	Location
Revelle and Fleming (1942)		10	San Diego Harbor
Mosby (1946, 1949)		16	off Bergen, Norway
Lesser (1951)		50	N.A.
Bowden and Fairbairn (1952)		4	Mersey River, Gr. Br.
Francis, Stommel, Farmer, and Parsen (1953)		20	Kennebec River, Maine
Bowden and Fairbairn (1956)		20	Red Wharf Bay, Anglesey
Bowden, Fairbairn, and Hughes (1959)		20	Red Wharf Bay, Anglesey
Bowden (1962)		20	Red Wharf Bay, Anglesey
Bowden and Howe (1963)		4	Mersey River, Gr. Br.
Charnock (1959)		20	Red Wharf Bay, Anglesey
Knauss (1965)		6000	Western Atlantic
Issacs, Reid, Schick, and Schwartzlose (1966)		4000	Pacific off Baja, Calif.
Sternberg (1969)		4000	Pacific off S. Calif.
Dyer (1970)		16	West Solent Channel

TABLE 1.2 (cont.)

Investigator	Sensor	Depth (m)	Location
Korgen, Bovarsson, and Kulm (1970)		3000	Pacific off Oregon
Wimbush and Munk (1971)		4000	Pacific off S. Calif.
Seitz (1971)	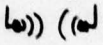	12	Patuxent River, Md.
Channon and Hamilton (1971)		100	off S.W. England
Weatherly (1972)		800	Straits of Florida
Hartlett and Kulm (1972)		3000	Cascadia Channel
McCave (1973)		20	North Sea
Thorpe, Collins, and Gaunt (1973)		1000	Gulf of Cadiz
Gordon and Dohne (1973)		7	Choptank River, Md.
Gordon (1974, 1975)		7	Choptank River, Md.
Gordon and Witting (1977)		7	Choptank River, Md.
Heathershaw (1974, 1976)		60	Irish Sea
Vincent and Harvey (1976)		35	North Sea
Sternberg (1976)		40	Gulf of Mexico
Everdale (1976)		50	E. Long Island Sound
Bohlen (1977)		50	E. Long Island Sound
Butman (1977)		60	George's Bank

task was taken by Mosby (1946, 1949) who lowered a 3 meter tall mast to the sea floor (16 m depth). To the mast were affixed twelve cup-wheel anemometers which, when rotated by the flow, would close a switch thus lighting one of twelve lightbulbs in the main lab of the M.S. ARMAUER HANSEN. A watchstander (or perhaps one of twelve watch-standers) would log the time of flash to the nearest second. From calibration data revolutions per minute could be converted to flow speed. Velocities down to 4 cm per sec could be measured in this way and Figure 1.2 in section 1.2 is a sample of Mosby's results. This incredible procedure produced many time series, some being as long as six hours.

Since 1946 there have been a host of researchers who have used mechanical sensors to investigate horizontal bottom current speeds. Interestingly, the first attempt at measuring the vertical fluctuations of bottom currents was made by scientists from Woods Hole (Francis, et al., 1953). Using a pivoted von Arx propeller meter, the magnitude and the inclination of the flow to the vertical was recorded. The current meter was lowered on a flexible cable for profiling experiments and also mounted on a tripod resting on the bottom to obtain time series at a fixed depth ($\sim$ 20 m). The importance of this work is that is points out the difficulties of making Reynolds stress measurements with mechanical sensors which cannot respond quickly enough to three dimensional velocity fluctuations in the flow.

Bowden offered a solution to this problem by using a tri-pod equipped with two electromagnetic current sensors (Bowden and

Fairbairn, 1956). This was the first detailed observation of both horizontal and vertical velocity fluctuations. These were crude measurements in light of the instrumentation to be described in this thesis, but the calculations of Reynolds stresses and correlation functions which resulted were seen as a major advance in benthic boundary layer investigations. Bowden and Fairbairn's instrumentation suffered from zero drift problems which are critical when making fluctuation measurements. The zero drift had to be balanced electronically on board the attending ship which was tethered to the instrument by electrical cables. Their records were only five to ten minutes long and showed large variations from one record to another which required considerable averaging in their analyses. Measurements could only be made of two components of velocity at a single level above the sea bed at a given time and no measurements were made of the amplitude or direction of the mean velocity.

Measurements of near bottom velocities proceeded from the near shore work of Bowden out onto the continental shelf (Sternberg, (1966); Dyer (1970) and others) and then into the deep ocean (Wimbush and Munk (1971); Weatherly (1972); and others). Fluctuations in the vertical component of velocity have yet to be measured in the deep ocean.

Heathershaw (1974), using an electromagnetic current sensor, and Gordon (1974) using a gimballed propeller current meter both reported observations of high stress events in marine boundary layers. Their remarks on the intermittency of the vertical transport of

momentum made it clear that new sensors were required which had faster response times and less flow interference than the sensors which they had used. A strong case was also made for careful time series analyses on velocity fluctuation data so as to more accurately describe the important length and time scales in the flow. The major purpose of the research described in this dissertation is to remedy this observational deficiency.

As an historical aside to this thesis, Wiseman's 1969 doctoral dissertation describes a three axis acoustic Doppler shift current sensor for estuarine turbulence studies in the Chesapeake Bay. It was cabled-lowered, shallow water device which produced analog tape records of the three velocity components. Data was obtained in the Patuxent River and, despite problems with data dropout, inroads were made into the structure of high frequency turbulence in a tidal estuary.

The next chapter describes a new velocity sensor designed to reliably measure three dimensional velocity fluctuations at any depth in the ocean.

Chapter 3 details a field experiment using the instrumentation, and Chapter 4 presents the results of the measurements.

1.4 Summary of Objectives

Marine scientists investigating near bottom flows need data, unattainable with existing instrumentation, to understand and then parameterize boundary layers in the sea. To this end the aims

of this research can be summarized as:

- to design, construct, and develop a system for measuring the mean and fluctuating components of the velocity vector at four levels above the sea bed.

- to demonstrate the capability of the instrument as a tool for a contribution to the understanding of boundary layer flows which could not be made with presently available instrumentation.

- to compute Reynolds stresses and observe their variation with such factors as mean velocity profile, state of the tide and distance from the bottom.

- to see how the intensity of the turbulent fluctuations varies with the tide.

- to demonstrate how this particular instrument system can be used to infer from velocity measurements the dominant length and time scales in a marine boundary layer, and to observe intermittency in this type of flow.

CHAPTER 2

INSTRUMENTATION

The Development of the Benthic Acoustic Stress Sensor (BASS)

From the discussion in the previous chapter, it is seen that the historical data set is highly skewed towards laboratory observations. The scant number of field experiments has employed instrumentation which was not capable of directly measuring the three velocity components simultaneously at various points in the flow. The size and operational characteristics of the sensors prohibited the measurement of length scales of velocity important to the internal structure of the flow. This structure is the prime agent responsible for the transport of mass, momentum, and chemical species at the sediment-water interface. The crucial measurement to be made is seen by ocean scientists to be a time series of three component velocity measurements at varying distances from the bottom. Seeing this need, a new instrument was designed and built which would hopefully remedy the observational deficiencies in the understanding of the structure of marine boundary layers. This chapter describes the development and capabilities of this new instrument.

2.1.1 Sensor Requirements

In view of the objectives set forth previously, a sensor capable of accurately measuring the three dimensional velocity vector in the ocean was required. This sensor had to be small enough to

sample the scales of turbulence responsible for the Reynolds stresses, and it had to sample often enough so that aliasing of the high frequency components was avoided. The instrument had to provide a time series of suitable length so that intermittent processes such as bursting could be observed and related to continuously varying flow conditions. Long time series were desired not only to satisfy statistical requirements, but also to see how low frequency driving forces might affect the boundary layer flow structure.

Since the fluctuations of velocity in the flow are many times smaller than the mean velocity, the sensor had to be linear and exhibit a high degree of sensitivity. Linearity was required by the nature and number of Reynolds stress computations. For low velocity flows the sensitivity of the sensor had to be high in order to discern turbulent momentum transfer; an approximate limit of sensitivity being 1% of the mean flow. To achieve meaningful values of turbulent stress at low flow speeds, the measurement of small vertical fluctuations had to be made; failure in this regard would have underestimated the stress considerably (Williams and Tochko, 1977).

2.1.2 The Choice of the Acoustic Travel Time Sensor

Many of the boundary layer experiments cataloged in Table 1.2 used mechanical sensors. These sensors beside physically interfering with the flow are non-linear at low flow speeds and cannot respond to small fluctuations which makes them unsuitable for Reynolds stress

measurements. Pulsed dye systems although rendering useful qualitative results require elaborate data reduction schemes. Hot wire and hot film probes are inadequate for oceanic conditions because of deterioration of the sensors and poor directional sensitivity (Frey and McNally, 1973).

Considering the objectives of this research, there are two general types of sensors which possess the qualities needed for a good Reynolds stress sensor. These are the scattering sensors and the volume averaging sensors. Laser Doppler and acoustic Doppler velocimeters are of the former type while electromagnetic and acoustic travel time are of the latter (Williams and Tochko, 1977).

Scattering sensors receive velocity information by measuring the frequency shift of reflected energy from particles moving with the fluid. This type of sensor has an accurate zero point making flume calibration unnecessary and senses the velocity in a small volume removed from the flow disturbance of the sensor itself. The major drawback in using scattering sensors is the problem of data dropout when there is a paucity of suspended particles in the flow. This requires added sophistication in the data processing software (Wiseman, 1968). Because of the small scattering volumes involved, the data acquisition rate must be high in order to avoid aliasing high frequencies and, therefore, either a large capacity data storage system or <u>in situ</u> processing is required. Despite these limitations, scattering velocimeters are the only means of measuring the smallest scales of turbulence in the ocean, as in experiments

dealing with the viscous sublayer or the fine scale of turbulent dissipation.

Volume averaging sensors integrate the velocity over a length scale comparable to the characteristic dimension of the sensor itself. This dimension should correspond to the smallest scale of interest in the flow.

In electromagnetic sensors the averaging volume is related to the configuration of the electromagnetic field, and roughly this is of the order of the diameter of the field coil. Ideally the field is solenoidal and well-defined; in practice, however, this is not the case and flow from regions outside the solenoidal field contribute to the measurement in a manner which is usually unknown. An ill-defined averaging volume is the chief disadvantage to electromagnetic sensors. Ducting the flow, while reducing this problem, is a concession to greatly reduced directional sensitivity. However, some of the best work on turbulence in marine boundary layers (see Table 1.2) has been done using two axis electromagnetic current meters.

Acoustic travel time sensors average velocities over the volume defined by the acoustic axes of the sensor. This volume is undisturbed except near the transducers in general, so that an accurate velocity estimate can be obtained. However, if the velocity is in line with an acoustic axis, the wake of the upstream transducer will cause a velocity defect in the averaging volume. Thus measurements of the flow near the direction of the acoustic axes must be avoided.

Unknown flow interference in the acoustic travel time sensor and unknown electromagnetic field configuration in the electromagnetic current meter, coupled with zero point offsets in both sensors demand flume calibration of these volume averaging devices. Even so, the two techniques of volume averaging have gone through several iterations of design, and sensors using these methods have proved themselves rugged and reliable in the marine environment.

With these considerations in mind and having had the experience of constructing a successful two axis acoustic travel time sensor for oceanic velocity microstructure research, it was decided to utilize these techniques for the study of the structure of bottom boundary layer flows. The remainder of this chapter deals with the design construction, operation and performance of such a device.

2.2.1 The Acoustic Travel Time Sensor - Basic Technique

In order to use acoustics in measurement systems, transducers are required to ensonify the medium and to detect sound waves in the medium. Acoustic travel time sensors use piezo-electric ceramics for this purpose. Piezo-ceramics are materials which convert electrical energy into mechanical energy and vice versa. When a voltage is applied to a piezo-electric crystal, it changes shape slightly and a compression wave propagates from it. Likewise, when acoustic energy impinges on the element, the material is strained and responds by producing a voltage.

This piezo-electric effect is exploited in the acoustic travel time technique as illustrated in Figure 2.1. Each transducer plays the dual role of transmitter and receiver. To transmit, the two transducers are simultaneously pulsed with equal voltages. The component of fluid velocity lying along the path between the transducers increases the speed of the acoustic pulse travelling in the direction of the flow and decreases the speed of the pulse travelling against the flow. Since each pulse traverses the same distance, d, but at different speeds, there will be a difference in the time of their arrivals at the opposing transducer. Formally, the arrival times are given by

$$t_{A\to B} = \frac{d}{c-v} \qquad t_{B\to A} = \frac{d}{c+v}$$

where c is the speed of sound in seawater (~1500 m/s). Subtracting the two, the time difference $\Delta t = t_{A\to B} - t_{B\to A}$ is obtained:

$$\Delta t = d\left[\frac{c+v-(c-v)}{(c-v)(c+v)}\right] = \frac{2dv}{c^2-v^2}$$

Oceanic currents are always much less than 150 m/s, hence v^2 is negligible compared to c^2 and $\Delta t \approx 2dv/c^2$. By measuring Δt and knowing c and d, the velocity component along the acoustic axis can be determined. The velocity found in this way is the integrated velocity along the path of length, d, and this means that the transducer separation determines the smallest scale of motion which can be monitored.

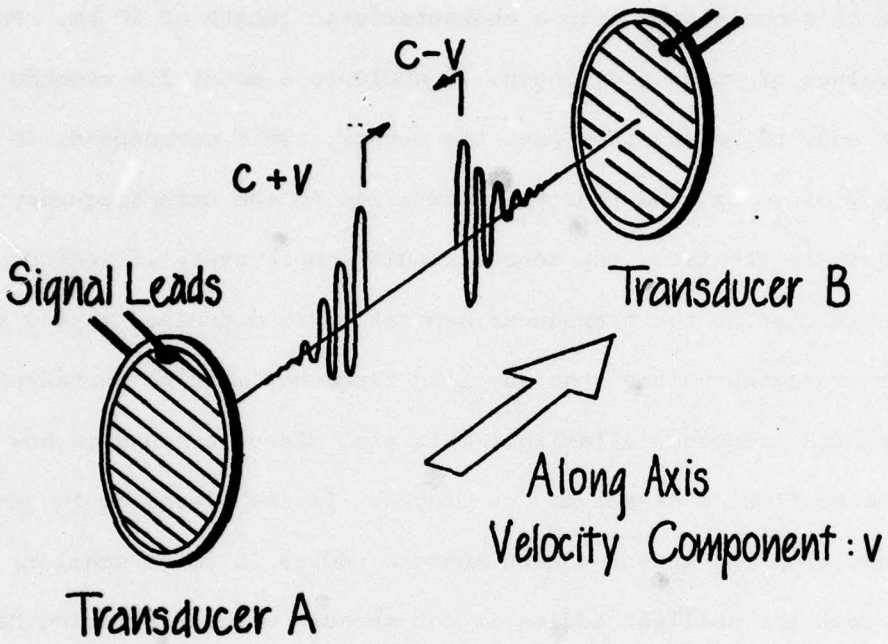

Sketch showing basic principle of the acoustic travel time technique. The transducers are separated by a distance "d". The shaded region on the transducer discs represents silver electrode material plated on the transducer faces.

Figure 2.1

Theory suggests that the scale of the most energetic eddies at a given height above the bottom in a turbulent boundary layer is of the order of that height. In a current of 30 cm/s, a sensor with transducer spacing of 15 cm located at 50 cm above the seafloor should be able to sense eddies with a characteristic length of 50 cm. For these values of speed and length, it would take about 1.6 seconds for a 50 cm eddy to be advected past the sensor. This corresponds to a frequency of .6 Hz, and thus to avoid aliasing the high frequency components in the flow, the sensor should sample every .8 seconds. This shows that as the transducer separation is decreased making a smaller averaging volume, the sampling frequency must be increased to curb high frequency aliasing. This also places a bound on how near the seafloor a sensor may be placed. If the averaging length is 15 cm, then the sensor cannot measure eddies 15 cm or smaller; and in fact the smallest eddies it can measure without aliasing have a characteristic dimension of 30 cm. A sensor with 15 cm transducer spacing should not be placed closer to the bottom than 30 cm assuming once again that the energetic eddies at a given distance above the bottom are the same size as that distance.

2.2.2 The Acoustic Travel Time Sensor - Mechanical Design

Two constraints which were placed on the instrumentation described in this thesis were deep ocean (5000 m) measurement capability and minimization of sensor-induced flow disturbances. Careful attention was paid to a streamlined physical arrangement and

a rugged mounting scheme so that the fragile piezo-ceramic transducers could sample undisturbed flows in the deep ocean.

The general principle of operation shows that each pair of transducers determines the projection of the velocity vector along the line between them. From two sets of transducers lying in the horizontal plane, the horizontal components of velocity can be resolved. The addition of a third pair of transducers not in the same plane allows the determination of the vertical component.

The sensors developed for this study of boundary layer processes have four acoustic axes arranged on two parallel rings as shown in Figure 2.2. The rings are separated by 15 cm and each acoustic axis has one transducer on each ring. The transducer spacing is 15 cm and the acoustic paths intersect the horizontal plane at approximately 45 degrees. Although only three axes are needed to determine the three velocity components, the redundant axis acts not only as a spare, but also as part of the design to minimize the effects of sensor induced wakes. When the flow is aligned with one acoustic path, the velocity measurements derived from that path are contaminated by the flow disturbance of the upstream transducer, thus by having a redundant axis, the measurement from the disturbed path can be rejected in the data processing and there are still enough measurements to compute the three velocity components.

From observations made during tow tank calibrations, it was noted that deviations from the ideal cosine response occurred only when the flow direction was within 20 degrees of being coincident

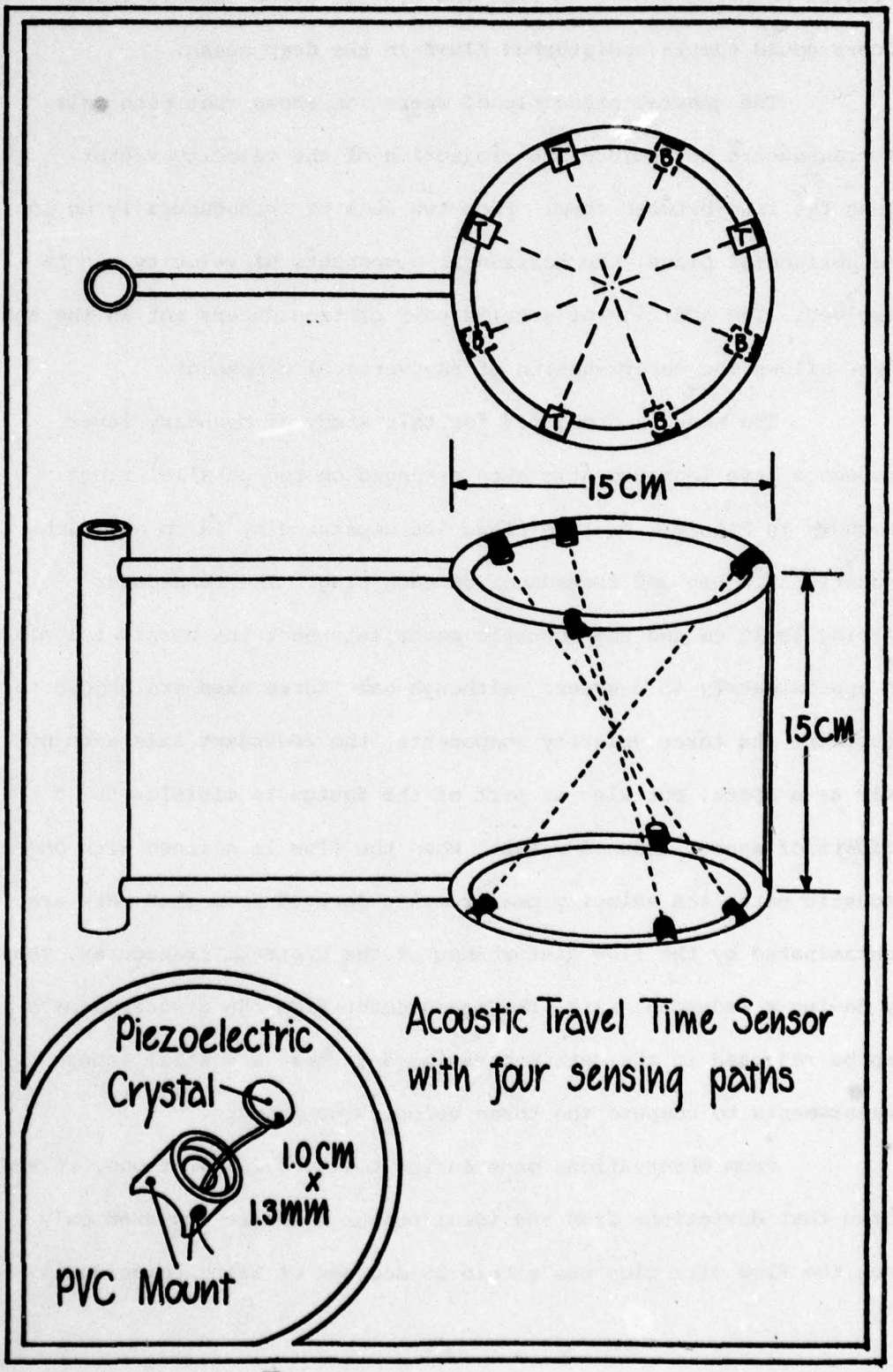
T
B
15 CM
15 CM
Piezoelectric
Crystal
1.0 cm
x
1.3 mm
PVC Mount
Acoustic Travel Time Sensor
with four sensing paths

Figure 2.2

with the measurement axis. Since bottom flows rarely make an angle of 45 degrees to the horizontal, the physical arrangement as illustrated in Figure 2.2 seems to minimize sensor wake effects which can be almost completely eliminated with the redundant axis.

Experience in constructing a two-axis velocimeter modelled after a design by Gytre (1975) for a free falling instrument showed that for deep ocean deployments the piezo-electric transducers should be pressure compensated. The air-backed transducer in the two axis version worked well to 2000 m depth but the air-backed design could not be modified for great depths without a substantial increase in size and fabrication complexity which would increase wake effects and construction costs. The inset in Figure 2.2 shows the details of the epoxy encapsulated transducer mount which was designed to be depth independent and to maximize the acoustic energy entering the water. Prototype mounts were pressure tested in fresh water to 6500 psi and cycled ten times from 0 to 6500 psi over a 48 hour period with no change in the travel time difference between the two transducers even though the one-way travel times did reflect the change of sound speed with increased pressure.

Four sensors as depicted in Figure 2.2 were built and mounted on a vertical staff which in turn was attached to a tripod. The sensors were mounted so that they would be logarithmically spaced at distances of 26, 46, 96, and 210 centimeters above the seafloor. Figure 2.3 shows the tripod. Since the instrument system acoustically senses turbulent stresses in the ocean, it was named the Benthic

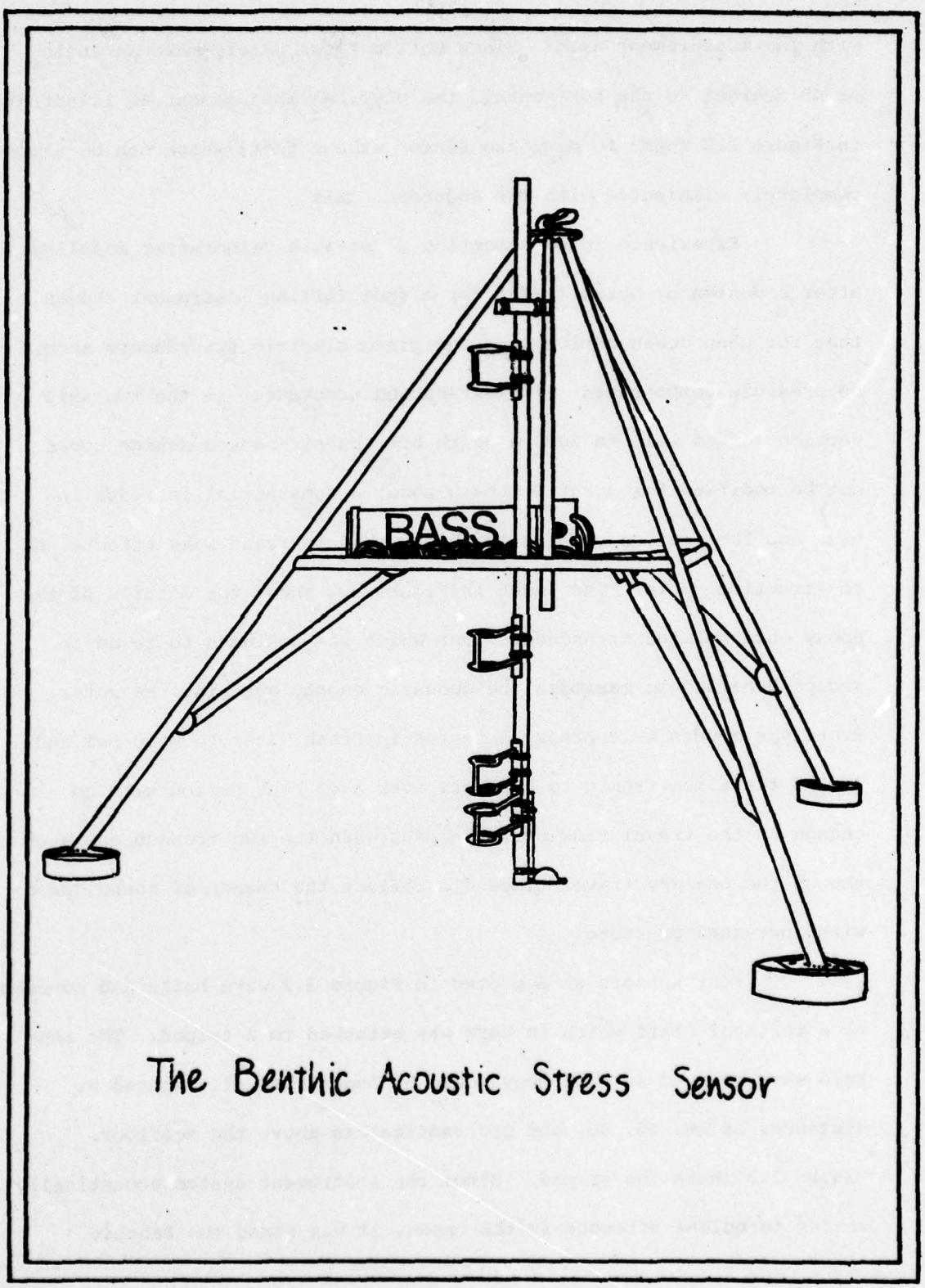

The Benthic Acoustic Stress Sensor

Figure 2.3

Acoustic Stress Sensor (BASS). The instrument as illustrated is a shallow water prototype of the deep ocean version. All the components of the prototype have been designed and tested for use in the deep sea, and the only things lacking for deep water deployment are the anchor release, flotation, radio beacon, and flashing light for recovery.

2.3 BASS Electronics

The systems engineer designing autonomous oceanographic measurement systems is inevitably faced with trade-offs in regard to power consumption, accuracy, speed of performing logical and arithmetic operations, and sensitivity to temperature. Fortunately the state of the art in electronic technology allows a choice among devices which satisfy these varying needs.

In BASS there is a hybrid system of electronics in which some sections of hardware deal with analog signals, and other portions employ different types of digital signals.

Digital signals, derived from low power circuits, are employed for the timing, logic, and recording phases of the measurement. Fast digital electronics are used in BASS where high speed comparisons are made, for example, in looking at the arrival times of leading edges of acoustic pulses. Analog circuits amplify the difference in voltage generated by integrators controlled by the fast logic.

Two classes of integrated logic circuits are used in BASS, namely CMOS and TTL. The former is short for Complimentary Metal Oxide Silicon, while the latter initials stand for Transistor-Transistor Logic. CMOS is a family of integrated circuits noted for their simplicity, noise immunity, and low power consumption which accounts for their use in mass market consumer electronics, as in some pocket calculators and digital watches. In BASS, CMOS circuits are employed as power saving devices where high speed of operation is not required. CMOS logic operates best at supply voltage levels of 12 volts whereas TTL requires a 5 volt level. TTL devices have the property of very fast response times at the expense of increased power drain. Because of their high speed, TTL has found wide use in digital computer systems. The minute travel time differences (4.8×10^{-11} seconds per least bit) that must be measured accurately by BASS necessitate the use of TTL logic at the expense of greater power loss.

Armed with this brief background into the design philosophy and jargon of the electronics section of BASS, hopefully one will be able to follow the way acoustic travel time flow velocity measurements are made.

2.3.1 Transmitter Circuitry

The first step in making a velocity measurement with the acoustic travel time technique is to simultaneously produce two acoustic pulses travelling in opposite directions along a measurement

path. The acoustic pulses are generated by applying a high voltage transient (500 V) to the piezo-electric transducers.

In the early design (Gytre, 1975) the electrical impulse was delivered by considering the capacitance of the transducer to be part of a tuned circuit driven to resonance. The amplitude of the voltage becomes sufficient for good acoustic transmission during the second quarter cycle after the trigger pulse. The voltage then appears across the transducer faces thus generating the acoustic pulses travelling through the measurement volume.

Dissatisfaction with performance inconsistencies and the time consuming process of matching each transducer pair with the proper inductive and resistive circuit elements for a tuned circuit prompted experimentation with alternative designs. The final transmitter design was simpler, provided a consistently sharp leading edge for the acoustic pulse, and required no component matching. Basically a low voltage (CMOS) triggering pulse trips a solid state switch (in reality a silicon controlled rectifier or SCR) which allows a 500 V voltage residing across a capacitor to be simultaneously applied to the two transducers of a measurement axis. In Appendix B, Figure B.1 is a schematic diagram of the transmitter circuit for the four axis sensor used on BASS. Each pair of transducers has its own transmitting circuit and the sixteen SCRs (four sensors with four axes each) are fired individually and sequentially. In a later section the timing of these events will be discussed.

Because of the high frequencies and voltages used in the transmitting circuitry, judicious design in the layout of the printed circuit boards was required. The tuned circuit design was fraught with group loop problems which hindered performance. Ground loops are unwanted sources of electrical noise owing to currents travelling in ground connections between points at slightly different voltages even though they both supposed at ground potential. On the BASS transmitter circuit boards, these ground loops were engineered out of the design by careful attention to the details of the physical arrangement of the circuit boards.

2.3.2 Receiver Circuitry

The key to the success of this velocity measurement system is the ability to measure the minute time differences in the arrival of the acoustic pulses at opposing transducers. This time difference is on the order of 1.3×10^{-8} seconds (18 nanoseconds) for a 10 cm/sec current and a transducer spacing of 15 cm. The receiver circuitry used on BASS is an improved version of Gytre's design (Gytre, 1975) and rather than discuss the nuances of transistor integrators, the purpose of this section is to explain how nanosecond time differences are measured on BASS.

Figure 2.4 is an illustration showing the transmitted and received signals at one pair of transducers. The received pulses are detected by high speed voltage comparators arranged in what is technically called a Schmitt trigger configuration. When the voltage

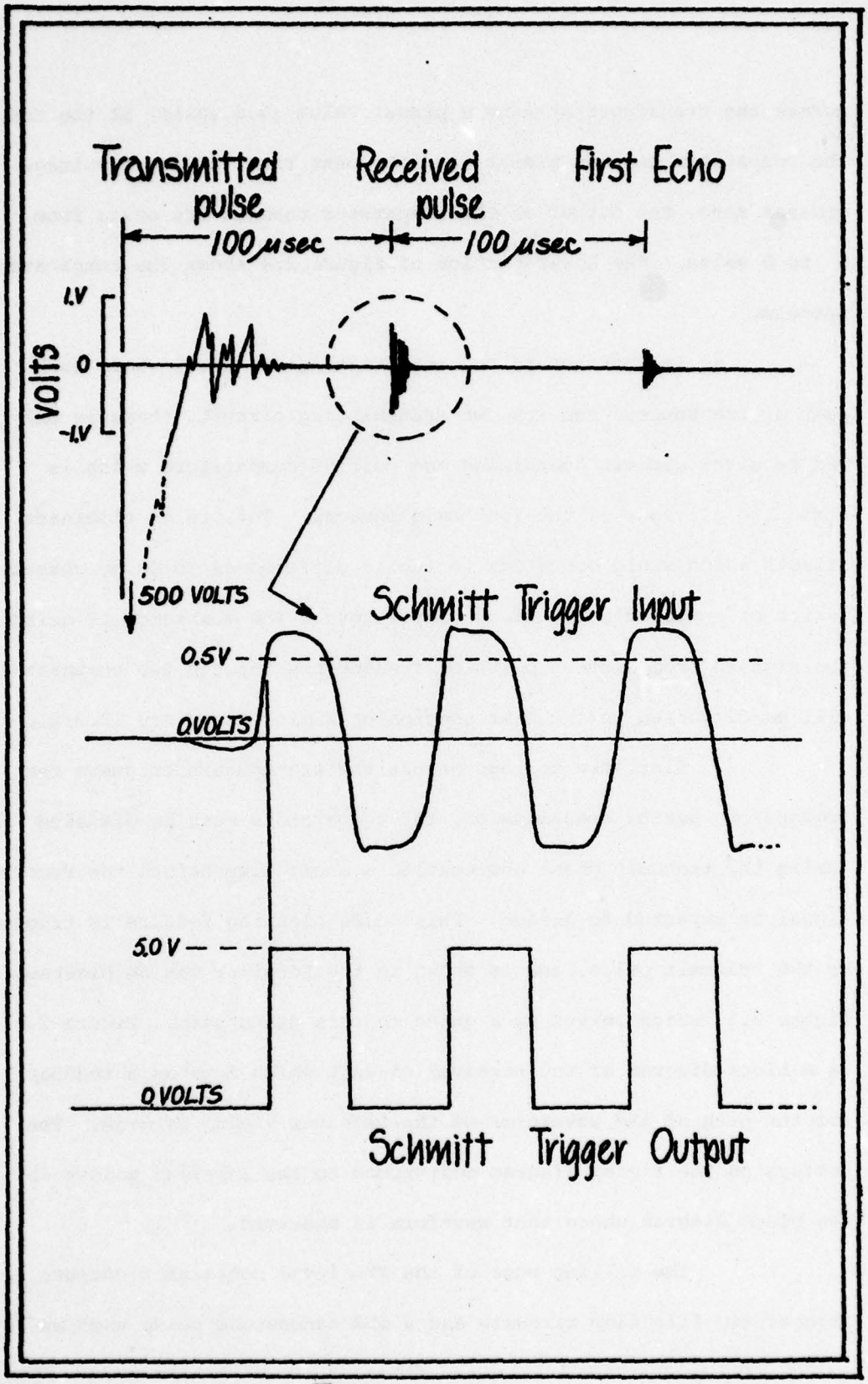
Transmitted pulse
Received pulse
First Echo
100 μsec
100 μsec
1.V
0
-1.V
volts
500 VOLTS
Schmitt Trigger Input
0.5V
0 VOLTS
5.0 V
0 VOLTS
Schmitt Trigger Output

Figure 2.4

across the transducer attains a preset value (0.5 volts) at the input, the comparator becomes preset, and the next time the input voltage crosses zero, the output of the comparator changes its state from 5 to 0 volts. The lower portion of Figure 2.4 shows the comparator outputs.

In contrast to the transmitting circuitry where each pair of transducers has its own transmitting circuit, there is only one receiver circuit containing one pair of comparators which is common to all four of the four axis sensors. This is to eliminate offsets which would occur due to subtle differences in delay characteristics of supposedly identical comparators. The mechanics of switching the signals from sixteen pairs of transducers through two comparators will be discussed in the next section on Timing Circuitry (2.3.3).

Since the voltage across the transducers triggers the comparators during transmission, the comparators must be disabled during the transmit phase and enabled a short time before the received signal is expected to arrive. This pulse blanking feature is triggered by the transmit pulse, and is shown in the Receiver Timing Diagram, Figure 2.5, which serves as a guide to this discussion. Figure 2.6 is a block diagram of the receiver circuit which acts as a roadmap for the path of the waveforms of the Receiver Timing Diagram. The letters on the timing diagram correspond to the labelled points in the block diagram where that waveform is observed.

The falling edge of the TTL level comparator outputs trigger two flip-flop circuits and a 650 nanosecond pulse used as an

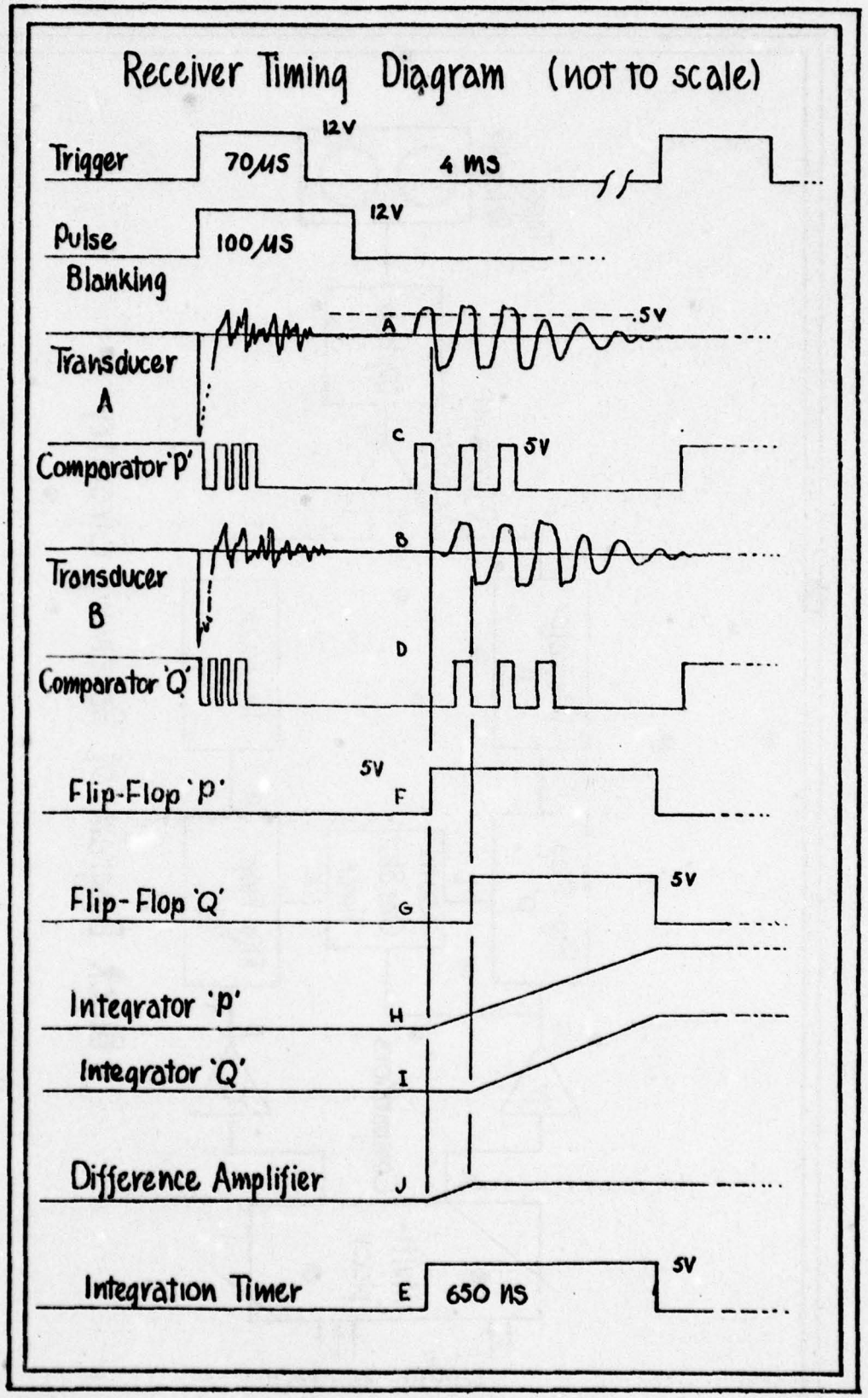
Receiver Timing Diagram (not to scale)
Trigger
12V
70μS
4 MS
Pulse
Blanking
12V
100μS
Transducer
A
A
5V
Comparator 'P'
C
5V
Transducer
B
B
Comparator 'Q'
D
Flip-Flop 'P'
5V
F
Flip-Flop 'Q'
G
5V
Integrator 'P'
H
Integrator 'Q'
I
Difference Amplifier
J
Integration Timer
E
650 NS
5V

Figure 2.5

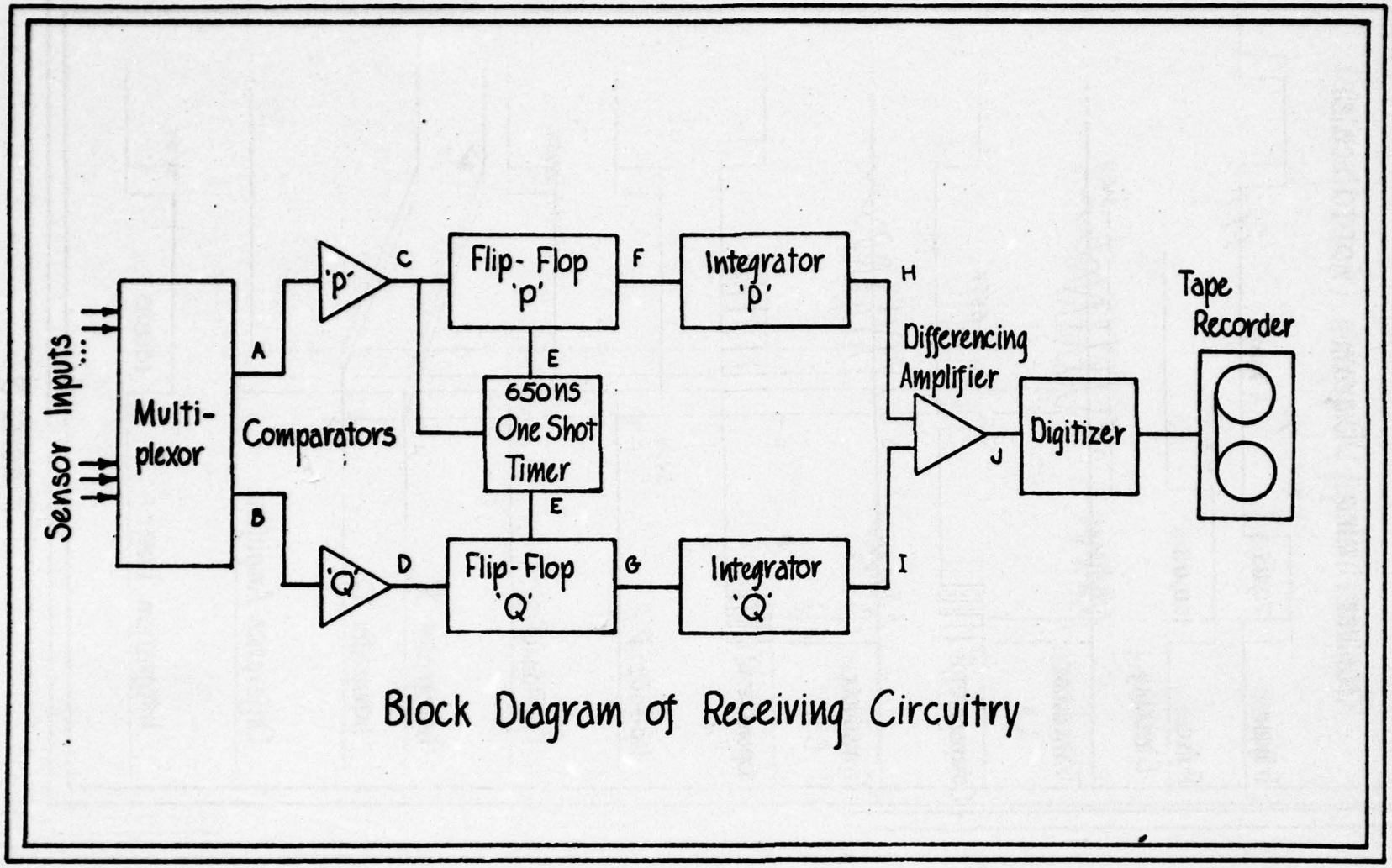

Block Diagram of Receiving Circuitry

Figure 2.6

integration time base. A flip-flop is a device which changes its output state when it experiences a specific transition on its input. In this case when the comparator output goes from 5 volts to 0 volts (a high to low transition), the output of the flip-flop goes high, that is, from 0 to 5 volts. A low to high transition at the input has no effect on the output state of the flip-flop. A glance at the Receiver Timing Diagram will make the operation of the flip-flop clear.

The comparator output which undergoes a transition first, that is, the first pulse arrival to be sensed, also generates the 650 nanosecond pulse mentioned previously. This pulse too is an input to the flip-flops and when it ends both of the flip-flops are reset to their initial state (0 volts) thus ending that phase of the measurement.

The outputs of the flip-flops are fed to an integrating circuit in which transistors integrate the area under the flip-flop output waveform. These integrations appear in time as linearly increasing ramp functions. Since one received pulse arrives earlier than the other, the ramp corresponding to the first acoustic pulse to arrive will be at a higher voltage than the ramp from the other transducer. The integrators are stopped after 650 nanoseconds with the difference in voltage between the ramps being linearly proportional to the travel time difference. This difference is calculated by a differencing amplifier whose output is proportional to the velocity along the transducer axis. This value is digitized in 360 μsec and recorded

on a magnetic cassette tape. During the integration and digitization, a 2 ms pulse blanks out any echoes from the transducers. The receiver circuitry is then reset for the next measurement. The entire process starting with the triggering of the transmitted acoustic pulse and ending with the recording of the digitized data on tape takes 1.5×10^{-2} seconds (15 milliseconds) for one axis. All sixteen axes of the instrument can be serviced in 240 milliseconds. A detailed schematic of the receiver circuit is found in Figure B2 of Appendix B.

Non-linearities in the ramp integrators or differences in ramp shapes can produce zero point errors in the measurement and these were indeed present in the previous design; however, a sensor switching scheme was devised for BASS and this multiplexing circuitry is described in the next section.

2.3.3 Timing and Multiplexing Circuitry

In the previous discussion mention was made of the error introduced by unequal signal propagation delay times through identical solid state devices. Even by carefully matching the two comparators, this error could still be discerned, and therefore, a switching circuit was introduced to eliminate it.

Let A and B be opposed transducers on the same sensor axis, and P and Q be the two comparators in the receiving circuit. In this sensor-transposing scheme two cycles of transmission are required for each velocity measurement from a single axis. The first cycle has transducer A connected to comparator P and transducer B

linked to Q. The transmit command is given and the receiving circuit records the travel time difference as in section 2.3.2. A CMOS multiplexer now interchanges the transducers A and B so that A is associated with comparator Q and B with P. The measurement is again performed and recorded on magnetic tape. In the subsequent data processing, the two values are subtracted from each other thus nulling the errors introduced by delay times in the receiver circuitry and doubling the time difference signal. This assumes that these errors remain constant over the two transmission cycles which lasts about 30 milliseconds. This is reasonable since there is a lack of jitter in the output of the differencing amplifier when the transducers are kept in a quiescent bucket of seawater.

In practice two switching circuits are used employing CMOS multiplexers. One acts as a distributor of triggering pulses so that each pair of transducers is fired at a known point in the time sequence. The other multiplexing circuit prevents acoustic crosstalk in received signals. Crosstalk can arise when signals from transducers which are not members of the currently active pair change the shape of the input waveform at the comparators thus contaminating the measurement. The phenomenon was experienced on an earlier design and so a switching circuit was added to open gates which channel only the received signals of interest into the comparators.

Although complex, this multiplexing scheme has eliminated two possible sources of measurement error and has performed flawlessly

in the field. Detailed schematics of the multiplexing circuits are given in Appendix B (Figures B.4 and B.5).

One travel time difference measurement takes 15 milliseconds and in order to service all sixteen axes, 32 measurements must be made taking a total of 480 milliseconds. To avoid aliasing a sampling rate of 1.33 Hz was chosen (the rationale for this has been given in section 2.1.3). This means that BASS makes an entire suite of thirty-two measurements every 750 milliseconds. The actual measuring and recording is done in 480 milliseconds and the electronics are passive during the remaining 270 milliseconds.

2.4 Data Processing

BASS uses a Sea Data digital cassette recorder to store the travel time difference measurements on magnetic tape. The least significant bit (LSB) recorded corresponds to a velocity of 0.328 mm/sec, and a round of 32 measurements every 750 milliseconds allows slightly more than six hours of continuous recording.

Once the instrument is recovered the magnetic tape is read by a Hewlett Packard 2100 computer using a standard cassette reading program called CARP, developed at Woods Hole for processing Sea-Data cassette tapes. The twelve bit velocity words must then be unpacked and expanded into sixteen bit words to be compatible with the HP-2100 system for processing.

Being a new instrument system, computer programs were needed for diagnostics, calculations and graphic displays. A family

of more than ten software routines was designed for these purposes. The steps in the processing were as follows:

Samples of the raw data were plotted to check that all axes were operational and that the instrument was working properly. After this check, the data was subjected to a wild point editing program. Wild points are attributed to data drop out due to spurious signals in the electronics and solid objects such as seaweed and even fish entering the measuring volume. Fortunately, wild points were usually singular and the worst axis had 400 bad points out of the more than 32,000 recorded on the six hour tape.

The u, v, and w components of the velocity vector were calculated using three sensing paths with an adjustment being made for the zero offset in the electronics which will be discussed in the next section. The data presently in this work were taken in a strong tidal flow, and except for the twenty minutes when the tide was changing, the mean current was from either of two directions differing from each other by 180°. Wake effects were held to a minimum because the sensors were repositioned by divers once BASS was on the bottom. This is reflected in the fact that it did not matter which of the three sensing paths were used for the velocity vector computations. Plots of velocity using two different sets of axes were virtually indistinguishable; therefore, the same three axes were chosen on all four sensor pods for the calculations presented here. The redundant axis did have its use as will be seen later.

A sixth order polynomial fit was applied to the 6 hour u-velocity component to obtain the mean flow speed in the x-direction. The x-direction (longshore) was coincident with the mean flow direction for the entire experiment except during slack water. The cross stream (v) and vertical (w) velocities had means which were zero.

The polynomial fit allowed the u-velocity fluctuations to be computed by subtraction, and the data set was reduced to a time series of u, v, and w velocity fluctuations from which root mean squared values of the fluctuations and Reynolds stresses were calculated.

Further processing was performed on the data set using the HP-2100 Fast Fourier Transform system. Autocorrelations and cross-correlations were computed along with Power Density Spectra for the turbulent fluctuations and Co-Spectra for the Reynolds stresses.

Besides these calculations, many plots were produced which gave valuable insights into the selection of averaging times and the scales of intermittency in the boundary layer.

In summary the BASS software system and the basic data set of three components of velocity fluctuations plus the mean horizontal velocity at four points above the bottom allowed computation of mean velocity profiles, Reynolds stress levels, turbulent velocity intensities, velocity correlations, and frequency spectra. Figure 2.7 presents a block diagram which schematically reveals the processing path of the data.

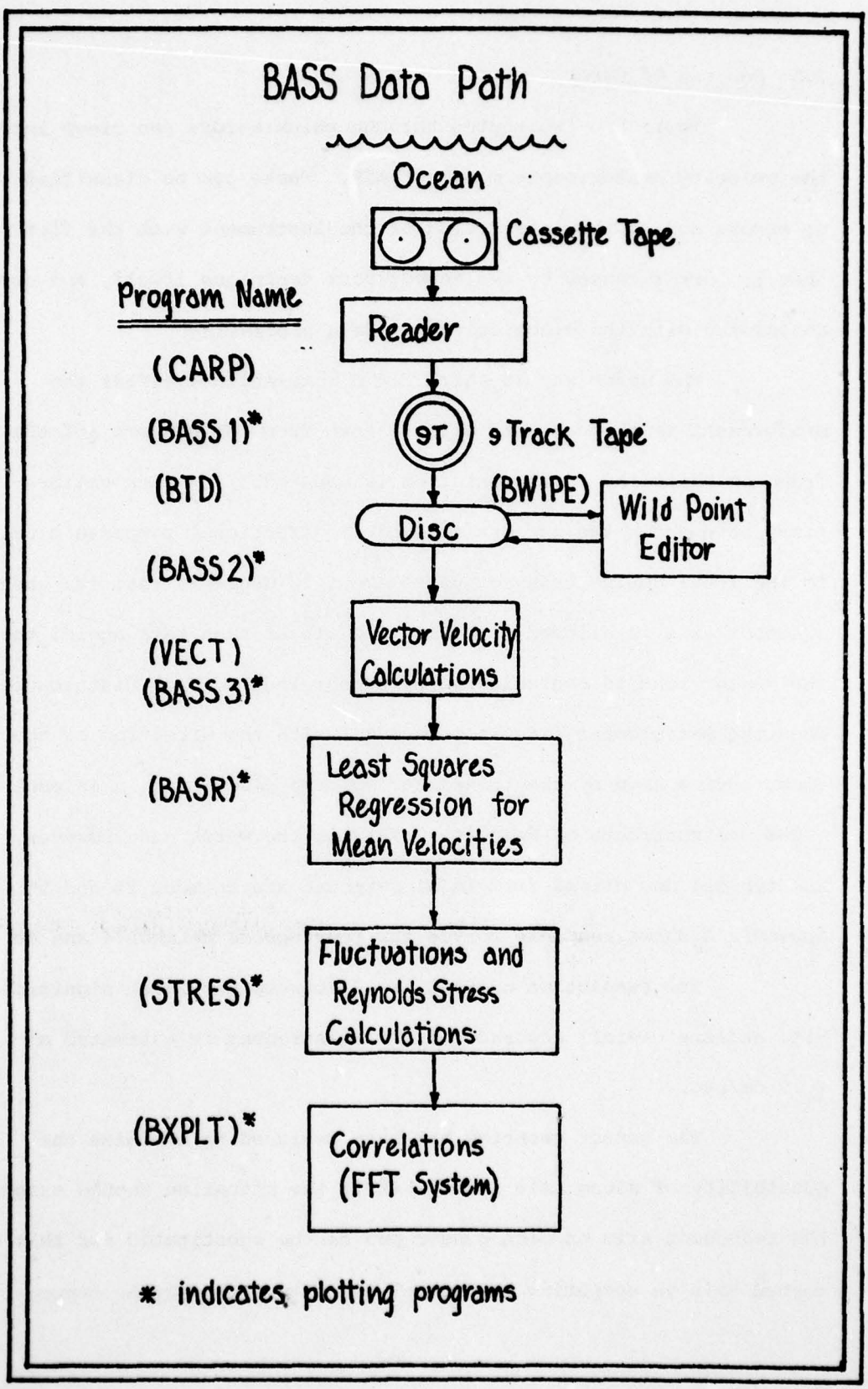
BASS Data Path
Ocean
Cassette Tape
Program Name
Reader
(CARP)
(BASS 1)*
9T
9 Track Tape
(BTD)
(BWIPE)
Wild Point Editor
Disc
(BASS 2)*
(VECT)
(BASS 3)*
Vector Velocity Calculations
(BASR)*
Least Squares Regression for Mean Velocities
(STRES)*
Fluctuations and Reynolds Stress Calculations
(BXPLT)*
Correlations (FFT System)
* indicates plotting programs

Figure 2.7

2.5 Sources of Error

There are two routes through which errors can creep into the velocity measurements made by BASS. These can be classified as errors due to the interaction of the instrument with the fluid, that is, error caused by the measurement technique itself, and errors associated with the electronics and data processing.

The major way in which fluid interactions effect the measurement is through wake effects both from the sensors and the frame on which the instrumentation is mounted. Tow tank calibrations have shown the sensors to exhibit directional response close to the ideal cosine behavior up to about 20 degrees, that is, when a sensor axis is aligned with the flow closer than this angle, then the measurement is contaminated by sensor-induced flow disturbance. When the measurement axis is coincident with the direction of the flow, eddies shed by the transducer holders can result in as much as a 20% underestimate of velocity. This is the worst case however, and typical deviations from ideal response are between 2% and 5%. Appendix A shows response curves for four speeds between 4 and 40 cm/sec.

The resolution of BASS is .33 mm/sec per least significant bit, and the overall accuracy of the measurement is estimated at $\pm$ .5 cm/sec.

The sensor geometry has been designed to minimize the possibility of along axis flows, but if the situation should exist, the redundant axis on each sensor pod can be substituted for this disturbed axis in computing the vector velocity. It must be remembered

that any velocity sensor will disturb the flow somewhat; however, the opened and streamlined design of the BASS sensor pods produces far less disturbance than any other sensor currently available for three axis velocity measurements.

The wake of the mounting frame also presents disturbances to the flow being measured; however, the sensors have been mounted in such a way as to reduce this effect. Fortunately in the experiment described for this thesis, the frame and sensors were aligned in the flow by divers who tried to keep the sensors out of the wake caused by components of the frame. The data indicates that the sensors were never in the wake of the frame.

Another sort of flow disturbance, and one which is difficult to detect, is the influence of unknown topographic features. Secondary flows or wakes stemming from mounds, hollows, or boulders on the seabed could lead to misinterpretation of velocity scales and directions. The effect of an uncharted depression or bump near BASS could result in the instrument measuring an induced mean vertical velocity, and since continuity demands zero mean velocity in the vertical, this could be mistakenly attributed to instrument tilt rather than to the topography. The only way to be sure is to make a detailed bottom survey of the experimental site, and to observe the levelness of the instrument itself.

Two other sources of error related to the fluid are density fluctuations and refraction of the acoustic pulses due to velocity

shear. Density fluctuations cause changes in the speed of sound and that effect has been treated in the discussion of the basic measuring technique (section 2.1.3). The range of density perturbations encountered in near bottom flows in the sea is so small that this effect is negligible. Acoustic refraction due to velocity shear would cause acoustic pulses to travel along paths which are not necessarily the shortest geometric distance between the transducers. However, as is shown rigorously in Appendix C, the travel time difference is independent of acoustic path and depends solely on the transducer spacing except for pathological velocity distributions.

An important consideration in the analysis of error for Reynolds stress calculations from velocity fluctuation measurements is orientation of the sensors with respect to the flow. If the instrument is tilted in relation to the actual mean flow direction, then when the vector components of the velocity are calculated, a portion of the horizontal velocity fluctuations will appear as vertical signal. This leakage of horizontal velocity into the vertical will give a false contribution to the Reynolds stress.

In the atmospheric surface boundary layer, the work of Deacon (1968) and Pond (1968) suggests estimates of the error in Reynolds stress measurements in the range of 8% - 10% for 1° of tilt. Kraus (1968) indicates that errors as high as 100% can occur with a 1° tilt of the sensor. Kaimal and Haugen (1969) present sonic anemometer data which show that large discrepancies in the momentum flux can be observed between sensors of apparently identical design sampling the

same flow even though other statistical quantities, such as the variance, agree very well. Subsequent testing proved that small alignment errors (less than 2.5°) were responsible for the observed discrepancies, and that excessively large errors in the Reynolds stress determination occurred during periods of low correlation between u and w.

Using the diagram below the effect on Reynolds stress computations of small misalignments of the sensor can be analyzed.

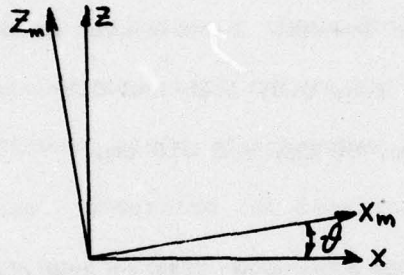

If the sensor is tilted by an angle θ, then the coordinate transforms between the velocity fluctuations measured in the tilted reference frame (subscript m) and the actual velocities are:

$$u_m = u\cos\theta + w\sin\theta$$
$$w_m = w\cos\theta - u\sin\theta \qquad (2.1)$$

Forming the product $u_m w_m$ yields:

$$uw_{mm} = uw\cos^2\theta + \cos\theta\sin\theta[w^2 - u^2] - uw\sin^2\theta$$

Considering small angles, that is, $\cos\theta \approx 1$ and $\sin\theta \approx \theta$, the above expression reduces to

$$\overline{u_m w_m} = \overline{uw} + \theta[\overline{w^2} - \overline{u^2}]$$

where the overbar represents an appropriate time average. For typical values of $\overline{u^2}$, $\overline{w^2}$, and $\overline{uw}$ (13 minute averages) from the BASS data set, equation 2.3 yields errors in the Reynolds stress of 7%, 20%, and 33% for tilts of 1°, 3°, and 5°, respectively.

The absolute error in Reynolds stress due to tilt is thus seen to be a function of $(\overline{w^2} - \overline{u^2})\theta$. The value of $\overline{u^2}$ is larger than $\overline{w^2}$ in this data set so that the Reynolds stress error due to tilt is principally scaled by the turbulent energy. This varies by a factor of 2 1/4 from the uppermost sensor to the lowest. From a tilt error of 3° the Reynolds stress error would be 1.8, 0.8, 1.25 and 0.8 dynes/cm^2 for the sensors at 26 cm, 46 cm, 96 cm, and 210 cm, respectively.

Another way of investigating the effect of tilt on the computation of Reynolds stress is to enter the wrong values of sensor orientation in the angle transformation program. This was done for a piece of the BASS time series during which the mean streamwise velocity at 96 cm over the bottom was 32 cm/sec. Each of the four sensors were given effective tilts of 3°, 5°, and 10°, and the averages of all the per cent errors in the Reynolds stress were 12%, 20%, and 36%, respectively. These values compare well with those obtained from equation 2.3.

Errors in measuring the angles that the individual measurement axes subtend with the horizontal plane also cause errors in the computed velocities and Reynolds stresses. A computer simulation of a measurement error of 1° in elevation angle of an acoustic axis has

shown that a 1% error in the Reynolds stress can result. In the construction of BASS, great care was taken both in aligning the sensing paths and in positioning the sensors on the tripod so that the angles the sensing paths subtended with the horizontal plane were known. These angles were subsequently measured to 1° in elevation and azimuth.

The real problem in Reynolds stress measurements is that the Reynolds stresses have some inherently unpleasant attributes. Although the measured streamwise and vertical velocity components are nearly Gaussian in their distribution and have known statistics, the product uw, which determines the momentum flux, is far from Gaussian (Stewart, 1974; Heathershaw, 1976). Stewart points out that the theory governing the statistics of unusually distributed variables is not well established, and that there is no theoretical basis for determining, for example, the duration of the time series required to yield the value of $\overline{uw}$ within the given limits of a specific situation.

In a recent paper by Heathershaw and Simpson (1978), it is shown that an average sampling variability of ±45% can be expected in Reynolds stress measurements in the range of 1 dyne/cm^2 and down to ±10% in the 8 dyne/cm^2 range. This is due to auto-correlations of the uw product extending over ten or more successive samples. In other words, an increased variability in the measured Reynolds stress can occur due to the fact that each stress realization is not independent. Those working with atmospheric boundary layer data observe that $\overline{uw}$ does not "settle down" rapidly, and it is difficult to obtain a value before the overall mean flow conditions change (Stewart, 1974). The

experimental scatter which this type of effect might produce leads to the questions of choosing the best procedure for subtracting the mean velocity in order to obtain the fluctuating components, and of choosing the appropriate averaging time for the computation of turbulent stresses once the mean has been removed.

As discussed previously in section 2.4 on the data processing for BASS, a least squares sixth order polynomial fit was used to define the mean component of streamwise velocity. This choice was made on the basis of numerous computer experiments using techniques such as fitting lower order polynomials to pieces of the data set and sliding various sized averaging windows through the data. Fitting a polynomial to the entire time series seemed to give the best estimate of the mean, and the only differences which could be discerned among the fifth, sixth and seventh order fits were near the beginning and end of the experiment.

Regardless of the method used to extract the mean, the real question is: how is the error in estimating the mean velocity reflected in the computation of Reynolds stress?

Analytically this can be seen by considering the fluctuating velocity components u and w to be contaminated by the addition of constant mean components u_m and w_m. The expression for the contaminated Reynolds stress is then:

$$\begin{aligned}\overline{(u+u_m)(w+w_m)} &= \overline{uw} + \overline{uw_m} + \overline{u_m w} + \overline{u_m w_m} \\ &= \overline{uw} + \overline{u}w_m + u_m\overline{w} + u_m w_m\end{aligned}$$

Both $\overline{u}$ and $\overline{w}$ are zero by definition, and so the above equation reduces to:

$$\overline{(u+u_m)(w+w_m)} = \overline{uw} + u_m w_m$$

The term $u_m w_m$ reflects the error due to incorrect estimation of the mean velocities. A 1 cm/sec error in the means would cause a 1 dyne/cm^2 offset in Reynolds stress.

Using the diagnostic data processing software written for BASS, experiments were performed to discern this effect. After subtracting the mean, the time series of velocity fluctuations was used to form the uw product which was averaged over 12.8 minutes (1024 points) to give the Reynolds stress. By taking the same fluctuating time series, but artificially adding a 1 cm/sec mean velocity to the u component before averaging, a Reynolds stress was computed which shows the effect of an incorrect estimate of the mean velocity. Results of this exercise for different sensors at various times in the experiment show stress errors in the range 17% - 23% for a 1 cm/sec error in extracting the mean.

Table 2.1 shows how the calculated stresses for profile E varied for the sensors at 26 cm and 96 cm. For the 26 cm level the error is 1.8 dynes/cm^2 per 1 cm/sec added mean velocity while at the 96 cm level it is .9 dynes/cm^2 per 1 cm/sec. This is interpreted to mean that the mean vertical velocities were 1.8 and .9 cm/sec, respectively, during this particular piece of the time series. These results point out how crucial the proper definition of the mean velocity is on the calculation of Reynolds stress.

TABLE 2.1

Height	Added Mean Velocity			
	0 cm/sec	1 cm/sec	2 cm/sec	5 cm/sec
26 cm	-11.38 dynes/cm^2	-9.57	-7.67	-2.10
96 cm	-2.89 dynes/cm^2	-1.91	-0.92	+2.08

With these types of errors in mind, a worst case error analysis for Reynolds stress can be made by assuming a sensor tilt of 3°, a measurement axis misalignment of 3°, and a 20% error in Reynolds stress due to inaccuracies in extracting the mean velocity. If these errors are independent, the effect per cent error is 26%. Applying this to the largest Reynolds stress measured during the experiment (11.48 dynes/cm^2), error bars of ±3 dynes/cm^2 are obtained, and these will be assumed for the results presented in Chapter IV.

Reynolds stresses are by definition time averaged quantities, and the duration of the averaging interval is critical to any conclusions to be drawn from Reynolds stress measurements. In unsteady flows, such as in the tidal channel considered here, the choice of the averaging interval is difficult since a long interval is desirable for stability of the estimate of Reynolds stress, while a short one will produce results which are less affected by changes in the overall flow due to unsteadiness.

Table 2.2 illustrates the effect of averaging length on the calculation of Reynolds stress for a 25.6 minute piece (2048 points) of BASS data taken when the tidal current was at its maximum. The 25.8 minute time series was first broken up into sixteen 96 sec segments (128 points), and the $-\rho uw$ product was averaged for each segment. These results are shown in the second column. The next three columns show the results of dividing the time series into 8, 4, and 2 data segments. The values of the computed mean, variance and standard deviation are listed at the bottom of each column. For the 12.8 minute averages, an adjacent 25.6 minute record was added to calculate the variance. The results from the table show the reduction in the sample variance with longer averaging times. On the basis of a number of similar experiments at different times in the tidal cycle and with each of the four current sensors, it was felt that a 12.8 minute (1024 points) averaging interval provided the best estimate of the Reynolds stress. Over 12.8 minutes the mean conditions were fairly steady, and the value of the Reynolds stress was stable from one 12.8 minute record to the next. Doubling the averaging interval, that is, making it 25.6 minutes did not significantly change the variance, but changes in mean flow conditions were discernible over that time scale.

In shallow water, swell can be important in the analysis of velocity fluctuation measurements. Wave orbital velocities can

AD-A062 842 WOODS HOLE OCEANOGRAPHIC INSTITUTION MASS F/G 8/3
A STUDY OF THE VELOCITY STRUCTURE IN A MARINE BOUNDARY LAYER - --ETC(U)
DEC 78 J S TOCHKO N00014-74-C-0262
UNCLASSIFIED WHOI-78-90 NL

2 OF 3
AD
A062 842

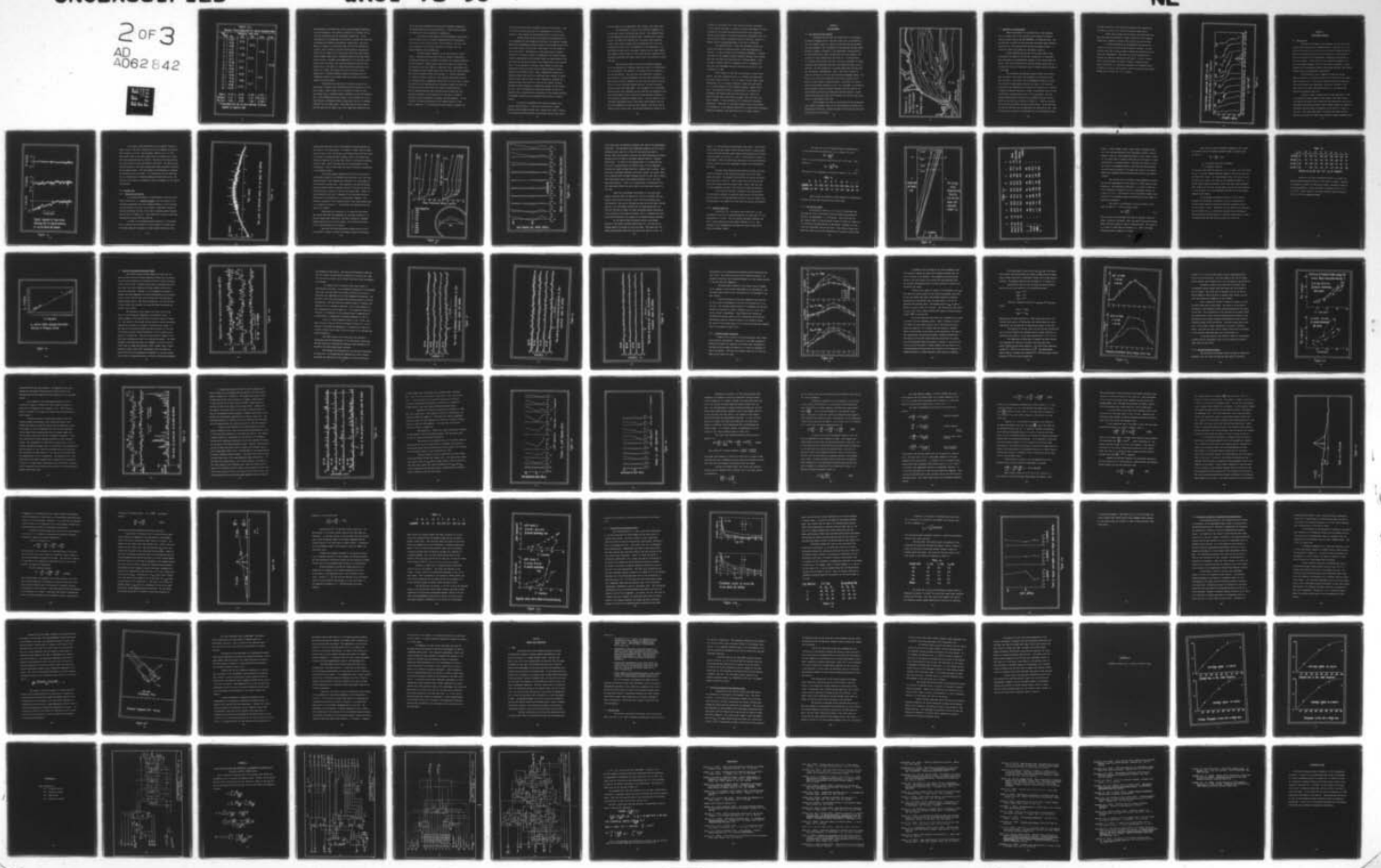

TABLE 2.2

Reynolds Stress (dynes/cm²) for various averaging times

Data Piece	Averaging time (sec) 96	192	384	768	1536
1	11.95	10.73			
2	9.50		9.73		
3	6.28	8.72			
4	11.15			11.45	
5	13.43	11.59			
6	9.74		13.18		
7	19.17	14.77			
8	10.36				12.29
9	15.61	13.01			
10	10.40		14.11		
11	14.91	15.02			
12	15.49			13.14	
13	9.52	8.96			
14	8.40		12.17		
15	16.69	15.37			
16	14.05				
Mean	12.29	12.29	12.29	12.29	
Variance	11.32	6.42	2.67	*(2.57)	
Std. Dev.	3.36	2.53	1.64	(1.60)	

* calculated with the use of an additional 25.8 min. segment of adjacent data.

make substantial contributions to the root-mean-squared amplitudes of the fluctuations. This effect is difficult to evaluate, but no swell was observed during the experiment treated here. As an illustration of the magnitude of this effect, consider two waves with wavelengths of 20 meters and 40 meters, respectively. The water depth is 10 meters so the 20 meter wave will feel the bottom only slightly, and its effect on the near bottom velocity fluctuations should also be slight; the 40 meter wave, being four times longer than the depth, should have a noticeable effect in the near bottom velocity field. Assuming a wave amplitude of 10 cm and using first order linear wave theory, the resulting horizontal velocity fluctuations due to the waves at 2 meters above the bottom are on the order of 1.8 cm/sec and 5 cm/sec for the 20 m and 40 m waves, respectively. Detailed frequency analysis and perhaps even an independent measure of the surface wave field would be required to separate the wave effects.

Considering the piezo-electric crystals as part of the electronics, the major error associated with the electronics is zero point offset. When a sensor is in a container of water at rest, the voltage that is digitized should correspond to zero flow velocity. This is not necessarily the case either in the laboratory or in the ocean because a systematic offset voltage exists which is in general different for each sensor pair. Much effort was put into tracking down the cause of the offset, and it was hoped that having only one

set of receiving electronics and using the transducer transposing system discussed earlier would eliminate it. These efforts reduced the offset, but did not eradicate it completely.

Zero point offset plagues both electromagnetic and acoustic current meters, and it is usually compensated for by calibration. In the case of the acoustic travel time velocimeter, the true cause of the magnitude of the offset phenomenon is unknown, but the prime candidates can be enumerated.

The most suspect component is the piezo-electric crystal itself. Influencing factors such as aging, pressure, temperature, and applied voltage all can affect the dynamic and electrical behavior of the transducer. These factors cannot only cause zero offset, but can possibly cause that offset to change with time. Experiments with the transducers used on BASS lasting over four times the typical deployment time have shown no drift with pressure. A six-hour experiment in a bucket initially filled with iced seawater showed that the offset associated with a temperature change from ~0°C to 20° was .6 cm/sec. The crystal can be characterized by a transmit transfer function that converts electrical excitation into acoustic response and by a receive transfer function that converts acoustic excitation into electrical response. Each crystal has its own pair of transfer functions that are temperature, pressure, and age dependent. If the variation of transfer functions for two crystals match, no zero drift is expected. If the variation of each crystal's transmit and

receive transfer function is matched, there is no zero drift. Only if all four transfer functions vary independently is zero drift observed. This remains the uncorrectable error in the zero point.

Besides these factors which change the characteristics of the transducers and thus change the zero point, the physical arrangement of the transducers can cause signals to be received by the front end of the receiver circuit which could result in a zero offset or even a zero drift. Specifically, if the piezo-electric crystals continue to ring after a pulse is transmitted, this ringing voltage could be superimposed on the received signal and cause offset of the zero point by changing the shape of the leading edge of the received pulse. In the presence of ringing, large changes in travel time differences could occur with relatively small changes in sensor spacing or the speed of sound. Aging, temperature, pressure and applied voltage could occur with relatively small changes in sensor spacing or the speed of sound. Aging, temperature, pressure and applied voltage could also enter into the zero offset and drift problem by either enhancing or damping the tendency of the crystals to ring. Also, the signals are travelling through a total of 12 meters of wire in going from the electronics to the sensors and back, and perhaps reflections at the terminals could also be a form of ringing.

All acoustic measurements face possible problems from multiple acoustic paths. In the case of the sensors on BASS, multiple paths through the water and, although less likely, through the transducer mounting hardware could produce signals which add to

the true signal at the comparators thus causing a zero point error.

The performance of some of the electronic components in the receiver circuit could also cause offset. The threshold level on the comparators which determines when a received pulse actually arrives, the slope and time base for the arrival time integrator circuit, and voltage leakage from the transistors which turn the integrators off and on are all dependent on the temperature of the electronics housing and on the supply voltage from the power supply. These effects should cancel to first order when the transducers are transposed (switched) but subtle effects here could produce an erroneous zero.

The zero point offset could not be predicted a priori since the experimental operating conditions could not be duplicated in the laboratory, and therefore, the offset had to be adjusted in the data processing. This was done using laboratory calibration zero points as a guide and demanding that with these adjustments the mean vertical velocity component was zero and that when the current was at its fully developed maximum velocity, the mean horizontal velocity profile was logarithmic. This assumption of a logarithmic profile during fully developed flow was based on the repeated occurrence of this type of flow in both field and laboratory studies of fully developed turbulent boundary layers. The zero offsets of the individual measurement axes of each sensor were adjusted, and then the three components of velocity were computed. The worst case of offset was 6% of full scale, and two axes required no change at all.

Although the adjustments are slight and the technique reasonable, if they had not been made, a constant 15 cm/sec mean downward vertical velocity at 26 cm above the seafloor would have to be explained. Clearly this solution to the offset problem was distasteful since the hope was that a bucket calibration would be sufficient, however, it appears that an in situ measurement of the zero is necessary.

The important point is that this adjustment of the zero offset only serves to change the level of the mean component of velocity. It has no effect on the fluctuating components. Changing the offset in the computer produces identical velocity traces except that they are offset from each other by a constant amount. Since the mean is removed from the u-component and the w-component has zero mean, the adjustment does not contribute to any error in the calculation of $-\rho\overline{uw}$.

Three courses are open for removing the zero point uncertainty. The most satisfying course is to discover and understand the actual source of drift. If it is crystal ringing, damp it more effectively; if it is acoustic multipath, remove the other paths; if it is deterioration of the transducer assembly, improve the design. The practical solution in shallow water is to deploy the instrument with plastic bags over each sensor pod. These will remove the mean flow and provide an in situ zero after which they can be removed. A third possibility is to physically interchange transducers. While this is the proper approach from an instrumentation standpoint, it has numerous difficulties including flow disturbance, mechanical complexity, and impossibility with a simple rotation.

CHAPTER 3

THE EXPERIMENT

3.1 Site Motivation and Location

Originally the plan for this research was to investigate the benthic boundary layer in the deep ocean since, as mentioned in the first chapter, there is a paucity of detailed deep sea boundary layer measurements. The instrumentation was designed for deep ocean operation; however, confidence in the measurement technique had to be established before a deep sea deployment could be planned. The criteria for site selection were put forth as: a location which has a simple shallow water flow over a flat bed, accessible to divers, and where some interesting scientific and engineering data could be obtained. The site chosen was in Vineyard Sound about one-half mile off the Falmouth, Massachusetts, shore. The chart in Figure 3.1 shows the location of the site and the bottom topography nearby. The depth at the time of the experiment was slightly greater than 10 meters and the bottom is characterized by a relatively flat bed of gravel having pebble diameters in the 1 to 2 cm ranges. A biological coating tended to hold the pebbles together, and this acted as effective armor protecting the underlying sand from erosion. Divers reported that when the gravel was disturbed, the sand was swept away readily at the height of the tide.

The instrument sat level on the bottom, and the orientation with respect to magnetic North of the staff holding the sensors was obtained by divers from a compass attached to the bottom of the staff which rested on the sea bed.

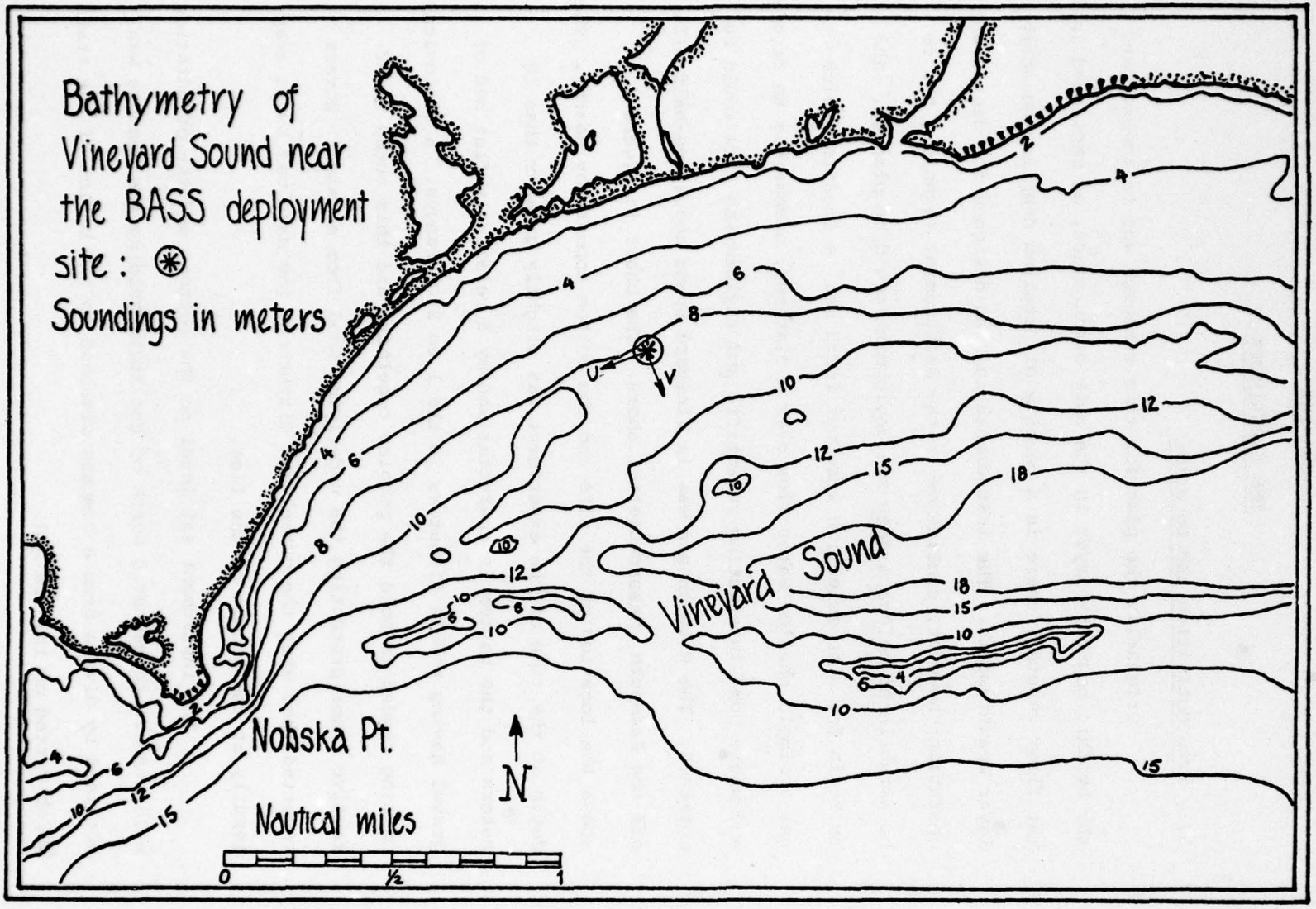
Bathymetry of
Vineyard Sound near
the BASS deployment
site : ⊛
Soundings in meters
U
V
Vineyard Sound
Nobska Pt.
N
Nautical miles
0
½
1

Figure 3.1

3.2 Deployment and Measurements

BASS was designed to be launched from a small workboat, and on 11 August 1977 it was lowered into the waters of Vineyard Sound using the crane on the M/V WHITEFOOT, a 65 foot tug boat. The sea was calm, no swell could be discerned, and under these favorable conditions the 300 kilogram tripod was easily managed on deck. A tether and small float marked the instrument's position.

Divers adjusted the position of the sensor staff, took photographs and samples of the bottom, released dye to investigate flow disturbances, and measured the heights of the sensors above the bottom. The divers observed small baitfish swimming around the instrumentation and also occasional pieces of seaweed getting entangled on the frame.

The instrument was deployed slightly before slack tide to make the divers' work easier, and remained on the bottom for more than six hours. During that time the WHITEFOOT remained on station and a series of hydrographic profiles were taken. The electrical conductivity and temperature of the water were measured as a function of depth by repeated lowerings of SCIMP, an autonomous vehicle having an internally recording CTD as one of its sub-systems. The data amassed enabled density profiles to be computed and these are presented in the form of σ_t profiles in Figure 3.2. BASS was launched forty-five minutes before the first profile shown. Slack tides were at 1000 and 1352 ETD, and the experiment was completed at 1530. When the current was running at its maximum rate, the hydrodynamic forces

on SCIMP prevented it from reaching the bottom; this accounts for the partial σ_t profile at 1150 and no profiles after 1302 h.

Before hoisting BASS off the bottom, the divers were sent down again and they reported no change in position of the compass needle and no apparent sinking of the tripod's leg into the bed.

A similar experiment was performed the previous day in a different site off the south beach of Martha's Vineyard. At that location there was a strong longshore current which had wave orbital velocities superimposed. That data will not be presented here; however, two important observations did result. First, a cursory look at the data shows that BASS is capable of measuring wave orbital velocities in a flow which represents the combined effects of waves and currents, and secondly, launch and recovery were readily managed even in swells of 1 to 1.5 meters.

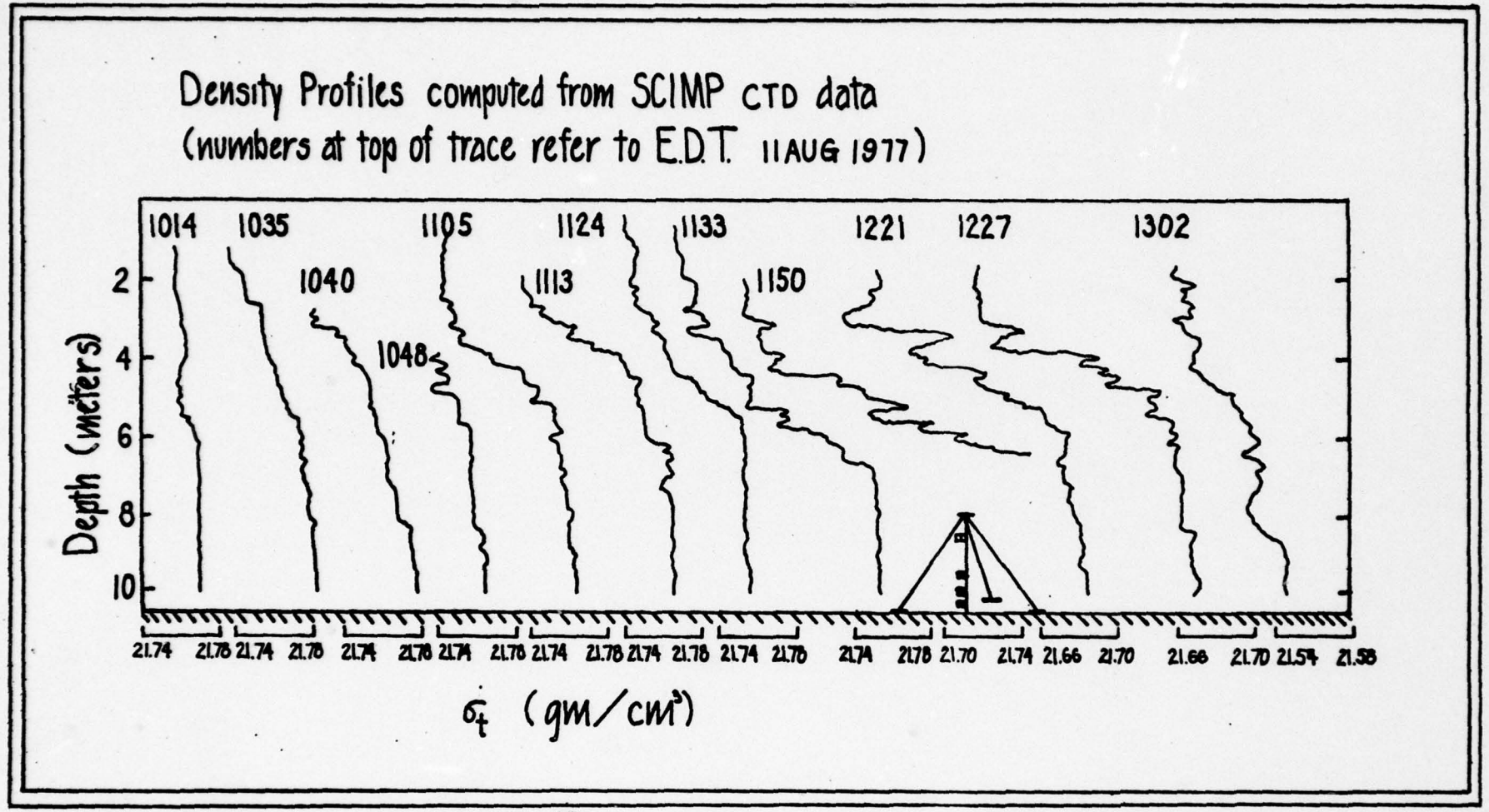
Density Profiles computed from SCIMP CTD data
(numbers at top of trace refer to E.D.T. 11AUG 1977)
1014
1035
1040
1048
1105
1113
1124
1133
1150
1221
1227
1302
Depth (meters)
2
4
6
8
10
21.74 21.78 21.74 21.78 21.74 21.78 21.74 21.78 21.74 21.78 21.74 21.78 21.74 21.78 21.74 21.78 21.70 21.74 21.66 21.70 21.66 21.70 21.54 21.58
σt (gm/cm³)

Figure 3.2

CHAPTER 4

EXPERIMENTAL RESULTS

4.1 The Data Set

The data set discussed in this chapter is a six hour record of near bottom velocities in Vineyard Sound at a depth of 10 m. Sensors were located at 26 cm, 46 cm, 96 cm, and 210 cm above the bottom, and for each sensor the basic data set consists of a time series of velocity resolved into the rectangular coordinate system defined in the first chapter. Recall that $\tilde{u}$ is the streamwise component, $\tilde{v}$ is the cross-stream component, and $\tilde{w}$ is the vertical component; a tilde represents an instantaneous quantity while upper and lower case letters signify means and fluctuations, respectively.

The direction of the U component of velocity has been taken as parallel to the depth contours at the location of the experiment (see Figure 3.1). The flow was generally along this direction during the course of the experiment, and as will be shown in the next section, the mean cross-stream velocity, V, was nearly zero except near times of slack tide.

Figure 4.1 shows a typical piece of the time series. This is a thirty-two minute segment of the velocity data from a sensor 26 cm above the bottom, and it shows the tide approaching slack water. The figure illustrates the detail that the BASS sensors are capable of providing, and also gives an indication of the wealth of scales in the flow. Only every tenth point is plotted; this makes the plot easier to read but also causes some abruptness between adjacent points.

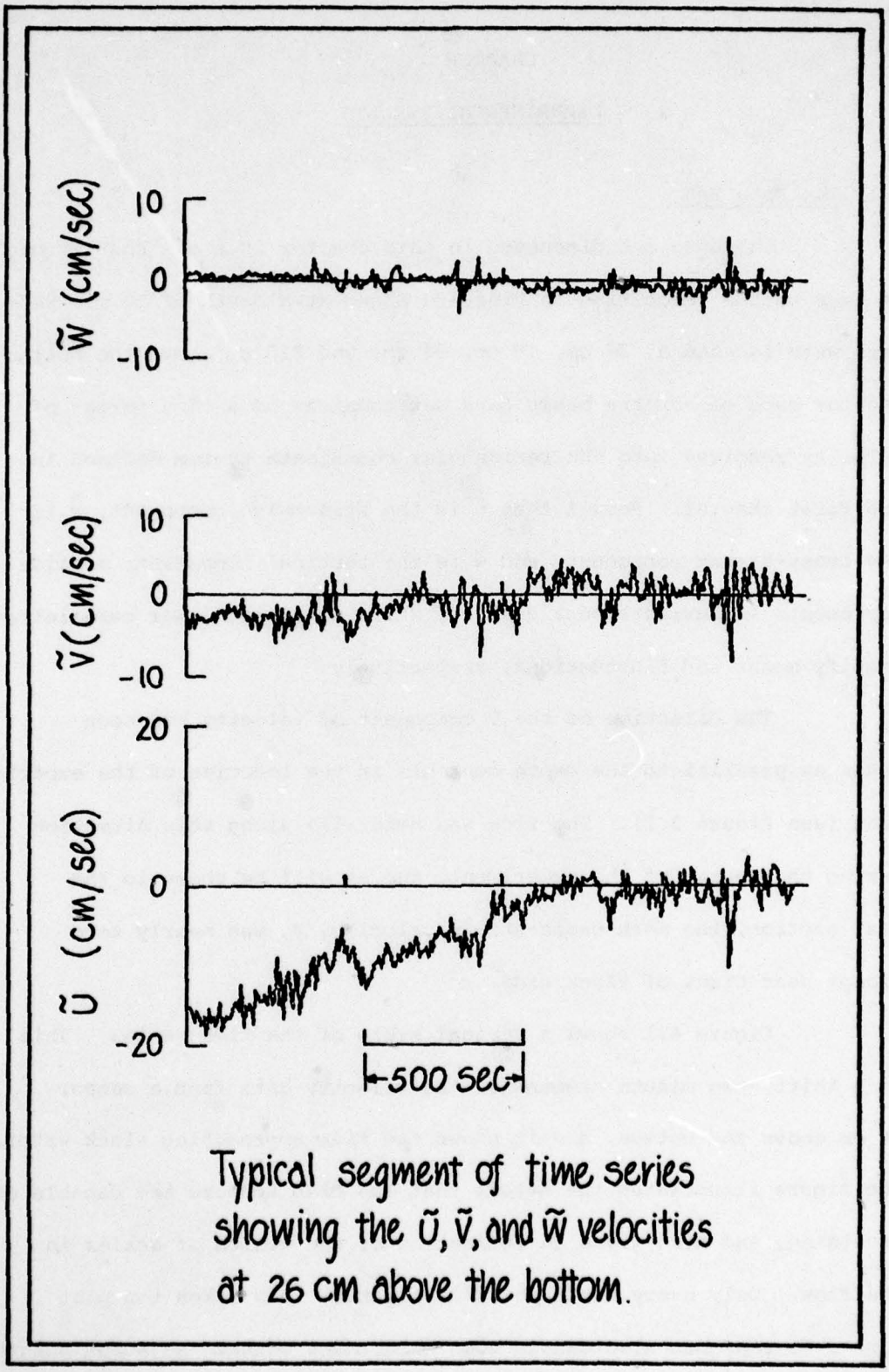

Typical segment of time series showing the $\tilde{U}$, $\tilde{V}$, and $\tilde{W}$ velocities at 26 cm above the bottom.

Figure 4.1

As a guide to many discussions in this chapter, Figure 4.2 shows a plot of the entire time series of the u-component of velocity for the sensor at 96 cm. The instrument sampling rate is 1.33 Hz which means there are 133 data points every 100 seconds, but in this plot every twentieth point is plotted. Had every point been plotted, the curve would be a dark fuzzy band on this scale. The smooth curve through the data is the least squares sixth order polynomial representing the mean velocity. The time series of u-fluctuations is obtained by differencing the two curves. It is interesting how the amplitude of the u-fluctuations is modulated during the half-tidal cycle. The letters in the figure are intended to serve as guideposts in the following sections.

4.2 The Mean Flow

4.2.1 Mean Velocity Profiles

As mentioned previously in the discussion of the zero point offset (see Section 2.5, Sources of Error), the zero points of the individual measurement axis were adjusted slightly to force the mean vertical velocity to be zero, and to force a logarithmic profile to the mean horizontal velocity at the time of maximum current (between points E and F in Figure 4.2). This caveat must be kept in mind when interpreting the mean velocity profiles.

In order to investigate Reynolds stresses in a non-steady flow, a decision must be made as to the treatment of the mean flow. The simple approach of passing a sliding average through the time

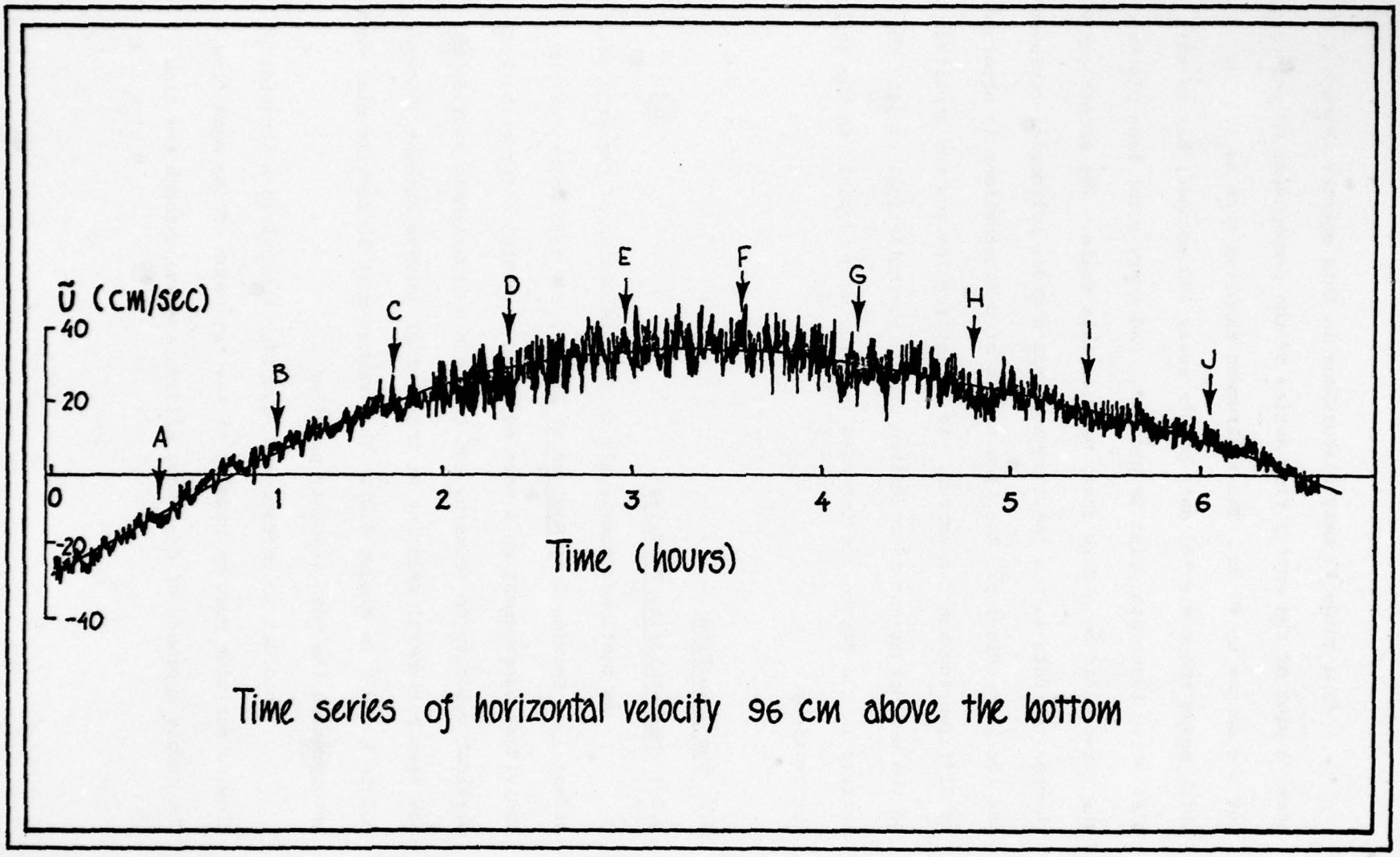

Time series of horizontal velocity 96 cm above the bottom

Figure 4.2

series misses the mark in this case because of the multiplicity of the scales of the fluctuations. As Figure 4.2 shows, both the amplitude and scale of the fluctuations are changing during the tidal cycle. If too short an averaging time is chosen, some of the larger scale motions become part of the mean flow; while if too large an averaging window is used, some of the mean flow can be superimposed on the fluctuations. Both of these cases can lead to incorrect calculations of the Reynolds stress.

The sliding average approach was tried, but it proved unsatisfactory because of the problems just mentioned, and so the more complex method of least squares was utilized to fit a polynomial to the horizontal velocity data. This resulted in the mean horizontal velocity profiles shown in Figures 4.3a and 4.3b which were derived from plots akin to Figure 4.2 for all four sensor pods. Figure 4.3a shows profiles of the mean U component of the horizontal velocity, while Figure 4.3b presents the V (cross-stream) component. The profiles correspond to the lettered points on the inset diagram which is a schematic of Figure 4.2. The profiles are separated from each other by 34 minutes.

Considering the U profiles, it is seen that the current was flowing East when the experiment was initiated (profile A); it quickly became slack (profile B), and then increased to a maximum between profiles E and F of 36.4 cm/sec, 210 cm above the bottom. At 26 cm the velocity was 28.2 cm/sec.

Even with the forced log profile between points E and F, the profiles in Figure 4.3a show the gradual increase and decrease

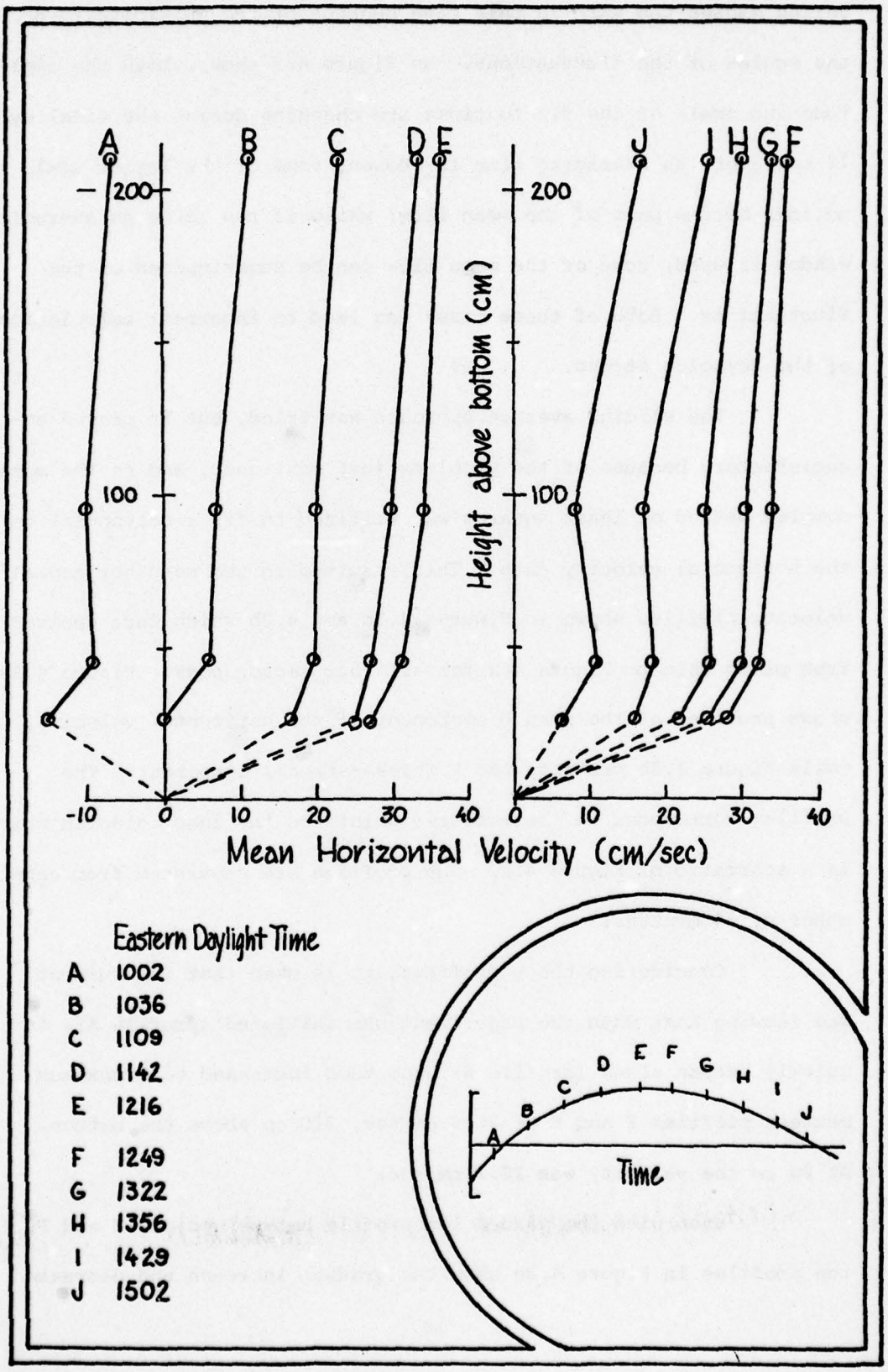
A
B
C
D
E
F
G
H
I
J
200
100
Height above bottom (cm)
-10
0
10
20
30
40
Mean Horizontal Velocity (cm/sec)
Eastern Daylight Time
A 1002
B 1036
C 1109
D 1142
E 1216
F 1249
G 1322
H 1356
I 1429
J 1502
Time

Figure 4.3a

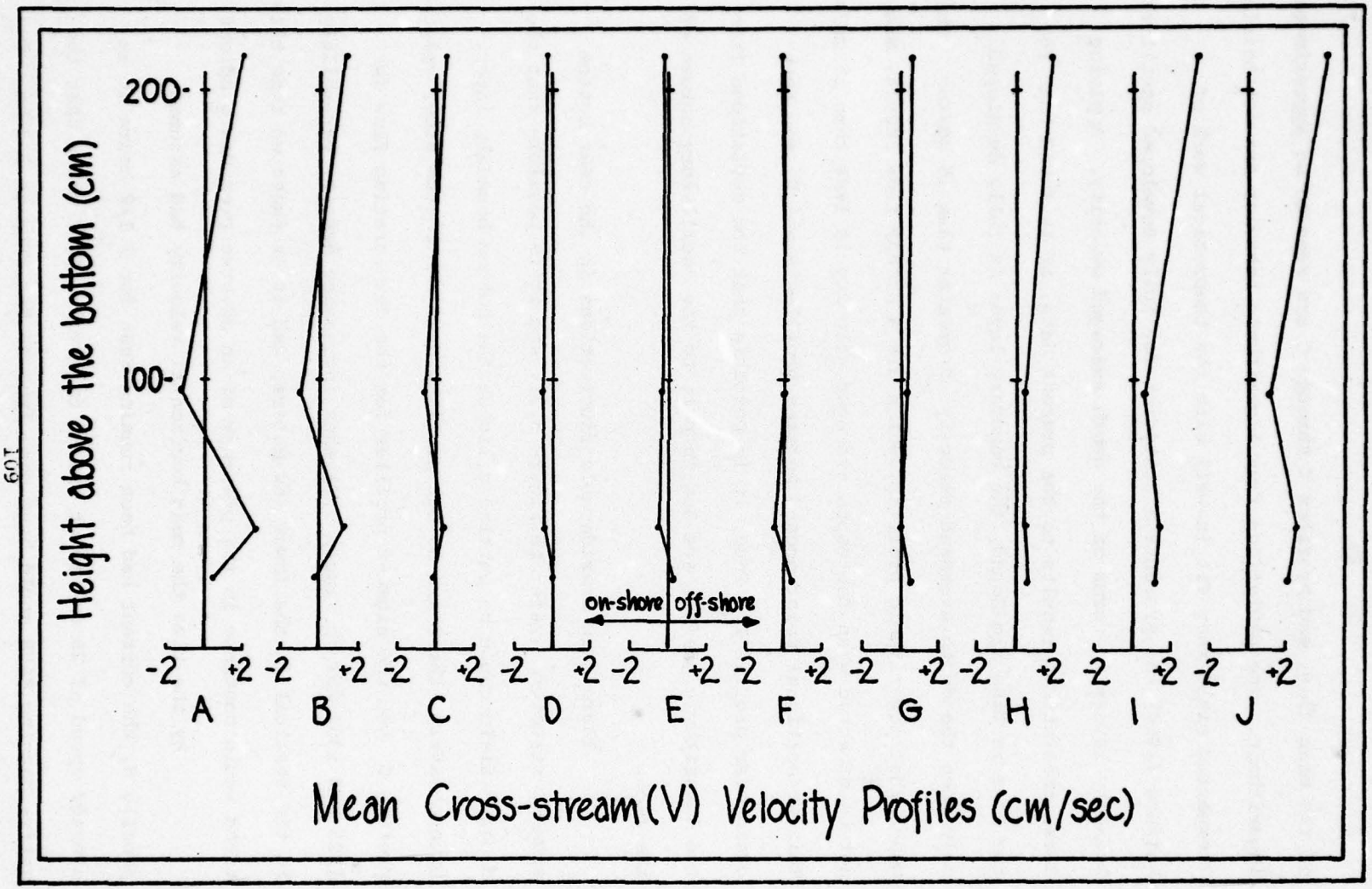
Height above the bottom (cm)
200-
100-
on-shore
off-shore
-2
+2
A
B
C
D
E
F
G
H
I
J
Mean Cross-stream (V) Velocity Profiles (cm/sec)

Figure 4.3b

of the mean flow, and profiles C through G are seen to be approximately logarithmic. The deviations from logarithmic behavior are not totally unexpected since they fit in well with the theoretical work of Kajiura (1964) who presents a criterion for fully developed oscillating boundary layers in terms of the depth averaged velocity. Applying those theoretical results to the present data, it is found that for the site in Vineyard Sound, the boundary layer is fully developed only when the depth averaged velocity is greater than 15 cm/sec. This means that logarithmic profiles, which are a steady flow result, might not be expected when the depth averaged velocity is less than 15 cm/sec. This transitional point occurs between profiles B and C, and then again near profile I. Thus, it is possible that the deviations from the logarithmic profile are due in part to the oscillatory nature of the flow.

There were considerable fluctuations in the near bottom sigma-t structure (refer to Figure 3.2), and it is possible that the density field could be putting a lid on the bottom boundary layer. Unfortunately, there are no CTD profiles near the bottom after velocity profile G, but the sigma-t profiles for the decelerating flow (at 1227 and 1302 EDT in Figure 3.2) show increasing density variability in the vertical in the lower few meters, and it is expected that this trend would continue in the presence of an adverse pressure gradient.

By the time the mean horizontal velocity had assumed profile H, the current had been running East for 3 1/2 hours at an average speed of 26 cm/sec at the 96 cm level. This means that the waters passing BASS could have come from as far away as 3.3 km. On

Figure 3.1, this would be the easternmost point shown. Flow disturbances caused by the current flowing through regions of varying depth would be advected downstream past BASS and could produce the velocity structure shown in profiles H, I, and J. The profiles of Figure 1.2 after Mosby (1946) also show these variations in the mean horizontal velocity, and in that study topographic features were delineated as the cause.

The mean cross-stream velocity profiles (Figure 4.3b) show hardly any veering of the horizontal velocity vector with height above the bottom. The maximum off-shore flow is 4 cm/sec at profile J for the sensor at 210 cm. Only at times near slack tide are the mean cross-stream velocities greater than 1 cm/sec; when the flow is fully developed, the mean V velocities are almost non-existent.

In the next two sections, estimates of the bottom stress will be made by applying the quadratic drag law and the logarithmic profile method to the mean horizontal velocity curves of Figure 4.3a. The remainder of the chapter will deal with the velocity fluctuations.

4.2.2 Quadratic Drag Law

In section 1.2.1 a frictional drag coefficient, c_f, was calculated for the site in Vineyard Sound and its value was 5.0×10^{-3} referenced to Z = 96 cm. This was obtained assuming turbulent flow over a rough surface with a mean pebble diameter of 1 cm. (The mechanics of the computational procedure are found on page 248 of Daily and Harleman (1966)).

The value of u_* can be obtained from the quadratic drag law by substituting the definition of u_* in terms of τ_b into

$$\tau_b = \frac{c_f \rho U^2}{2}$$

where $U = U_{96}$ (the reference velocity for c_f in this case). This results in

$$u_* = \left(\frac{c_f}{2}\right)^{1/2} U_{96} \tag{4.1}$$

The results of the computation are shown in Table 4.1 ($c_f = .005$).

TABLE 4.1

	A	B	C	D	E	F	G	H	I	J
U_{96} (cm/sec)	10.0	7.0	20.0	30.0	34.2	34.3	30.7	25.8	17.2	8.4
u_* (cm/sec)	.50	.35	1.00	1.50	1.71	1.75	1.54	1.29	.86	.42

These results are similar to those obtained by investigators studying the same type of shallow water tidal flows.

4.2.3 The Profile Method

As discussed in section 1.2.2, u_* can be calculated from the slope of a plot of horizontal velocity versus the logarithm of height of the measurement above the bottom. Such a plot for the data taken by BASS in Vineyard Sound is given in Figure 4.4; Table 4.2 is a listing of the data plotted in the figure. Profiles A, B, and J were not logarithmic and are not shown. These three occurred near slack water when the vertical distribution of horizontal velocity was

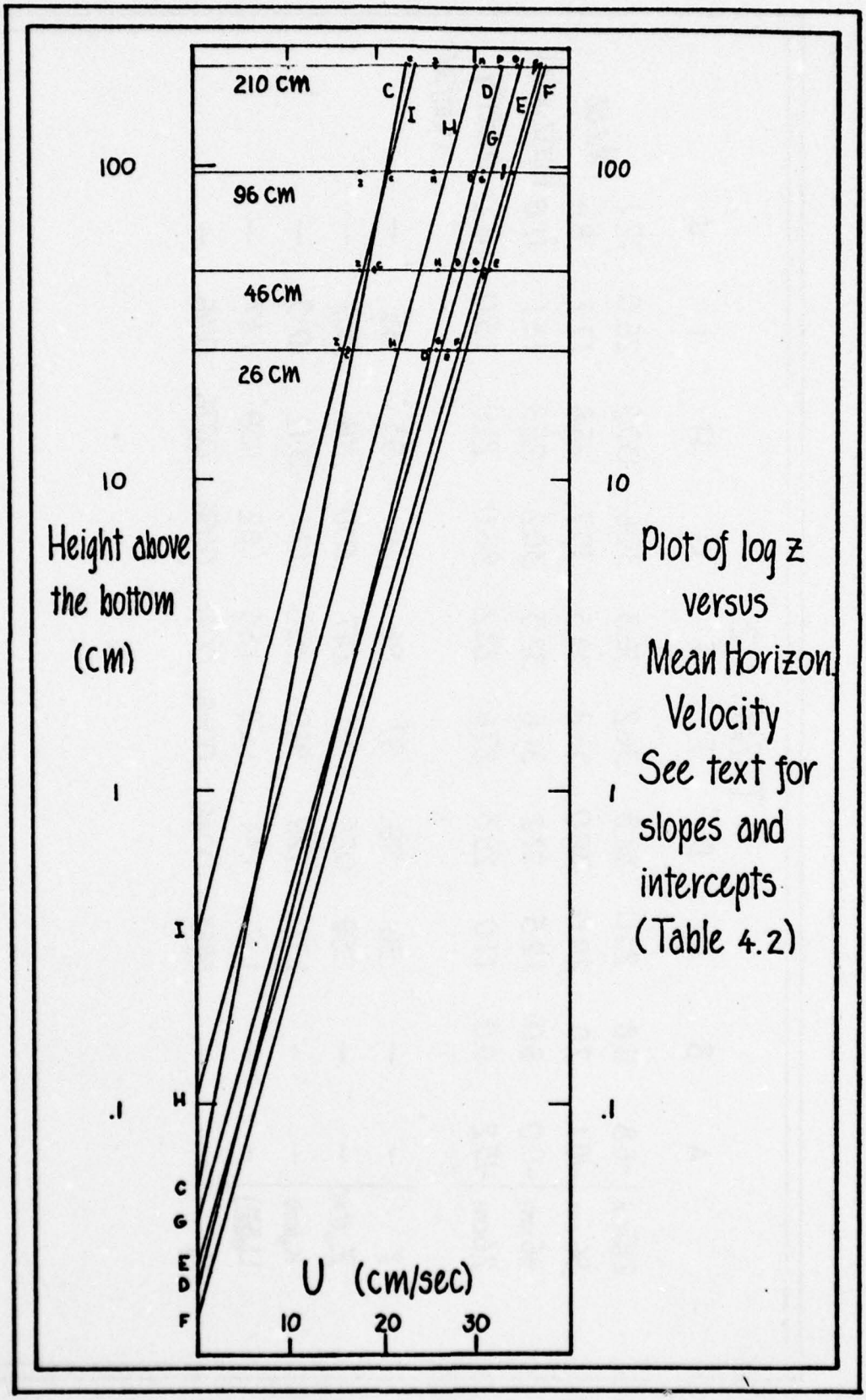
210 cm
96 cm
46 cm
26 cm
100
10
1
.1
Height above the bottom (cm)
Plot of log z versus Mean Horizon. Velocity See text for slopes and intercepts (Table 4.2)
C
I
H
D
E
F
G
U (cm/sec)
10
20
30

Figure 4.4

TABLE 4.2

	A	B	C	D	E	F	G	H	I	J	
210cm	-6.8	11.8	23.0	32.8	36.2	36.3	34.6	30.2	26.0	17.1	Mean Horizontal Velocity (cm/sec)
96cm	-10.1	7.0	20.0	30.0	34.2	34.3	30.7	25.8	17.2	8.4	
46cm	-9.0	6.0	19.5	27.2	31.6	32.3	30.2	25.9	18.1	11.0	
26cm	-15.2	0.0	17.0	25.3	27.6	28.2	26.0	21.9	16.0	6.2	
r	—	—	.96	.99	.97	.96	.95	.93	.85	—	
Z_o(cm)	—	—	.059	.024	.031	.017	.039	.104	.337	—	
k_b(cm)	—	—	1.77	.729	.949	.526	1.17	3.12	10.0	—	
U_*(cm/sec)	—	—	1.12	1.44	1.68	1.58	1.62	1.59	1.47	—	
C_f	—	—	.0063	.0046	.0048	.0042	.0056	.0076	.0146	—	

chaotic. Others (Mosby) (1947), Lesser (1951), Sternberg (1970), etc.) have observed deviations from logarithmic profiles, and the probable causes are those enumerated earlier in this chapter except for the unique case of Charnock (1959) who put the blame on a large concentration of jellyfish nearby. This point is brought up since the effects of suspended material in the flow have been neglected here and could be important in the deep sea as well as in coastal flows since suspended material decreases the value of von Karman's constant.

The straight lines in Figure 4.4 were computed by subjecting the four measurements at each station to a least squares linear regression. The regression coefficient, r, is given in Table 4.2 as an indication of goodness of fit to a logarithmic profile (on a scale of 0 to 1). The analysis of the log profiles hinges on the validity of the assumptions made in determining the zero offset as mentioned in Chapter 2.

The value of c_f referenced to the 96 cm level is also given in Table 4.2. It was arrived at using

$$C_f = 2\left(\frac{u_*}{U}\right)^2 \tag{4.2}$$

and the results are consistent with those of Charnock (1959) and Bowden, Fairbairn, and Hughes (1959) who applied the profile method under conditions similar to those in Vineyard Sound. The values of c_f in Table 4.2 show that the estimate (c_f = .005) of the drag coefficient made in Chapter 1 is valid.

Rough turbulent flow as defined by Nikuradse (1933) obeys the criterion that the roughness Reynolds number is greater than 70, that is,

$$R_r = \frac{u_* k_b}{\nu} > 70$$

k_b = equivalent sand grain roughness

ν = kinematic viscosity

For typical values from the data set, $u_* = 1.5$ cm/sec, $\nu = 10^{-2}$ cm^2/sec and $k_b = 1$ cm, the roughness Reynolds number is 150 and the flow can be termed fully rough. For rough turbulent flow, the value of z_0 to be used is $z_0 = k_b/30$; that is how k_b was computed in Table 4.2. k_b should remain relatively constant if the flow stays fully developed which seems to be the case, and the mean of k_b for the seven profiles is 1.05 cm which is in close agreement with the size of the pebbles sampled by the divers.

If one assumes a roughness height of 1.05 cm, then by applying the logarithmic relationship u_* can be calculated for various heights above the bottom provided the horizontal velocity at that height is known. The results of this exercise are tabulated below and show that u_* is relatively constant over the bottom two meters suggesting the existence of a constant stress region at least two meters thick from the time of profile C to that of H.

TABLE 4.3

	A	B	C	D	E	F	G	H	I	J
210 CM	.31	.54	1.06	1.51	1.66	1.67	1.59	1.39	1.20	.79
96 CM	.51	.35	1.01	1.52	1.73	1.73	1.55	1.30	.87	.42
46 CM	.50	.33	1.09	1.52	1.76	1.80	1.68	1.44	1.01	.61
26 CM	.92	–	1.03	1.53	1.67	1.71	1.57	1.33	.97	.38

Values of u_* for $k_b = 1.05$ (u_* in cm/sec)

Figure 4.5 is a plot of friction velocity, u_*, versus the depth-averaged horizontal velocity in the lower 2.1 meters. The plot is analogous to Figure 1.5 (after Seitz (1971)) and shows a slope of .051 corresponding to a drag coefficient as defined by Eq. 4.2 of 5.2×10^{-3}. Seitz' result in an estuary yielded a drag coefficient of 2.8×10^{-3} for a smoother bottom.

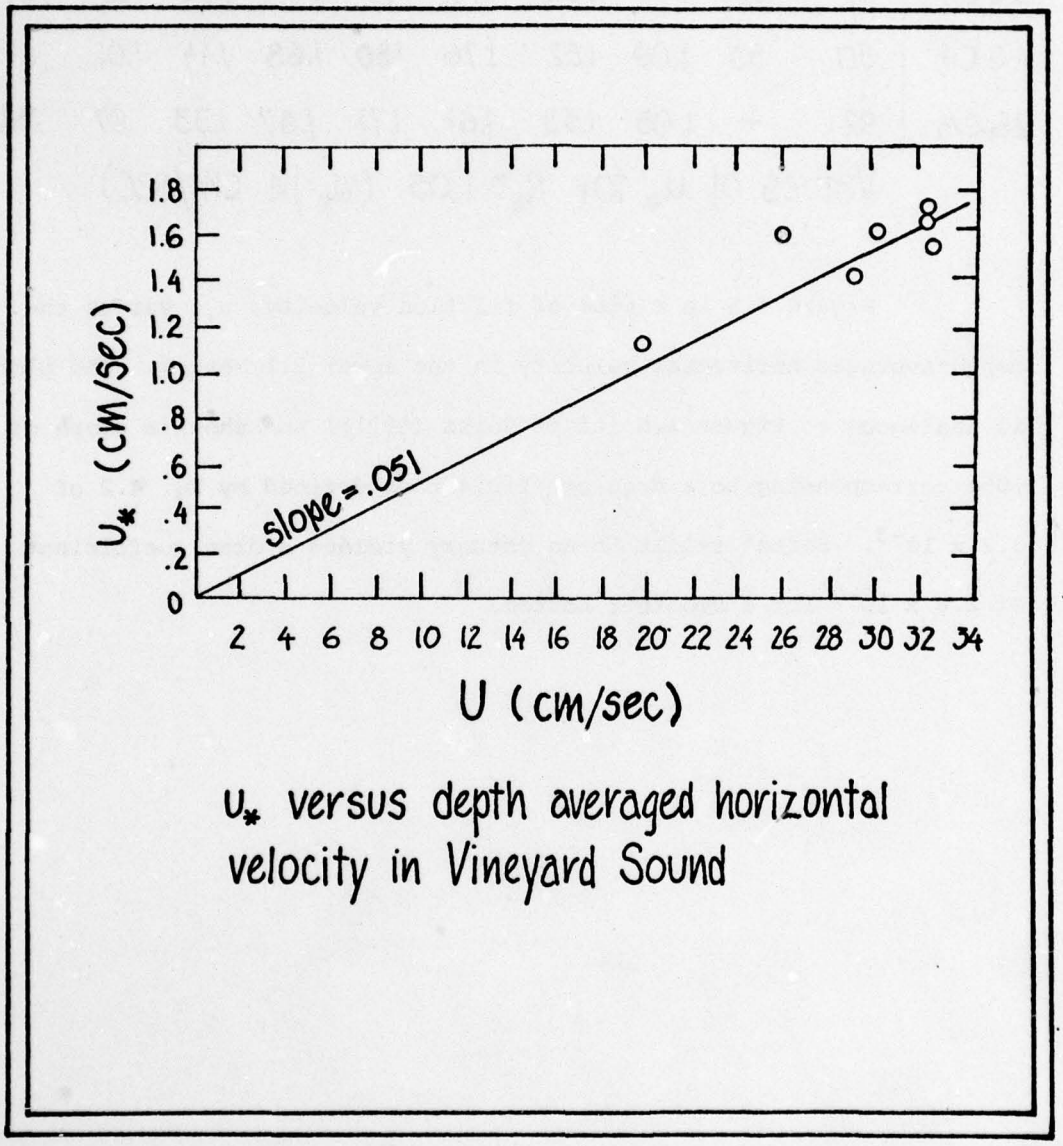

U_* versus depth averaged horizontal velocity in Vineyard Sound

Figure 4.5

4.3 Velocity Fluctuations Measured by BASS

The initial portion of this chapter has dealt with the mean horizontal velocity profiles measured by BASS, and the results that have been presented are consistent with what would be expected in this type of flow. Existing off-the-shelf instrumentation would have done a fair job at producing similar results and the story would have ended here. However, it is the capability of BASS to measure the three components of velocity fluctuations to an accuracy of $\pm$0.5 cm/sec that will give novel insight into the structure of marine boundary layers. The results presented in the last sections of this chapter will validate the claim that BASS can provide new insight in this field.

The remainder of this chapter will deal with the time series of the fluctuating components of the velocity field. A typical segment of the velocity record is shown in detail in Figure 4.6. The record is 143 seconds long and shows the three fluctuating components of velocity at a height of 26 cm above the bottom. At the time of this record, the mean horizontal velocity at 26 cm was ~28.0 cm/sec, and the record corresponds to a time slightly after profile E in Figure 4.2. Data of the type shown in Figure 4.6 has never been obtained previously in the marine environment. The other attempts at measuring more than one component of velocity fluctuations; that is, Bowden and Fairbairn (1956), Bowden (1962), Gordon and Dohne (1973), Seitz (1973, Heathershaw (1976) and Smith and McLean (1977) have only measured two components of velocity except Seitz (1973) who measured spectra of the three fluctuating components

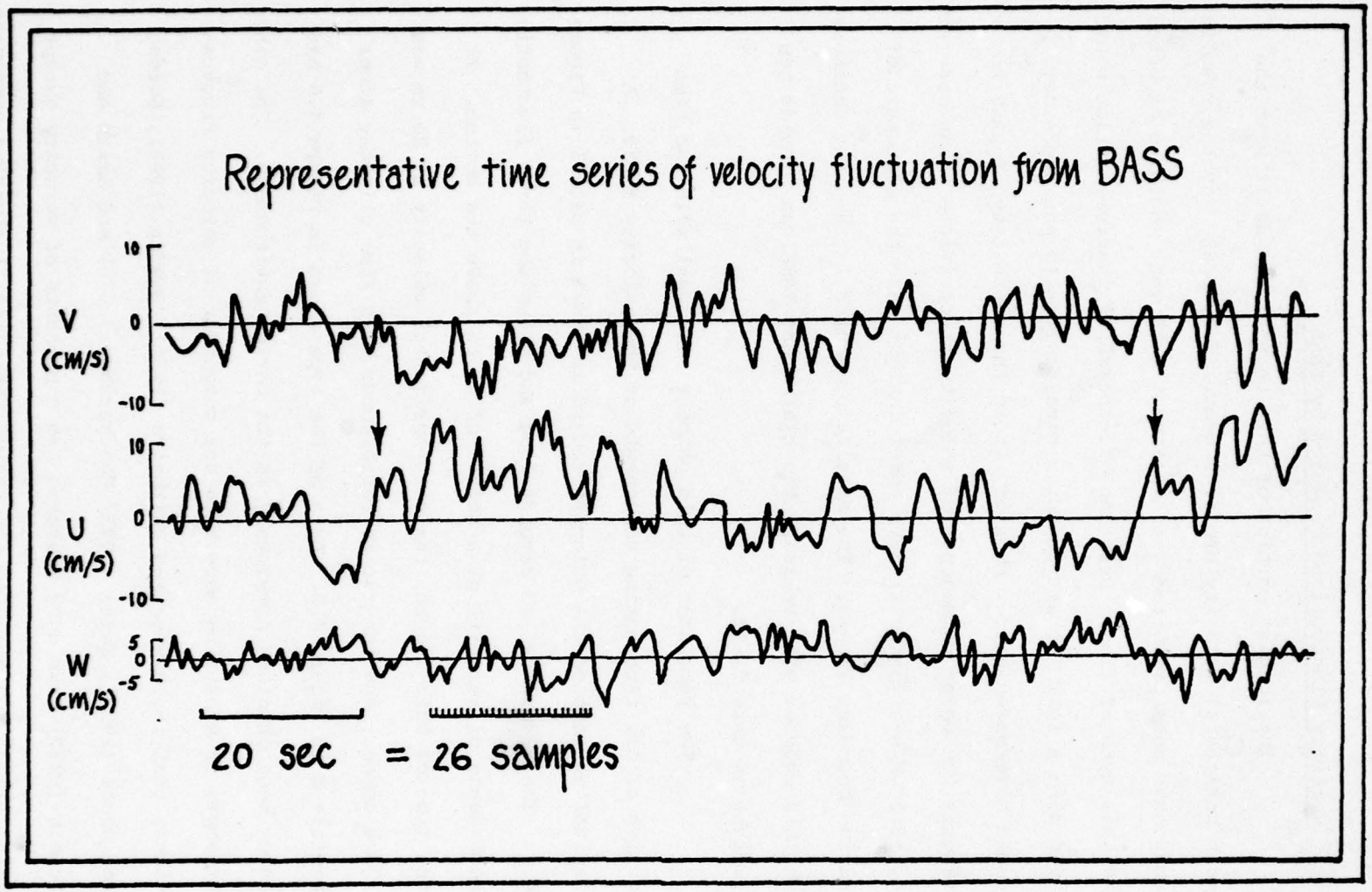
Representative time series of velocity fluctuation from BASS
V
(cm/s)
10
0
-10
U
(cm/s)
10
0
-10
W
(cm/s)
5
0
-5
20 sec = 26 samples

Figure 4.6

but produced no time series. The time series produced by BASS are not only longer, but have better resolution (0.33 mm/sec per least bit) and better accuracy ($\pm$ 0.5 cm/sec) than these other instrumentation schemes.

In looking at the u velocity trace, three scales of fluctuations can be seen. As a deliberate consequence of the expanded time scale, each data point is visible, and these point-to-point variations are responsible for the high frequency fluctuations. The bar next to the time scale marker shows the time spacing of velocity realizations. The next scale that readily stands out contains fluctuations of 6 to 7 seconds in duration. This is more apparent in the u component than in the other two. At an advection velocity of 28 cm/sec, a fluctuation of this duration might be represented as an eddy having a characteristic horizontal dimension of 200 cm.

There is a lower frequency visible in the u trace, and a whole cycle has been set off by the arrows in Figure 4.6; it has a period of 100 seconds corresponding to a characteristic eddy size of about 35 meters and is most likely the result of an upstream topographic undulation.

This small portion of the data was chosen because it illustrates typical characteristics of the fluctuation time series. The time scales just discussed are generally found throughout the records at all four current meter locations.

Now consider the correlations of the velocity fluctuations in Figure 4.6. In scrutinizing and comparing the u and w traces, the reader can eventually see the tendency of negative horizontal

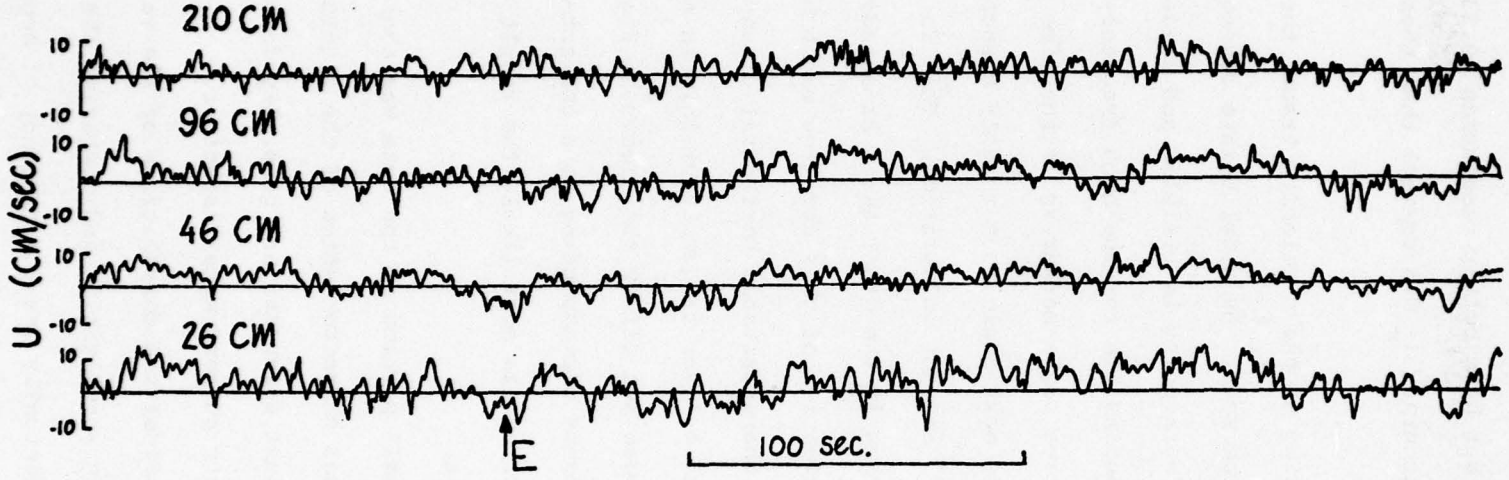

Time series of streamwise (u) velocity fluctuations at four elevations above the bottom

Figure 4.7

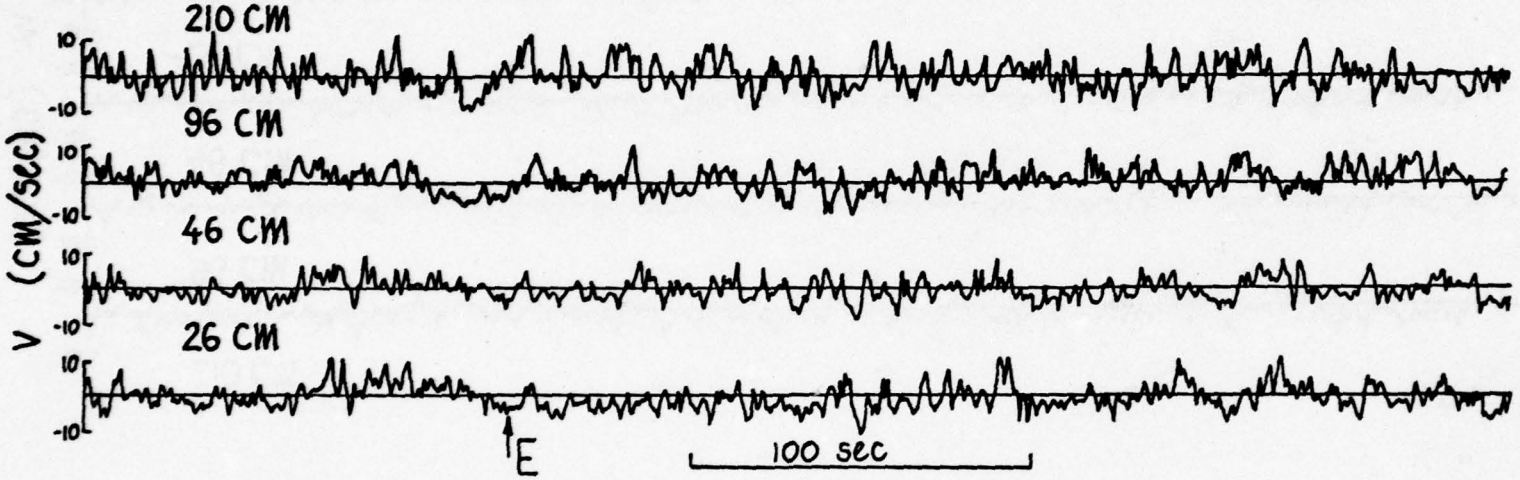

Time series of cross-stream (v) velocity fluctuations at four elevations above the bottom

Figure 4.8

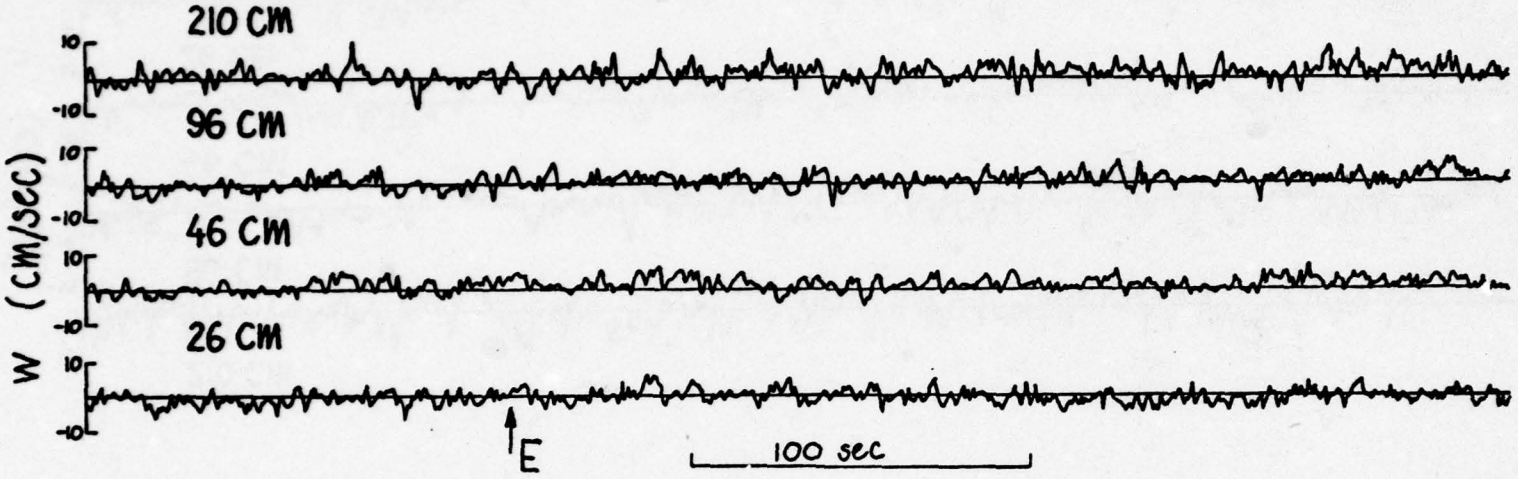

Time series of vertical (w) velocity fluctuations at four elevations above the bottom

Figure 4.9

fluctuations to be associated with positive vertical velocities and vice versa. The correlations give rise to Reynolds stresses. No apparent correlation can be observed between the cross stream velocity, v, and the other two components.

The final item to observe in the figure, which is common to all records, is the relative amplitudes of the fluctuations. The root-mean-square values of the fluctuations will be discussed in the next section.

A 400 second piece of the three component time series for all four levels is reproduced in the next three figures (4.7, 4.8, and 4.9). The location of mean profile E is indicated, and the mean horizontal velocities at levels 1 through 4 are 27.6, 31.6, 34.2, and 36.2 cm/sec, respectively. These figures are intended to illustrate the typical scales of the fluctuations and to show the correlations among the velocity signals at the different levels. The traces of the current meter at 26 cm directly precede the expanded trace of the previous figure (4.6).

4.3.1 Root-Mean-Square Velocities

Figure 4.10 is a plot of the root-mean-square (rms) values of the velocity fluctuations. Each point on the graph represents a 1024 point average (12.8 minutes); the letters again correspond to the mean velocity profiles of section 4.2.1 which are separated in time by 34 minutes. Note that the vertical scale for w is twice as large as the scales of u and v.

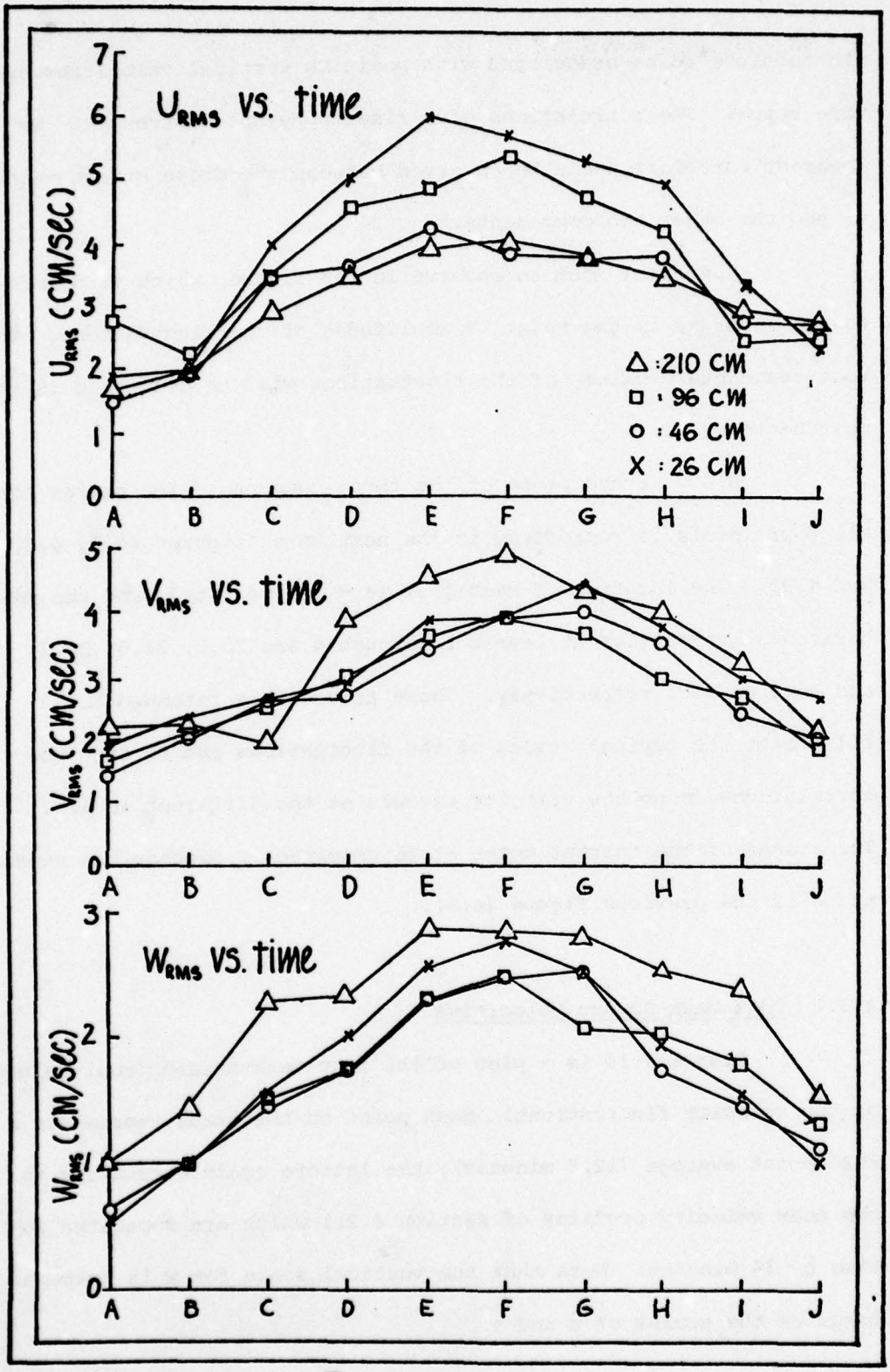
U_{RMS} vs. time
U_{RMS} (CM/SEC)
△ : 210 CM
□ : 96 CM
○ : 46 CM
X : 26 CM
V_{RMS} vs. time
V_{RMS} (CM/SEC)
W_{RMS} vs. time
W_{RMS} (CM/SEC)
A B C D E F G H I J

Figure 4.10

In general, the rms values of all three components track the horizontal current and reach their respective maxima when the tide is running at its maximum. The streamwise and cross-stream values of the rms velocity are of about the same magnitude while the vertical fluctuations seem to be about one-half as large as the horizontal rms values.

Looking at the graphs of Figure 4.10 individually, the u_{rms} plot shows the lowest sensor (26 cm) having the greatest value most of the time except near slack tide perhaps reflecting turbulence production near the bottom; while the upper sensor (210 cm) has generally the smallest value. The maximum value of u_{rms} occurs at profile E having a value of 6.0 cm/sec. The consistently high values of u_{rms} at the lowest sensor indicate high values of normal Reynolds stress ($-\overline{\rho u^2}$) at the sea bed.

The cross-stream rms velocities show a maximum of 5.0 cm/sec at profile F for the uppermost sensor. There is hardly any difference among the lower three sensors, and in fact they have nearly identical values at F (4.0 cm/sec) when the current is swiftest. There is more scatter of the points on the decelerating tide than on the accelerating, and this might suggest increased intermittency. The sensor at 210 cm has cross-stream rms values which are larger than the downstream values from profile D through I, and since this is not true for the others, it might suggest that the sensor is at a distance from the bottom where the structure of the turbulence is somehow different, or where different length scales are dominant.

This same effect is born out by the w_{rms} plot; the three lower sensors have values which are tightly grouped while the upper sensor stands alone with a consistently higher value of rms vertical velocity. The maximum value for the top sensor is 2.7 cm/sec at E.

Averaging the ratio of rms velocities to mean horizontal velocity for all four levels of the ten profiles yields:

$$u_{rms} = .16\ U$$

$$v_{rms} = .13\ U$$

$$w_{rms} = .08\ U$$

Similarly, forming the ratios of v_{rms}/u_{rms} and w_{rms}/u_{rms} yields:

$$v_{rms} = .9\ u_{rms}$$

$$w_{rms} = .5\ u_{rms}$$

Although data for only one-half of a tidal cycle were used in calculating these ratios, no differences were found between the ratios computed for the accelerating and decelerating phases of the tide.

Calculations of the rms values for the velocity fluctuations can be used to determine the turbulent kinetic energy intensity as defined by $\rho q^2/_2$ where ρ is the fluid density and $q^2 = u^2 + v^2 + w^2$.

The importance of being able to measure the three fluctuating components of velocity is brought into sharp focus here. Gordon (1975), since he cannot measure v, the cross-stream component, assumes $\overline{v^2} = .5\overline{u^2}$ for his calculations of $\overline{q^2}$. The measurements made by BASS in Vineyard Sound indicate $\overline{v^2} = .8\overline{u^2}$ which means Gordon's estimate of $\overline{v^2}$ can be off by almost 40%.

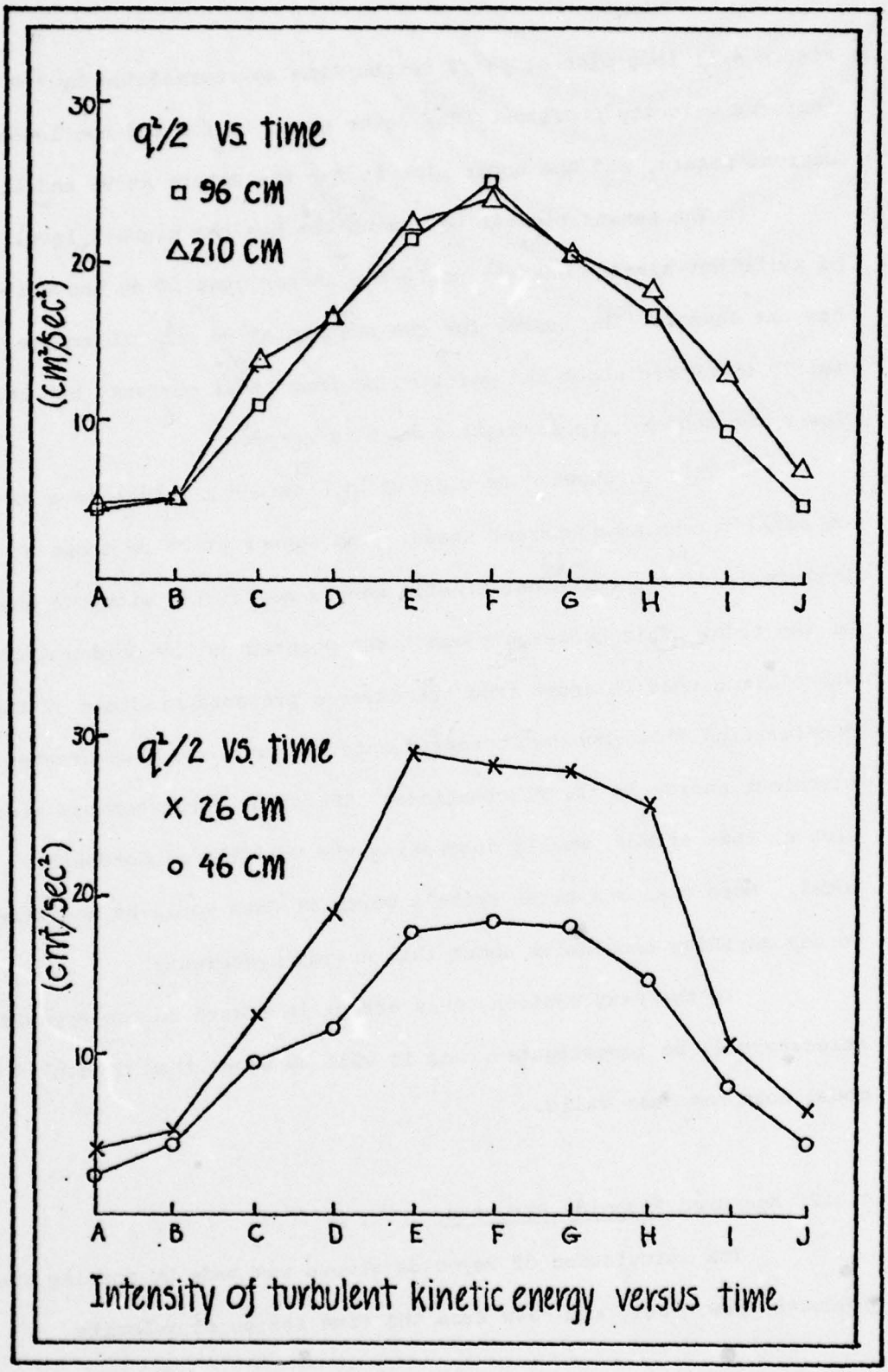
30
20
10
$q^2/2$ vs. time
□ 96 cm
△210 cm
(cm^2/sec^2)
A B C D E F G H I J
30
20
10
$q^2/2$ vs. time
× 26 cm
○ 46 cm
(cm^2/sec^2)
A B C D E F G H I J
Intensity of turbulent kinetic energy versus time

Figure 4.11

Figure 4.11 is a plot of $\rho q^2/2$ versus time as represented by the lettered velocity profiles. The lower graph is for the two lowest current meters, and the upper plot is for the meters at 96 and 210 cm.

The sensor closest to the bottom has the highest level of turbulent kinetic energy; while the sensor just 20 cm above it has the lowest. The curves for the sensors at 96 and 210 cm are fairly symmetric about the point of maximum tidal current, but the lower two sensors are asymmetric in this respect.

This is shown more clearly in Figure 4.12 which is a plot of $\rho q^2/2$ versus mean current speed. The sensor at 26 cm shows a hysteresis of the turbulent kinetic energy associated with the phase of the tide. This hysteresis was first pointed out by Gordon (1975) who claimed that it arose from the adverse pressure gradient of the decelerating flow causing increased intermittency and thus greater turbulent energy in the fluctuations. The other three sensors also hint at this effect, weakly suggesting the validity of Gordon's model. More than one tidal cycle's worth of data would be necessary to say anything conclusive about this energy hysteresis.

In the next section, this effect in regard to the Reynolds stresses will be investigated, and it will be shown that Gordon's model does not seem valid.

4.3.2 Measured Reynolds Stresses

The calculation of Reynolds stress was made by forming the products $-\rho uw$, $-\rho uv$, and $-\rho vw$ from the time series of velocity

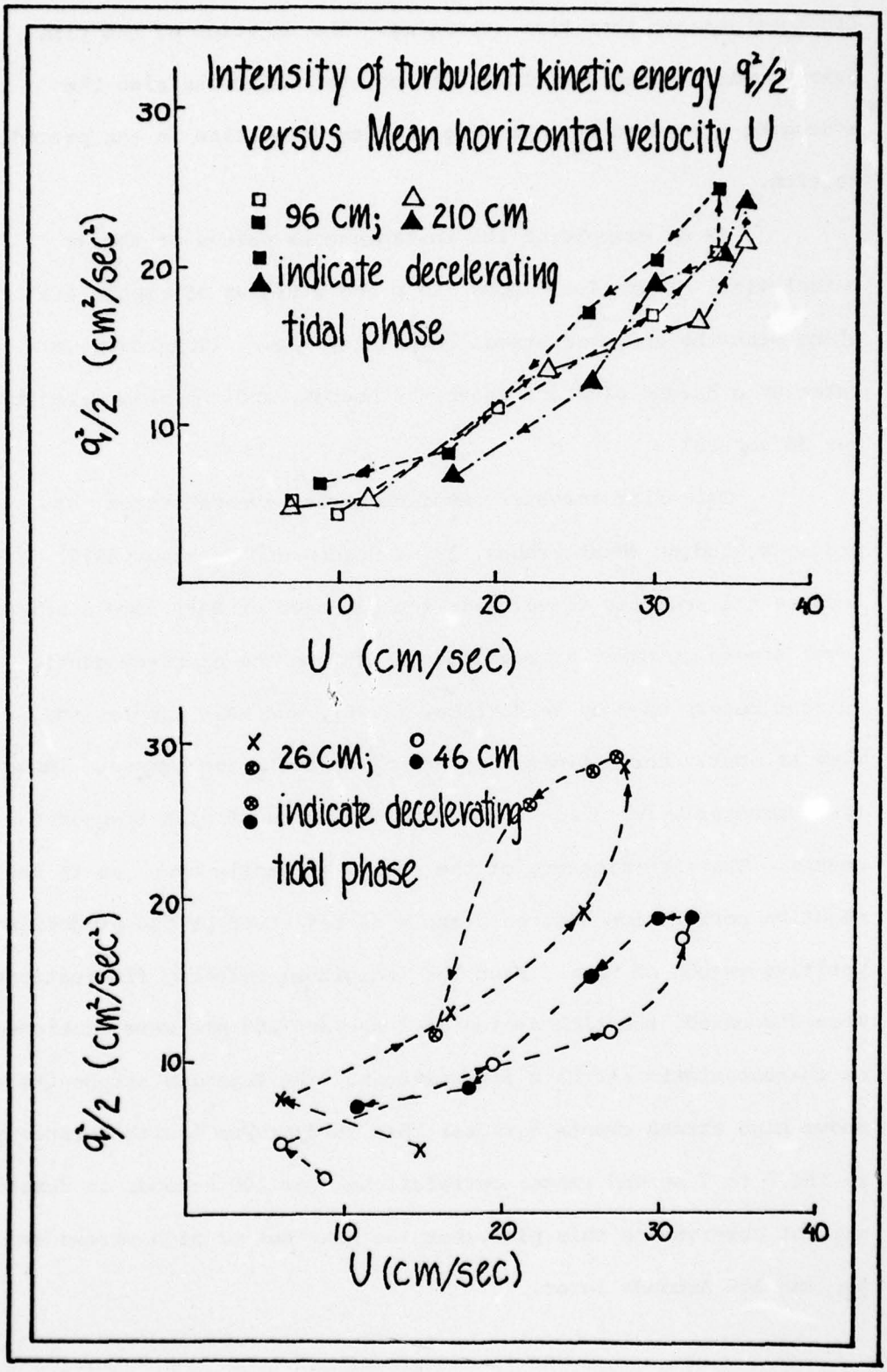
Intensity of turbulent kinetic energy q²/2
versus Mean horizontal velocity U
96 cm; 210 cm
indicate decelerating
tidal phase
q²/2 (cm²/sec²)
U (cm/sec)
26 cm; 46 cm
indicate decelerating
tidal phase
q²/2 (cm²/sec²)
U (cm/sec)

Figure 4.12

fluctuations and then time averaging. The duration of the time average was 768 seconds (1024 data points) which was also the averaging time used in computing the rms velocities in the preceding section.

As an example of the instantaneous values of the uw correlation, Figure 4.13 shows the u and w traces of Figure 4.6 along with the computed stress component, $-\rho uw$. (This data was taken at a height of 26 cm above the bottom, and the mean velocity was 28 cm/sec).

This plot resolves Reynolds stress events better than previous studies (Heathershaw, 1976; Gordon and Witting, 1977) because the acoustic travel time sensors used on BASS have a noise level almost an order of magnitude less than the electromagnetic current meters used by Heathershaw (1976), and BASS samples the flow at nearly three times the rate of Gordon's instrument. These two characteristics allow increased resolution of high frequency events. The intermittency of the stress is easily seen, as is the negative correlation between u and w as reflected by the predominantly positive values of $-\rho uw$. When the individual velocity fluctuations were discussed, the time scales of 7 sec and 100 sec were mentioned as characteristic of the u fluctuations. The Reynolds stress trace shows high stress events (greater than 15 dynes/cm^2) with durations in the 6 to 7 second range; correlations over 100 seconds in duration are not observed on this plot, but the next set of high stress events happens 100 seconds later.

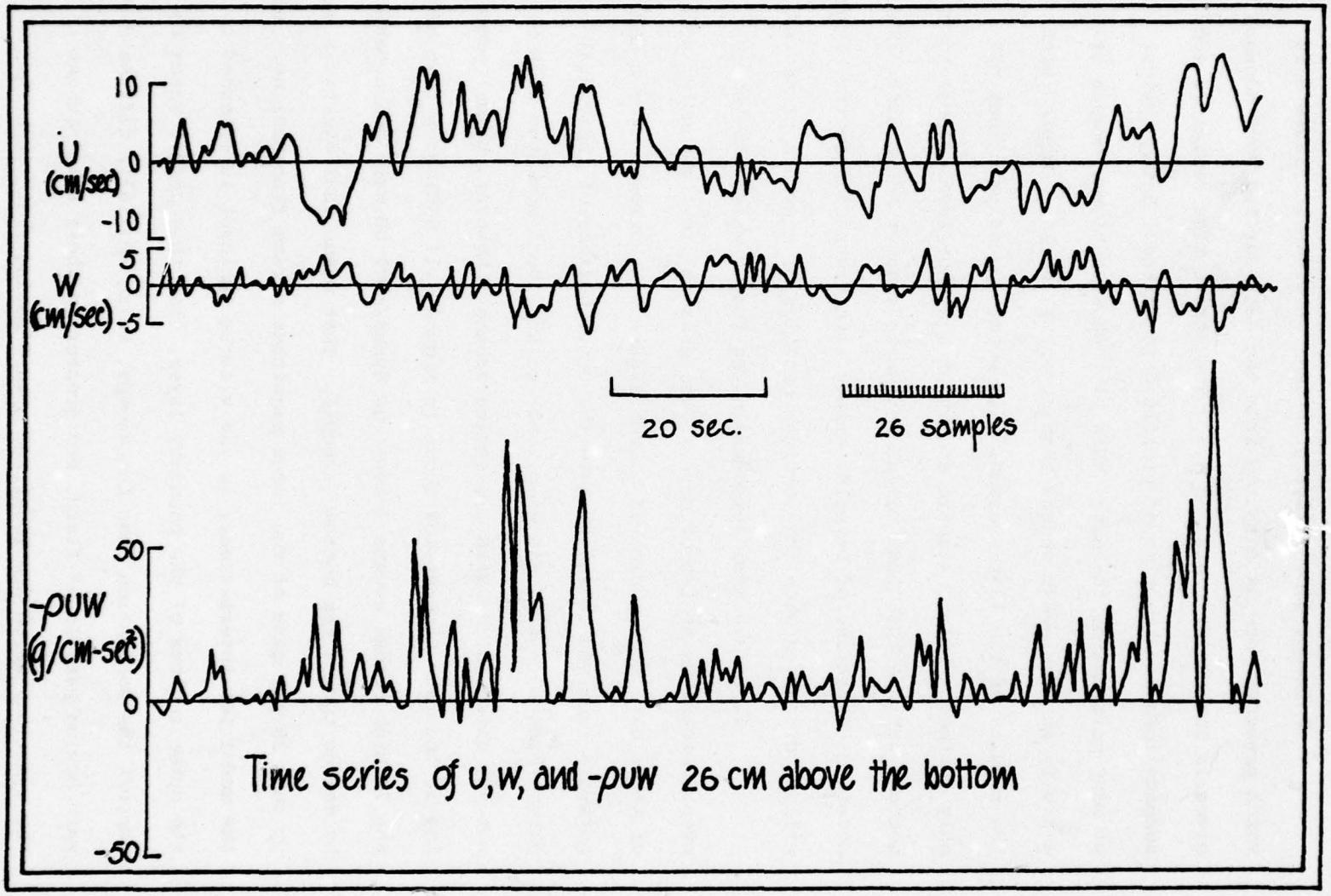

Time series of u, w, and -ρuw 26 cm above the bottom

Figure 4.13

A longer time series of stress is given in Figure 4.14 which presents $-\rho uw$ as computed from the data for the four sensors given in Figures 4.7, 4.8 and 4.9. The stress time series is 400 seconds long and the time of profile E is marked. Being typical of many portions of the data, this plot shows a higher degree of activity at the lowest sensor than at other levels. Coupled with the results of the last section, this seems to indicate that not only is the turbulent kinetic energy at a higher level closer to the bottom, but the turbulent momentum flux is greater there also. The detailed variations of Reynolds stress with distance from the bottom will be discussed when the vertical profiles of $-\rho\overline{uw}$ are presented.

There are some episodes in the traces which show stress events occurring at two or more of the sensors simultaneously; a few of these have been indicated in the figure with arrows. The complex software required to investigate the contributions of individual stress events (sweeps and ejections) to the total momentum flux does not yet exist in the BASS processing scheme. However, manual processing of the four time series shown in Figure 4.14 indicates that of the 70 high stress events ($-\rho uw > 30$ dynes/cm^2) 50 were characterized by motion toward the bottom (sweeps). That means that ejections made up only 28 per cent of the large magnitude stress fluctuations. If the model for intermittency in the viscous sublayer is extended to the outer regions of the boundary layer, then this result seems to support the contention that the sweeps, being spatially diffuse downward moving parcels of fluid, are greater in their areal extent than the ejections which are localized upward moving fluid jets; hence it

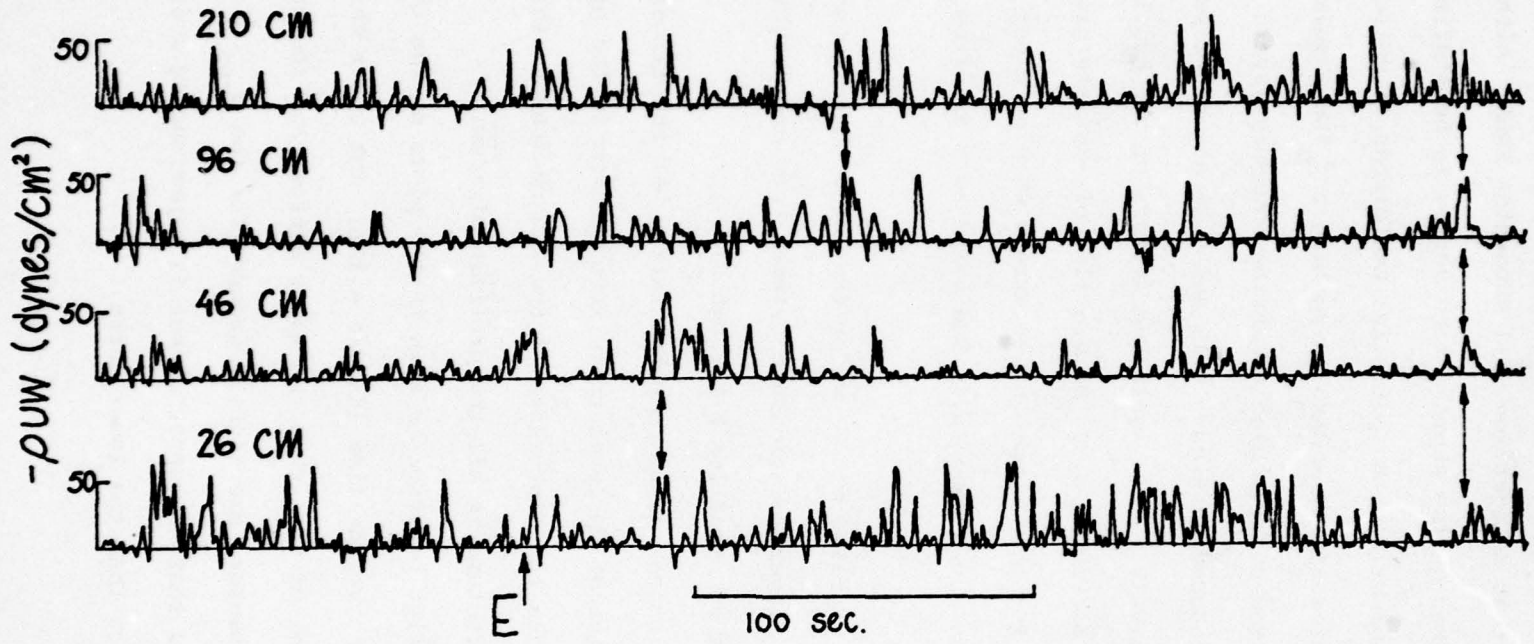

Time series of the -ρuw product at four points above the bottom

Figure 4.14

is less probable that an ejection will encounter BASS. Although this result is based on too short a time series to be statistically valid, it does demonstrate the potential usefulness of velocity fluctuation measurements from BASS in sorting out the problem of intermittency in the outer region of marine boundary layers.

Reproduced in Figure 4.15 and 4.16 are profiles of $-\rho\overline{uw}$ and $-\rho\overline{vw}$, respectively. Once again the letters of the profiles correspond to those of Figure 4.3. No profiles of $-\rho\overline{uv}$ are presented since the values for this component of stress were an order of magnitude less than the $-\rho\overline{uw}$ component. The error bars are from the analysis of error in Chapter II.

The profiles of $-\rho\overline{uw}$ for the lower three sensors indicate an approximately linear relationship between $-\rho\overline{uw}$ and height above the bed (at least for profiles B through G).

The sensor at 26 cm consistently has the largest value of stress while at the 96 cm level there is a minimum in the profiles. The Reynolds stress then increases at the 210 cm sensor; this increase is a persistent feature in all the profiles of $-\rho\overline{uw}$.

Similar behavior is seen in the plots of the rms values of the fluctuations versus time (Figure 4.10). The lower three sensors have higher values of u_{rms} than the upper sensor, and the curves for the lower three sensors are tightly grouped for the u_{rms} and w_{rms} curves suggesting that the upper sensor is experiencing a different type of turbulence than the lower three.

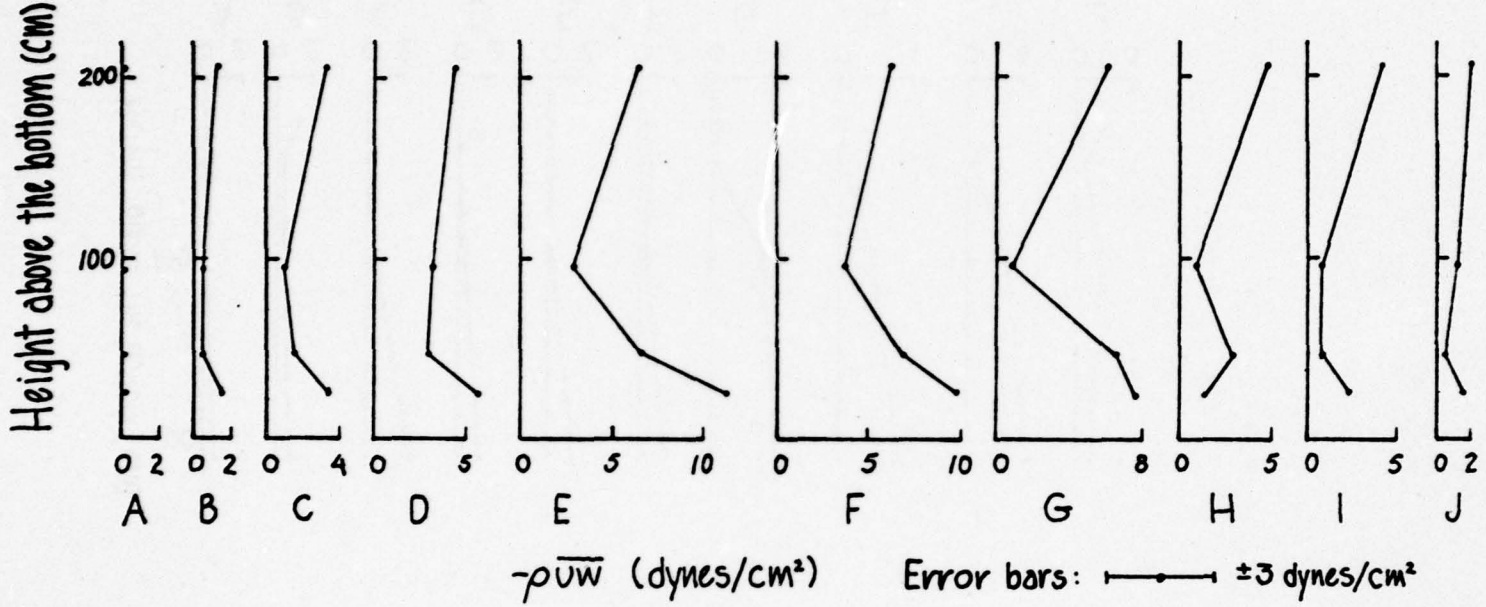

Profiles of $-\rho\overline{uw}$ Reynolds stress

Figure 4.15

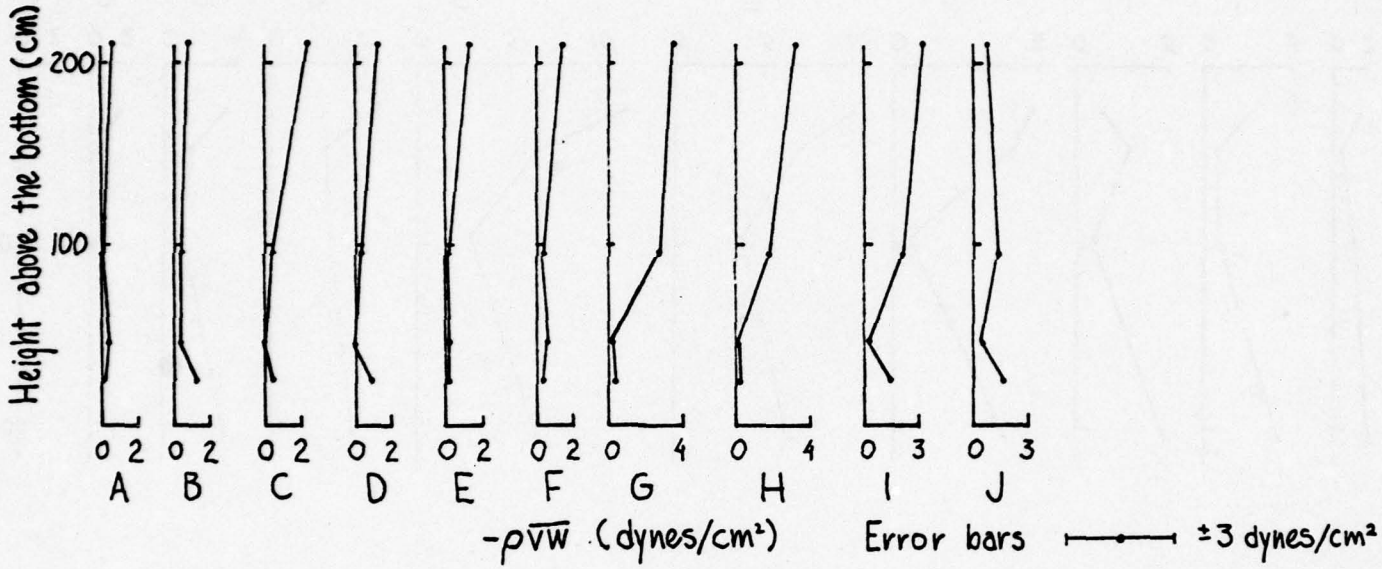

Profiles of $-\rho\overline{vw}$ Reynolds stress

Figure 4.16

Previously (in section 1.1) the constant stress layer assumption was invoked to derive the logarithmic velocity profile. It was assumed that in a steady, uniform, two dimensional shear flow over a flat bottom the stress should be nearly constant near the wall. For the experiment in Vineyard Sound described here, the conditions were hardly steady, uniform or over a flat bottom, and so it is not surprising that the stress is not constant at the heights above the bed where the measurements were made. In fact, the variability is slightly less than that predicted by the statistical analysis of Reynolds stress measurements done by Heathershaw and Simpson (1978). It is useful, however, to hypothesize as to the origins of the stress gradients shown in Figure 4.15.

The steady state Reynolds momentum equation given in Chapter I is:

$$\rho U_j \frac{\partial U_i}{\partial x_j} = \frac{\partial}{\partial x_j}\left[-p\delta_{ij} - \nu \frac{\partial U_i}{\partial x_j} - \rho \overline{u_i u_j}\right] \qquad (4.3)$$

Mean convection = pressure gradient + viscous stress + Reynolds stresses

The steady state equation is valid here if the rate of change of mean velocity with time is assumed to be zero during the averaging interval over which the time averages for Reynolds stress were taken.

Outside the boundary layer, the viscous and turbulent stresses can be neglected, and the overall flow in the tidal channel is governed by:

$$\frac{DU}{Dt} = -\frac{1}{\rho}\frac{\partial P}{\partial x}$$

For this large scale flow the frequency and wavelength of the tide are the scaling parameters.

Returning to equation (4.3) and applying it to the flow in the vicinity of the bottom, it is seen that viscous effects are small outside of the viscous sublayer, and hence the viscous stress terms $\nu \frac{\partial^2 U_i}{\partial x_j^2}$ can be neglected compared to the Reynolds stress terms. Equation 4.3 shows the pressure and Reynolds stress gradient terms balancing the convective term. Specifically, for two dimensional incompressible flow with zero mean vertical velocity (W = 0), equation (4.3) renders the horizontal momentum balance as:

$$\rho U \frac{\partial U}{\partial x} = - \frac{\partial P}{\partial x} - \rho \frac{\partial \overline{uw}}{\partial z} - \rho \frac{\partial \overline{u^2}}{\partial x} \qquad (4.4)$$

In order to determine the dominant terms in (4.4), the order of magnitude of each term must be found. This requires the identification of the scales of length and velocity in the flow. For a flat bottom with no stratification two velocity scales are apparent: U_∞, the mean flow just outside the boundary layer, can scale the horizontal flow in the streamwise direction, and u_*, the friction velocity, will be associated with turbulent motions in the boundary layer itself. Vertical distances can be scaled with the boundary layer thickness, δ, while horizontal distances associated with the rate of change of U_∞ downstream can be scaled with L where L, as defined by Tennekes and Lumley (1972) is:

$$L^{-1} \equiv \left| \frac{1}{U_\infty} \frac{\partial U_\infty}{\partial x} \right| \qquad (4.5)$$

For large Reynolds numbers, it can be assumed that $u_*/U_\infty << 1$ which implies that the bottom stress ρu_*^2 is small compared to ρU_∞^2. It is also assumed that the boundary layer thickness δ is small compared to the horizontal length scale L, that is $\delta/L << 1$.

The order of magnitude of each term in (4.4) can now be written:

$$\rho U \frac{\partial U}{\partial x} \sim O\left(\rho \frac{U_\infty^2}{L}\right) \qquad \text{convective effects}$$

$$\frac{\partial P}{\partial x} \sim O\left(\rho \frac{U_\infty^2}{L}\right) \qquad \text{pressure gradient} \qquad (4.6)$$

$$\rho \frac{\partial \overline{uw}}{\partial z} \sim O\left(\rho \frac{u_*^2}{\delta}\right) \qquad \text{Reynolds shear stress gradient}$$

$$\rho \frac{\partial (\overline{u^2})}{\partial x} \sim O\left(\rho \frac{u_*^2}{L}\right) \qquad \text{normal turbulent stress gradient}$$

The pressure term has been scaled with ρU_∞^2 by analogy to potential flow. The last term in (4.6) is negligible compared to the other Reynolds stress term since $\delta << L$; however, for an irregular bottom having large scale topography $\partial \overline{u^2}/\partial x$ would scale with u_*^2/ℓ where ℓ is related to the downstream influence of topographic features. If ℓ is of the same order as δ, then this term cannot be neglected. This case will be treated later in this section, but for now $\partial \overline{u^2}/\partial x$ will be considered small. This leaves three terms in the streamwise momentum balance.

$$\rho U \frac{\partial U}{\partial x} = -\frac{1}{\rho}\frac{\partial P}{\partial x} - \rho \frac{\partial \overline{uw}}{\partial z} \qquad (4.7)$$

Because of the assumptions regarding the scaling length ($\delta << L$) and scaling velocities ($u_* < U_\infty$), this balance only makes sense if the ratio $\frac{u_* L}{U_\infty \delta}$ remains of order 1, that is, the time scale of changes in the turbulence δ/u_* must reflect changes in the overall flow time scale L/U_∞.

Equation (4.7) is difficult to evaluate in the context of the BASS measurements since only one term, $\frac{\partial \overline{uw}}{\partial z}$, out of the three can be obtained from the data set. In addition, although the existence of an upstream topographic feature is likely, no bottom survey was taken, and so any arguments based on the presence of unknown topographic features must be considered speculation. It is important to note here that the pressure gradient in 4.8 is acting over the entire depth which means it can explain the decrease in stress with height above the bottom in the lower meter of the boundary layer, but it cannot explain the observed increase in turbulent stress in going from the one meter level to the two meter level.

Using profile E of Figure 4.15, the maximum value of the Reynolds stress gradient during the experiment is obtained:

$$\frac{\Delta \overline{uw}}{\Delta z} \simeq \frac{11.38 - 2.89}{26 - 96} = -0.12 \text{ cm/sec}^2$$

Under similar conditions in the Irish Sea, gradients of this magnitude have been measured (Heathershaw and Simpson, 1978).

These same workers found both positive and negative Reynolds stress gradients at various locations in the Irish Sea. Smith and McLean (1977) present even larger stress gradients for the flow in the Columbia River where the mean flow speed was ∿50 cm/sec; however, those measurements were clearly made in a field of sand waves.

It is instructive to see what kind of balance results from setting each of the three terms in (4.7) to zero. Neglecting the turbulent stress gradient yields the equation governing the overall large scale flow outside the boundary layer.

If the convective term is set equal to zero, then the stress gradient must balance the pressure gradient, that is,

$$\rho \frac{\partial \overline{uw}}{\partial z} = \frac{\partial P}{\partial x} \cong \rho g \frac{\partial h}{\partial x} \qquad (4.8)$$

where h is the water depth. In terms of the measured stress gradient, this would mean that $\frac{\partial h}{\partial x} = -1.2 \times 10^{-4}$ which corresponds to a sea surface elevation change of 12 cm in one kilometer. Very large accelerations of the overall flow would be produced by this surface slope, but there is no source for such a large elevation change in Vineyard Sound where $\frac{\partial h}{\partial x} \sim 10^{-5}$ is expected.

Assuming the pressure gradient to be negligible compared to the other terms in (4.7), there must be a balance between the Reynolds stress gradient term and the convective term:

$$\rho U \frac{\partial U}{\partial x} = \rho \frac{\partial \overline{uw}}{\partial z} \qquad (4.9)$$

For a mean velocity of 30 cm/sec, $\frac{\Delta U}{\Delta X}$ must be 4×10^{-3} sec^{-1} to balance the stress gradient term. This implies a change in velocity of 4 cm/sec in 10 meters of streamwise extent. One way this could happen is by a change in the geometry of the channel. For the velocity changes cited above this means that the bottom would have had a 13% slope at the deployment site. The divers reported no local slope near BASS, however, the possibility cannot be discounted without a detail survey. Figure 4.17 illustrates a possible bottom configuration for a 13% grade which the divers might have had difficulty discerning. Again, since U is the depth averaged velocity, this analysis, while explaining the magnitude of the stress gradient, does not explain the increase in stress in going from the sensor at 96 cm to the one at 210 cm.

It is physically unrealistic to imagine either the convective term or the pressure gradient term to be negligible in Equation (4.7), however, all the terms in the equation must be considered in terms of the averaging scales over which measurements are made. The pressure is an averaged quantity integrated over the water's depth, and the pressure gradient is usually measured over the largest scale in the flow. In contrast, the convective acceleration and Reynolds stress gradient are quantities highly dependent on the local geometry of the bottom. A small bump or depression in the sea floor ($\sim$1/2 m) causing a local pressure gradient would be reflected in the mean horizontal velocity gradient and in the Reynolds stress profile. The overall pressure gradient would hardly be affected if the bump was small compared to the depth. The stress gradients which were balanced

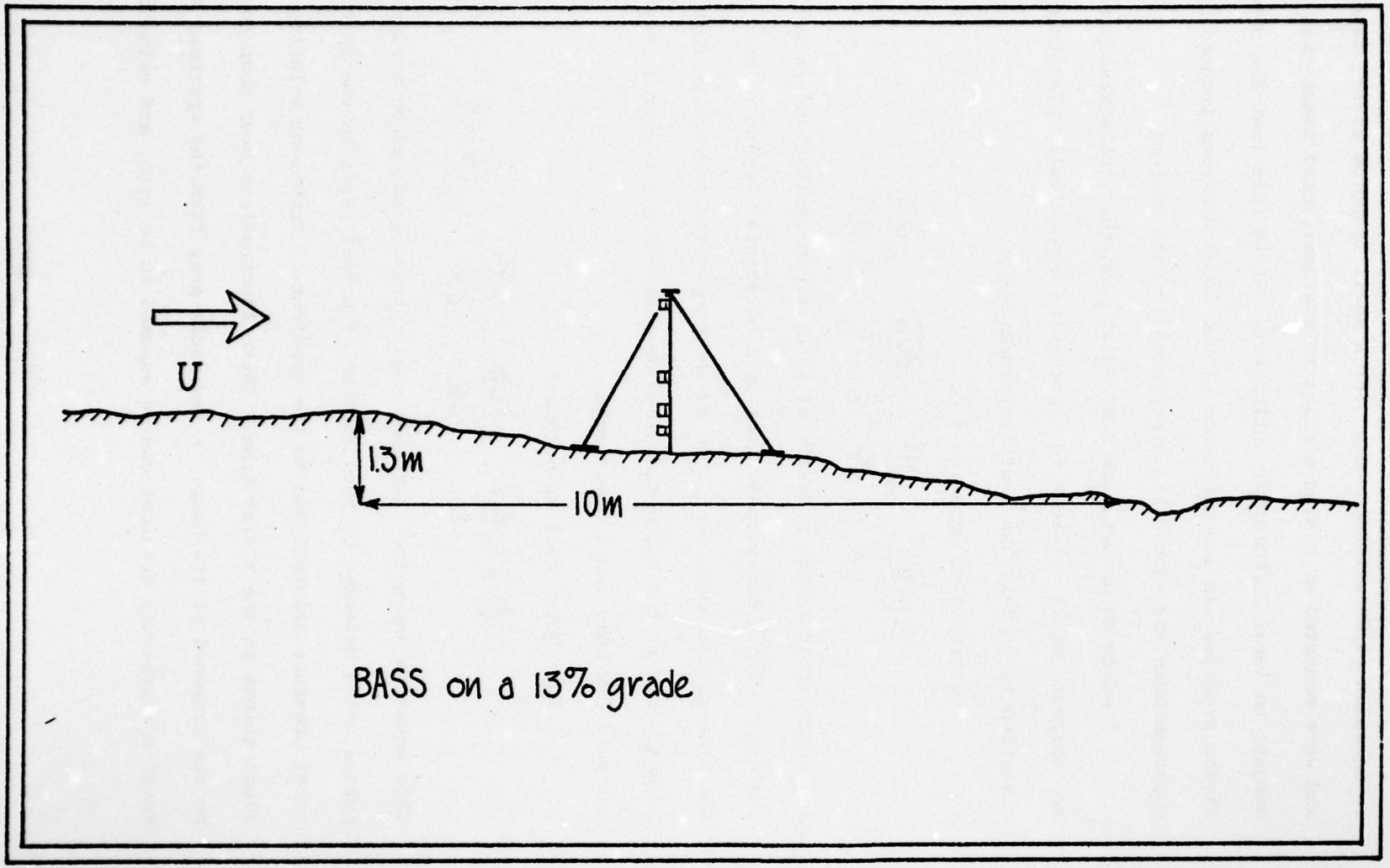

Figure 4.17

in Equation (4.7) extended only over a small fraction of the depth, and were measured at a single point in the horizontal plane thus being subject to local topographic influences. It is felt that the observed stress profiles are a consequence of the local dynamics induced by an upstream bump and should be interpreted in that context.

Assuming an upstream bump exists and that the stress profiles are correct, it is possible to hypothesize a physically plausible situation to explain the profiles dynamically.

Returning to Equation 4.4:

$$\rho U \frac{\partial U}{\partial x} = -\frac{\partial P}{\partial x} - \rho \frac{\partial \overline{uw}}{\partial z} - \rho \frac{\partial \overline{u^2}}{\partial x}$$

and noting that in the presence of an upstream feature $\partial \overline{u^2}/\partial x$ will scale not with L but with ℓ which is a horizontal length related to the flow disturbances generated by the bump. The convective term can be neglected if the assumption is made that $\partial U/\partial x = 0$ over a flat bottom a few bump radii downstream.

The above equation becomes:

$$0 = -\frac{\partial P}{\partial x} - \rho \frac{\partial \overline{uw}}{\partial z} - \frac{\partial \overline{u^2}}{\partial x} \qquad (4.10)$$

This equation shows the turbulent shear stress gradient on a fluid parcel being balanced by the gradient of normal stresses due to the local pressure gradient and to the gradient of turbulent velocity fluctuations in the x direction. These fluctuations have been enhanced by the presence of the bump. A few radii away from the upstream feature, the pressure gradient can be assumed to be zero, and using the

definition of Reynolds stress, $\tau = -\rho\overline{uw}$, the balance becomes

$$\frac{\partial \tau}{\partial z} = \rho \frac{\partial \overline{u^2}}{\partial x} \qquad (4.11)$$

indicating that both gradients must have the same sign.

From profile E of Figure 4.15, it is seen that the shear stress gradient is negative in the lower meter of the boundary layer, and positive from the one meter level to 2.1 meters. The gradient of the normal stress must balance this. Figure 4.18 illustrates how this might occur. The line labelled $\overline{u^2}_{max}$ can be considered the mean path of the eddies shed from the bump. Since the mean flow is changing slowly with time, it can be expected that the flow disturbances would follow this path in a fairly regular manner. From the figure it is seen that the gradients of the normal stresses are in the correct sense to balance the Reynolds stress gradients. The magnitude of the changes in normal stress with streamwise distance can be estimated by using the value of $\overline{u^2}$ at the current meter at 96 cm to be $\overline{u^2}_{max}$. From the plot of u_{rms} versus time in Figure 4.10, the curve for the sensor at 96 cm lies above the u_{rms} curves for the sensors at 46 cm and 210 cm. The sensor at 26 cm has the highest values of u_{rms} but it is influenced not only by the bump but also by locally generated bottom turbulence. For the sensor 96 cm above the bed $\overline{u^2}$ = 25 cm^2/sec^2 at the time of profile E.

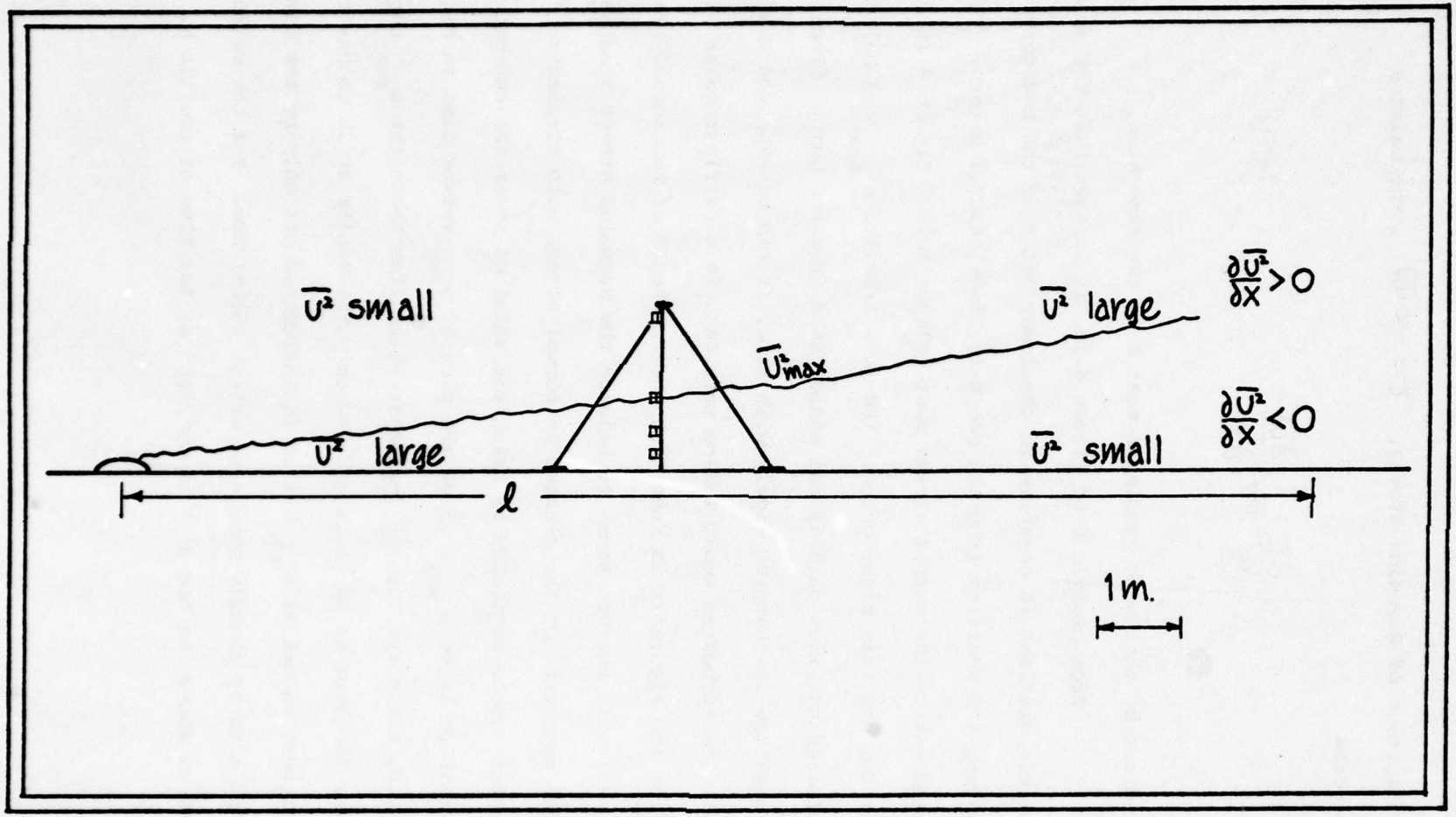
$\overline{u^2}$ small
$\overline{u^2}$ large
$\frac{\partial \overline{u^2}}{\partial x} > 0$
$\overline{u^2}_{max}$
$\frac{\partial \overline{u^2}}{\partial x} < 0$
$\overline{u^2}$ large
$\overline{u^2}$ small
ℓ
1m.

Figure 4.18

Equation 4.11 can now be used:

$$\frac{\Delta \tau}{\Delta z} = \rho \frac{\Delta \overline{u^2}}{\ell} = .012$$

Substituting $\Delta \overline{u^2} = 25$ cm^2/sec^2 yields a value of $\ell = 20$ meters which is a realistic length scale for the flow under consideration. In the next section it will be shown that the "average size" of the horizontal extent of the eddies computed from the autocorrelation of the time series is about 8 meters. Considering all the assumptions made in this analysis, these two numbers are relatively close.

Although the proposed situation as illustrated in Figure 4.18 is somewhat contrived, it does explain the observed profiles, but more importantly the analysis points out the necessity of sampling the flow in the horizontal plane as well as in the vertical.

Another approach for using the stress profiles is to assume that the average of the stresses measured by the lower three sensors is the Reynolds stress in the "constant" stress layer. Using $u_*^2 = - \overline{uw}$, the friction velocity can be calculated. Table 4.4 gives values of the average u_* in the lower meter. It was computed by assuming $u_*^2 = - \overline{uw}$ and averaging the three sensors.

TABLE 4.4

	A	B	C	D	E	F	G	H	I	J
U_* (CM/SEC) —	.90	1.36	1.71	2.63	2.58	2.17	1.29	1.18	1.02	

These values are slightly higher than those of Tables 4.1 and 4.2 which were calculated from the quadratic drag law and log profile method, respectively. The variations among the values in the three tables are probably due to the differences in averaging times used. Table 4.1 and 4.2 used the mean profiles which can be considered 34 minute averages while the Reynolds stresses were computed on a 10 minute average. Also, the log profile method used all four sensors; while only U_{96} was used for the drag law, and only the lower three values of $-\overline{uw}$ were used in the eddy correlation method.

Figure 4.19 shows plots of Reynolds stress versus mean velocity for all four sensors. Two things are apparent in the figure. Firstly, there is no significant hysteresis at any of the four levels. This is contrary to the results of Gordon (1975), but this lack of hysteresis has also been pointed out by Bowden et al (1959) and more recently by McCave (1973) and Bohlen (1977).

The second point of interest is the way in which the Reynolds stress at the 210 cm level varies almost linearly with mean current speed while the functional relationship between $-\rho\overline{uw}$ and U for the lower three measurement points does not seem to be linear at all. This again suggests a difference in the scaling of the processes

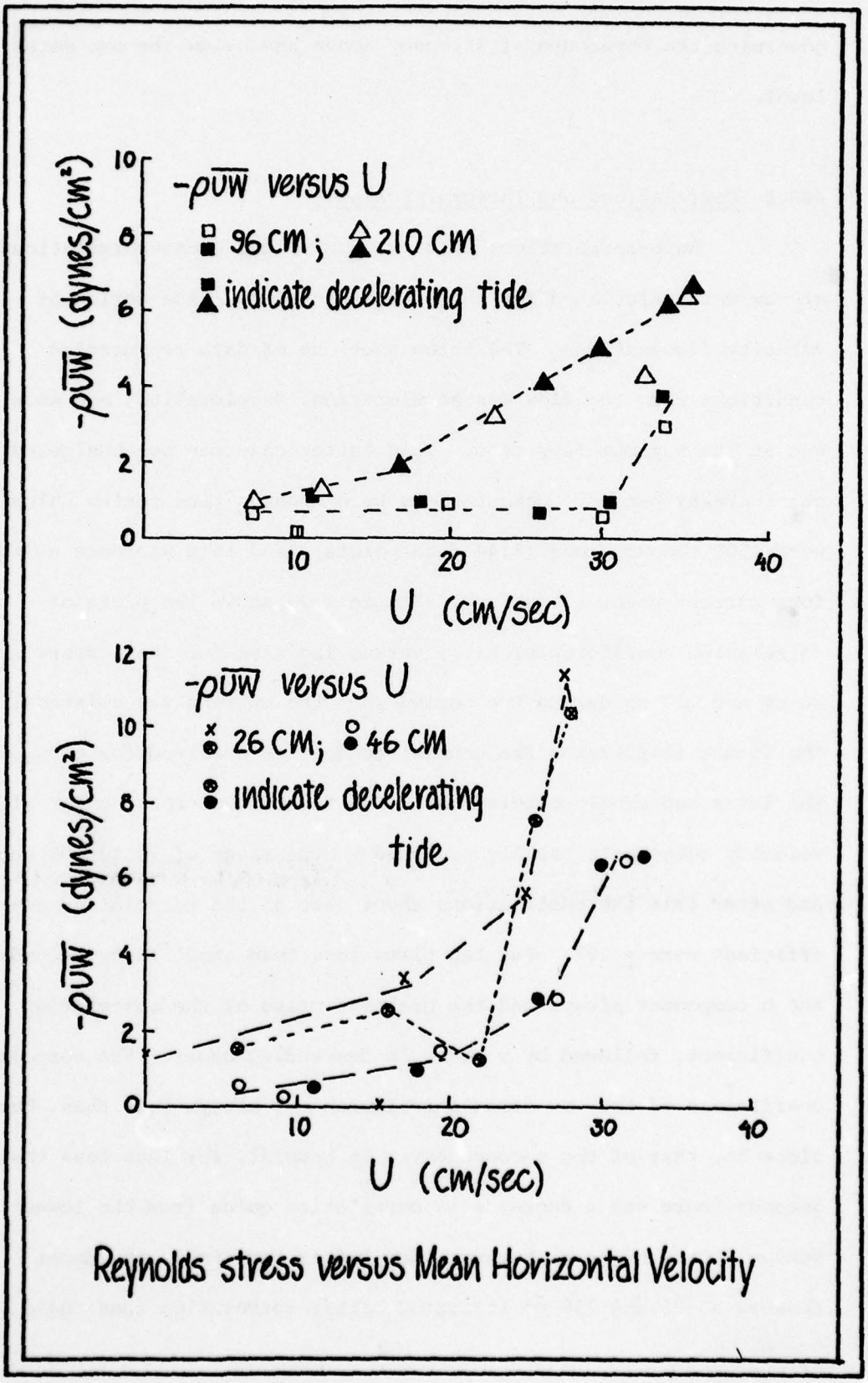

Reynolds stress versus Mean Horizontal Velocity

Figure 4.19

governing the structure of stresses above and below the one meter level.

4.3.3 Correlations and Integral Scales

Auto-correlations of u, v, and w, and cross-correlations of -uw were calculated for three segments of the time series of velocity fluctuations. The three sections of data represented conditions when the flow was accelerating, decelerating, and when it was at its maximum flow rate. This latter case can be considered a quasi-steady period. Computations were made on time series which were 4500 seconds long (6144 data points), and this was done at the four current meter elevations. Figure 4.20 shows two plots of correlation coefficients, $R(\tau)$, versus lag time for the sensors at 26 cm and 210 cm during the period when the current was swiftest. The figure illustrates the general tendencies observed for most of the auto- and cross-correlations. The first zero crossing for all velocity components usually occurred in the range of 70 to 100 seconds, and after this the oscillations about zero of the correlation coefficient were $\pm$ .07. For lag times less than about forty seconds, the u component always had the greatest value of the correlation coefficient, followed by v and w in descending order. The correlation coefficient of the -uw cross-correlation was always less than, but close to, that of the u-component. In general, for lags less than 10 seconds there was a decrease in correlation going from the lowest sensor to the highest; however, for longer lag times, the upper sensors at 96 and 210 cm indicated better correlation than those

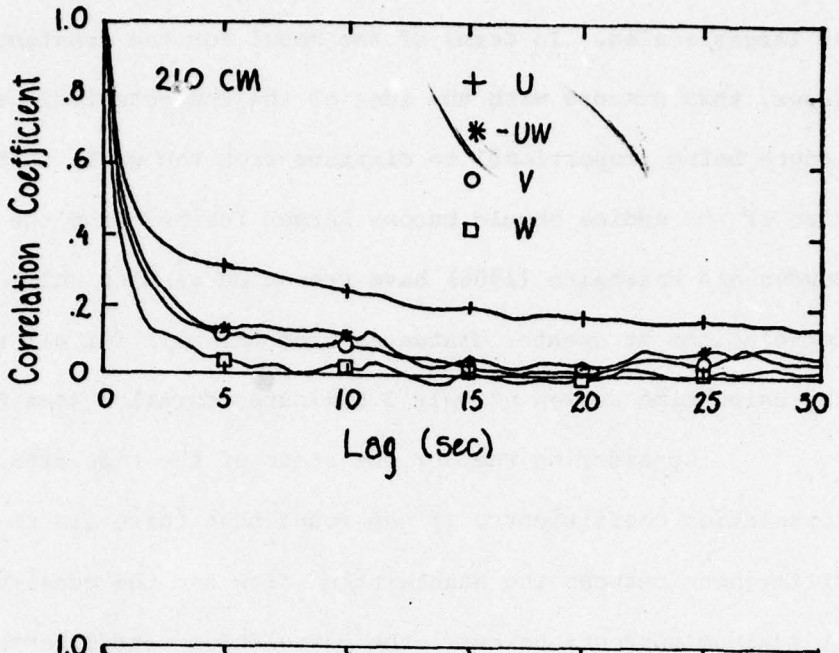

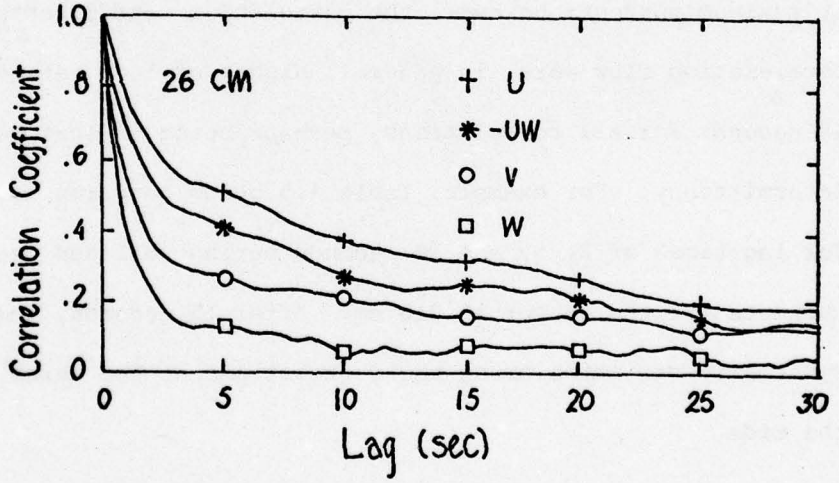

Correlation curves at 210 cm and 26 cm above the bottom

Figure 4.20

below, and this points to more organization in the flow structure at larger scales. In terms of the model for the constant stress layer, this concurs with the idea of the characteristic scaling length being proportional to distance from the wall; that is, the size of the eddies should become larger further from the wall. Bowden and Fairbairn (1956) have presented results which show higher correlations at greater distances from the wall for all values of lag using time series of only 3.5 minutes duration (see Figure 1.4).

Considering whether the state of the tide affects the correlation coefficients, it was found that there are no strong differences between the accelerating flow and the quasi-steady flow at maximum current; however, the correlation coefficients for the decelerating flow were, in general, higher at lags between 0 and 15 seconds for all correlations, perhaps being indicative of increased intermittency. For example, Table 4.5 below compares u, w, and -uw for lag times of 2, 5, and 10 seconds during full and decelerating currents for the sensor at 210 cm. After 15 seconds, there was no systematic variation among the correlations at the three stages of the tide.

Lag time (sec)	Full Tide			Decelerating Tide		
	R_u	R_{uw}	R_w	R_u	R_{uw}	R_w
2	.38	.30	.25	.50	.44	.31
5	.30	.15	.15	.47	.32	.22
15	.13	.05	.05	.25	.20	.10

TABLE 4.5

In Section 1, the concept of integral scale was introduced along with its definition; for example, the integral scale for the u-component is:

$$L_u = U\int_0^T R_u(\tau)\,d\tau$$

with U being the mean horizontal velocity, R being the correlation function and τ being lag time.

Recalling that the integral scales are measures of the characteristic eddy size (Tennekes and Lumley, (1972)), Figure 4.21 shows the functional relationship between integral scales and distance above the bottom. The values for the mean curves at the four heights in the figure are tabulated in Table 4.6.

TABLE 4.6

Height (cm)	L_u (m)	L_v (m)	L_w (m)
210	7.5	4.5	3.2
96	9.1	4.6	2.0
46	4.2	5.1	3.1
26	5.0	4.8	2.7
Mean	6.4	4.8	2.5

The values for L_v and L_w are relatively constant while L_u indicates two scales ~8.3 m and ~4.6 m with the larger scale occurring further from the wall. This last result also suggests the idea of two different scaling lengths governing the structure of turbulence

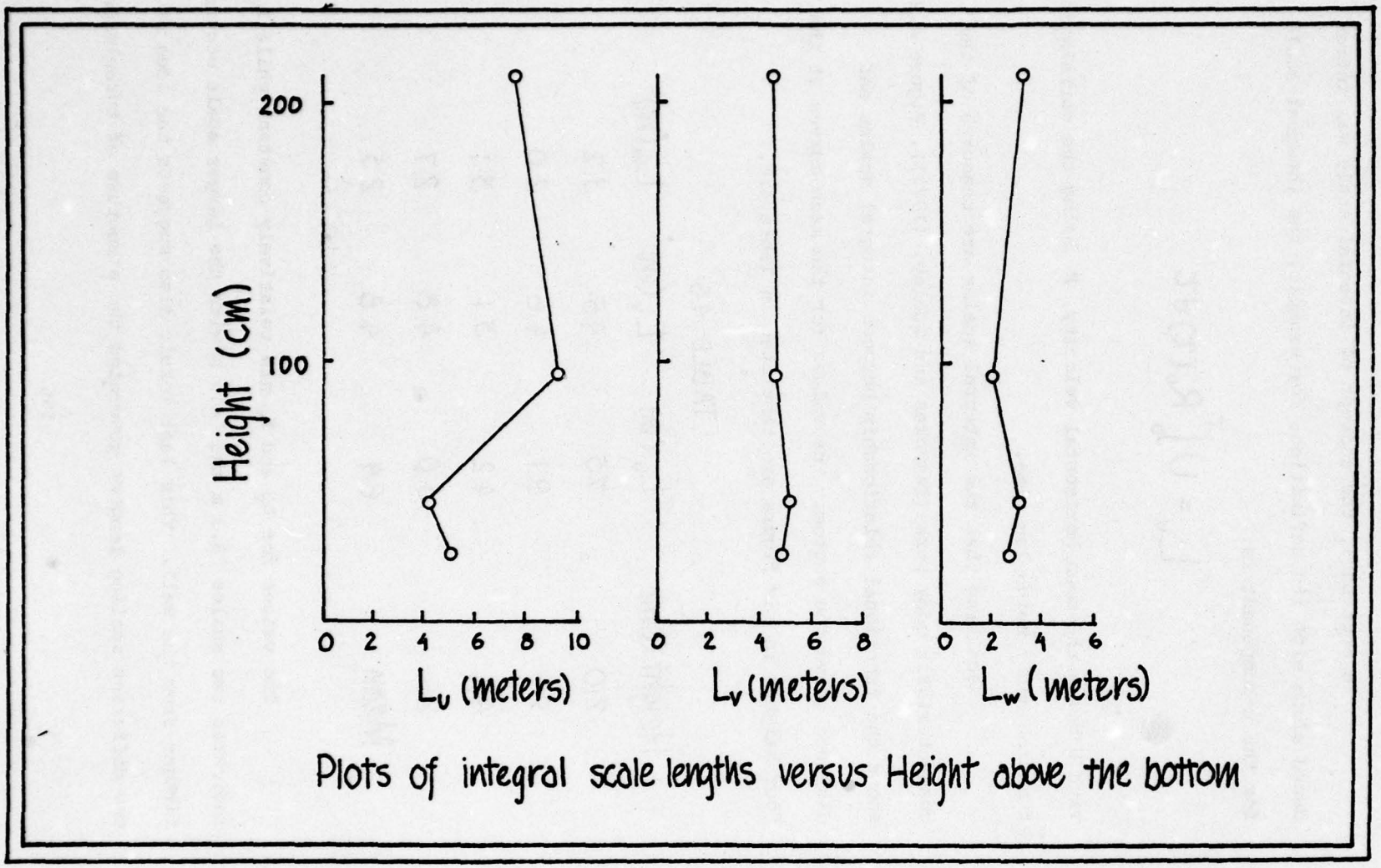
200
100
Height (cm)
0 2 4 6 8 10
L_u (meters)
0 2 4 6 8
L_v (meters)
0 2 4 6
L_w (meters)
Plots of integral scale lengths versus Height above the bottom

Figure 4.21

in the lower two meters. The value of L_w = 2.7 at 26 cm above the bottom suggests that simple mixing length arguments which generate the log profile might be invalid in a flow in which multiple length scales exist.

4.4 Alternative Validation of Reynolds stress Measurements

The preceding sections of this chapter have been devoted to an analysis of the measurements made by BASS in Vineyard Sound. The measurements have been presented to demonstrate the usefulness and capabilities of BASS as a tool for studying marine boundary layers. The response of the sensors to mean flows has been demonstrated in the tow tank, however, validation of the measured Reynolds stresses has not been possible for lack of an independent means of measuring these stresses. It is the purpose of this section to discuss alternative approaches which might be used to give an independent confirmation of the Reynolds stress measurements made by BASS. The experiments considered here have not been executed because of the constraints of time, economics, and availability of facilities and equipment. They will serve, however, as a basis for future work in investigating both the acoustic travel time sensors and the nature of the computations involved with Reynolds stresses.

Traditionally, the way to verify a new measurement system is to use it to measure a known quantity. Unfortunately Reynolds stresses, being terms in a turbulence model, are only predictable to the extent to which the model correctly represents the actual flow. Influencing factors not considered in the model could have a marked effect on the measured Reynolds stresses in a given situation. Because of possible unknown influences on the flow, it is difficult to predict the value of the Reynolds stress at a given location in a large flume or water tunnel. Validation of

Reynolds stress sensors in such a facility would be impractical because of the difficulties in differentiating among the effects of the model, the unknown influences in the flow, and the measurement characteristics of the sensor itself.

An alternative to this approach of verifying a new measurement technique is to adequately validate all the elements used in the derivation of the measurement under the assumption that the superposition of the elements does not add an unknown effect. This is the tack taken here.

Calibration experiments in a flume have been used to confirm the directional response of the BASS sensor to mean currents (as discussed in Chapter II). In order to better understand its performance as a stress sensor, the sensor's response to flows which fluctuate in a known manner must be checked.

Caution should be exercised in performing this type of verification because several effects can be present due to an unsteady flow which do not occur in the steady flow case. The structure of the sensor may induce flow disturbances which could cause the response to fluctuations to be different from the steady flow response. The individual measurement axes are serviced sequentially, and the time delay between measurements (30 ms) could produce phase shifts in an unsteady flow which affect the correlation of the u and w components. Fortunately, it is a relatively simple matter to perform tow tank tests to see the magnitude of these effects.

A method to test the phase response of the acoustic travel time sensor is to perform a tow tank experiment in which the sensor is oscillated in the tank. By orienting the sensor in such a way that the sensor's vertical axis is tilted at a 45° angle to the horizontal axis of the tank, the u and w axes of the sensor will be at 45° to the horizontal, and the response of these axes to horizontal flows should be the same in magnitude but of opposite sign (see Figure 4.22). The envisioned experiment could use the Woods Hole Tow Tank/Flume (20m x 1m x 1m) as the test facility. Various frequencies of oscillation will be used; the point being that the correlation between u and w should be independent of frequency. The ratio of the measured $\overline{uw}$ product to the mean squared horizontal velocity of the oscillating sensor should be a constant, that is,

$$\frac{\overline{uw}}{V^2} = \frac{(V \sin 45°)\ (-V \cos 45°)}{V^2} = -.5$$

The acoustic travel time sensor is a volume averaging device, and it should therefore be insensitive to turbulent motions which have characteristic eddy size smaller than the 15 cm averaging scale of the sensor. This small-scale turbulence insensitivity can be verified in flume experiments in which grids of various mesh spacings are positioned upstream of the sensor. Calculations of $\overline{uw}$ and of the spectra of fluctuating velocity components will show the effects, if any, of small scale turbulence on the stress measurements.

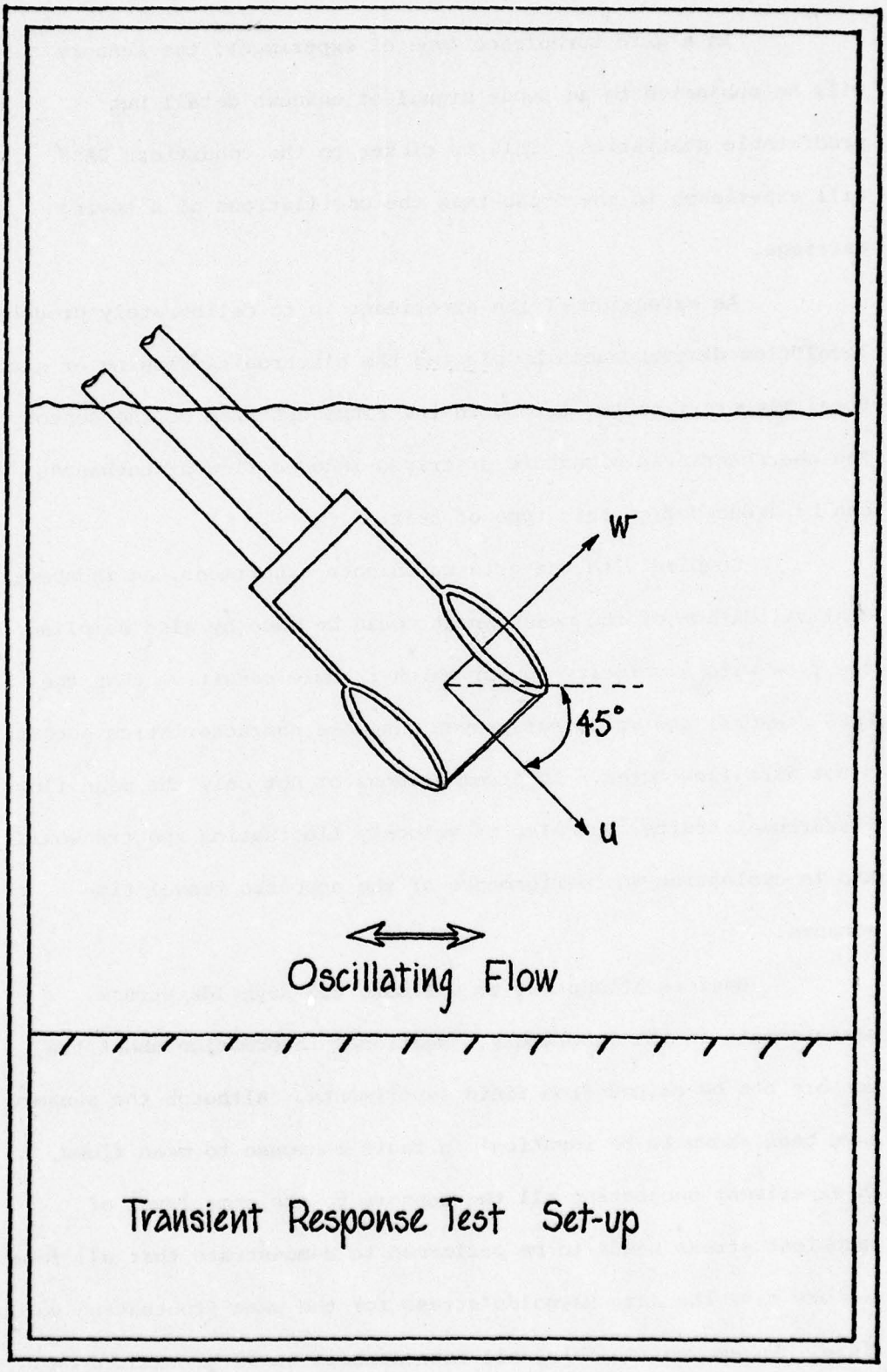

Figure 4.22

In a grid turbulence type of experiment, the sensors will be subjected to an input signal of unknown detail but predictable statistics. This is closer to the conditions BASS will experience in the ocean than the oscillations of a towing carriage.

An extension of the experiment is to deliberately produce local flow disturbuances by placing the electronics housing or structural members from the tripod in the flume upstream of the sensor. The characteristic signature of tripod-induced flow disturbances can be deduced from this type of test.

Coupled with the grid turbulence experiment, an independent validation of the measurement could be made by also sampling the flow with a velocity sensor which is more sensitive than the BASS sensors, and which has proven response characteristics such as a hot wire flow meter. Intercomparisons of not only the mean flow measurement traits, but also of velocity fluctuation spectra would aid in evaluating the performance of the acoustic travel time sensors.

Besides attempting to validate the Reynolds stress measurements in the laboratory, additional information about the sensors can be gained from field experiments. Although the sensors have been shown to be identical in their response to mean flows, an experiment subjecting all the sensors to the same level of turbulent stress needs to be performed to demonstrate that all four sensors give the same Reynolds stress for the same fluctuating velocity field. To accomplish this, all four sensors could be mounted on a

horizontal staff so that there is a 50 cm spacing between sensors. The staff would then be attached to the BASS tripod to monitor the flow one meter above the bottom. The experimental site should be similar to the site in Vineyard Sound, that is, a channel-like flow over a relatively flat bottom. In light of the results presented earlier in this chapter concerning the effects of unknown bottom topography, it is essential that all future field experiments include a detailed topographical survey of the deployment site.

Upon deployment, divers should orient the staff to be perpendicular to the mean velocity. In this way all the sensors will be measuring approximately the same velocity field at identical distances above the seabed. As an independent check, another velocity sensor using a different measuring technique (hot wire or electromagnetic current sensors) could be attached to the staff in order to make comparisons of the Reynolds stress measurements made by the different techniques.

Obviously, the success of such an experiment relies heavily on the assumption of horizontal homogeneity of the turbulence in the flow. It is critical to ensure that there are no upstream disturbances from either the tripod or features on the bottom which might give rise to horizontal inhomogeneities in the flow. The dependence on the assumption of spatial homogeneity can be reduced if the positions of the sensors were to be permuted during deployment. The problem would then be one of assuming temporal stationarity which should be valid over short time invervals (< 15 minutes). Changing

the positions of the sensors in a strong current will be a difficult task for divers. A viable alternative might be to permute the sensors in a large flume.

To summarize, in this section laboratory and field experiments have been proposed to confirm the performance of BASS as a Reynolds stress sensor. The laboratory experiments, using a tow tank and flume have been designed to establish the response of the sensors to unsteady flows and differing scales of turbulence. Additional flume experiments will then intercompare the acoustic travel time sensor with another velocity sensor which is above reproach in its transient response performance. Flow disturbances will be introduced upstream of the sensors in order to obtain baseline data for distances caused by the structure of the BASS tripod itself. In conjunction with these laboratory experiments, a field experiment has been proposed which, besides comparing the acoustic sensors with a more sensitive sensor, will intercompare the individual BASS sensors to confirm that they give the same value of Reynolds stress when subjected to the same flow field. It is felt that by executing these two classes of experiments, a better understanding can be gained of the errors involved in the measurement technique, and thus more confidence can be expressed for the results obtained from BASS data.

CHAPTER 5

SUMMARY AND CONCLUSIONS

5.1 BASS

The major goal of this research has been to develop instrumentation capable of making superior measurements of the velocity structure in a marine boundary layer. The data from BASS is the test of the accomplishment of this goal; the instrument performed its task well, and provided both mean vector velocity profiles and measurements of the Reynolds stress and turbulent fluctuations near the bottom in Vineyard Sound. In its maiden sea-trial, fifteen out of sixteen of the acoustic axes on BASS worked faultlessly. Since each sensor contains a redundant axis, the failure of one axis did not affect the capability of resolving the velocity vector into three rectangular components. The zero offsets were not determined before the experiment and had to be adjusted after the fact by forcing a zero vertical mean velocity and a log profile at maximum ebb. Both of these growing pains were eliminated in a recent deployment of BASS. In situ measurements of the zero point were obtained by covering the current meters with floodable plastic bags to simulate the no-flow condition in the working environment; the bags were subsequently removed, and velocity data collection was initiated.

The data collected in this field study demonstrate some key points which were not accessible with previous instrumentation.

These are:

- Measurements of u, v, and w, are required for the calculation of the intensity of turbulent kinetic energy ($\rho q^2/2$). The assumption used by Gordon (1975) of $\overline{v^2} = .5\ \overline{u^2}$ was shown to underestimate $\overline{v^2}$ by nearly 40%.

- Measurements of Reynolds stress must be made at a number of points above the bottom in order to show the variation of these apparent stresses with height above the solid boundary. Also, from vertically separated measurements of stress, the effects of multiple length scales in the flow can be better understood.

- Simultaneous measurements at four points above the bottom showed that high Reynolds stress events sometimes occurred at all four sensor locations at the same time, indicating the spatial extent of the flow's intermittency.

- Faster sampling rates and reduced noise in the acoustic travel time sensors provide a clearer picture of the structure of high frequency Reynolds stress events.

All of the sensors and components for BASS have been designed and tested for deep ocean experiments, and the successful measurements described in this study are an important first step in paving the way for deep sea studies of the benthic boundary layer. The experience gained in successfully handling the rather awkward tripod from a small vessel should aid in the future deployments from a rolling ship. Future work will include a frame with less flow disturbance.

5.2 The Mean Flow

The six hour time series of velocity at the four current meter locations in the lower two meters provided mean velocity profiles

for half of a tidal cycle. The experiment showed that the logarithmic velocity profile was a prevalent feature of the boundary layer, however, it was sometimes deformed owing to the unsteadiness of the flow or possibly the disruption of the flow by large scale upstream topographic features.

From the slopes of the logarithmic profiles the mean friction velocity, u_*, for the period when the boundary layer was fully developed, was found to be 1.60 cm/sec; while the value of 1.56 cm/sec for u_* was obtained by using an estimate of the drag coefficient for the conditions in Vineyard Sound and then applying a quadratic drag law. The logarithmic profile approach also rendered roughness height, k_b, commensurate with the 1 cm diameter pebbles observed by divers.

5.3 Velocity Fluctuations and Reynolds Stress

Examination of the velocity records from BASS showed the complexity of the motions in the boundary layer. The levels of the u, v, and w velocity fluctuations increase with increasing tidal velocity at all four levels above the bottom, reaching their maximum rms values when the current was the strongest. The relative rms amplitudes of the streamwise and cross-stream fluctuations were about equal, but the vertical rms value was half as large as either horizontal component. The lowest sensor tended to have the highest value of u_{rms}; the upper sensor having the lowest for a given point in time. This is interpreted as being a consequence of the production

of turbulence near the sea floor due to the increased velocity shear. Calculations of the intensity of turbulent kinetic energy also suggest this conclusion.

One of the surprising results which emerged from the calculation of the Reynolds stresses was the way in which the magnitude of ρuw would go through periods of relatively mild fluctuations, and then suddenly the fluctuations of the stress would become violent. These intermittent episodes alternated in time, but if the corresponding u and w signals were viewed without reference to the uw product, it was difficult to notice from the individual velocity fluctuations any difference between the quiet and the tumultuous periods of stress fluctuations.

The intermittency of the stress was quite noticeable, and by analyzing a 400-second portion of the record at all four levels, it was found that the mean duration of high stress events ($-\rho uw > 30$ dynes/cm^2) was 5 seconds and that more than 70% of these events could be classified as sweeps rather than ejections. This latter result can be explained by the more diffuse areal extent of sweeps in contrast to the localized nature of the ejections.

The profiles of Reynolds stress indicated that the flow which was sampled in Vineyard Sound was governed by two scale lengths - the smaller affecting the velocity structure in the lower meter of water, and the larger reducing the stress in the lower layer and influencing the upper reaches of the boundary layer. The former is thought to be due to the local bottom roughness; while it is speculated

that the latter stems from a larger roughness length associated with topographic protrusions upstream of the experimental site.

The Reynolds stress profiles also showed that the largest stresses occurred at the lowest sensor, and that the magnitude of the turbulent stresses tracked the speed of the tidal current. At its maximum, the bottom stress, τ_b, reached a value of almost 14 dynes/cm^2 as calculated by extrapolating the results of the Reynolds stress calculations to the sea bed. The error bars for the stress measurements from BASS were ±3 dynes/cm^2. It is no wonder that the bed at the site of the experiment consists of coarse pebbles bonded together with a biological armor - all lighter materials are swept away with each tide. The mean value of u_* from the Reynolds stress measurements in the lower meter was 1.9 cm/sec.

The results from one-half tidal cycle presented here show no hystersis in Reynolds stress in relation to favorable or adverse pressure gradients. However, the results for the intensity of turbulent kinetic energy do hint at the possibility of such a phenomenon especially in the region very close to the bottom.

Perhaps the most important result from the stress profiles measured by BASS is the limited usefulness of making stress measurements at one location in the horizontal plane if the bottom has topographic features. The topography and gradients of both the mean and fluctuating components of velocity must be measured to properly interpret the profiles of Reynolds stress.

Calculations of auto- and cross-correlations of the velocity fluctuations indicated that the correlation coefficients for lag times less than 10 seconds were higher at the lower current sensors; while for longer lag times, the upper two sensors showed larger correlation coefficients indicating the occurrence of larger eddies at increasing distances from the wall. This agrees with the mixing length assumption used to derive the logarithmic profile in that there are increasingly larger eddies as the distance from the solid boundary is increased; however, the magnitude of the integral scales calculated from the data seem to suggest that multiple length scales were present which would invalidate the mixing length approach.

Finally, much of the personal satisfaction derived from this research has come from playing a major role in providing the oceanographic community with an instrument capable of confidently probing the structure of bottom boundary layers, and it is hoped that the results presented here will aid others in their attempt to unravel the intricacies of boundary layers in the sea.

APPENDIX A

Response curves for a single acoustic axis

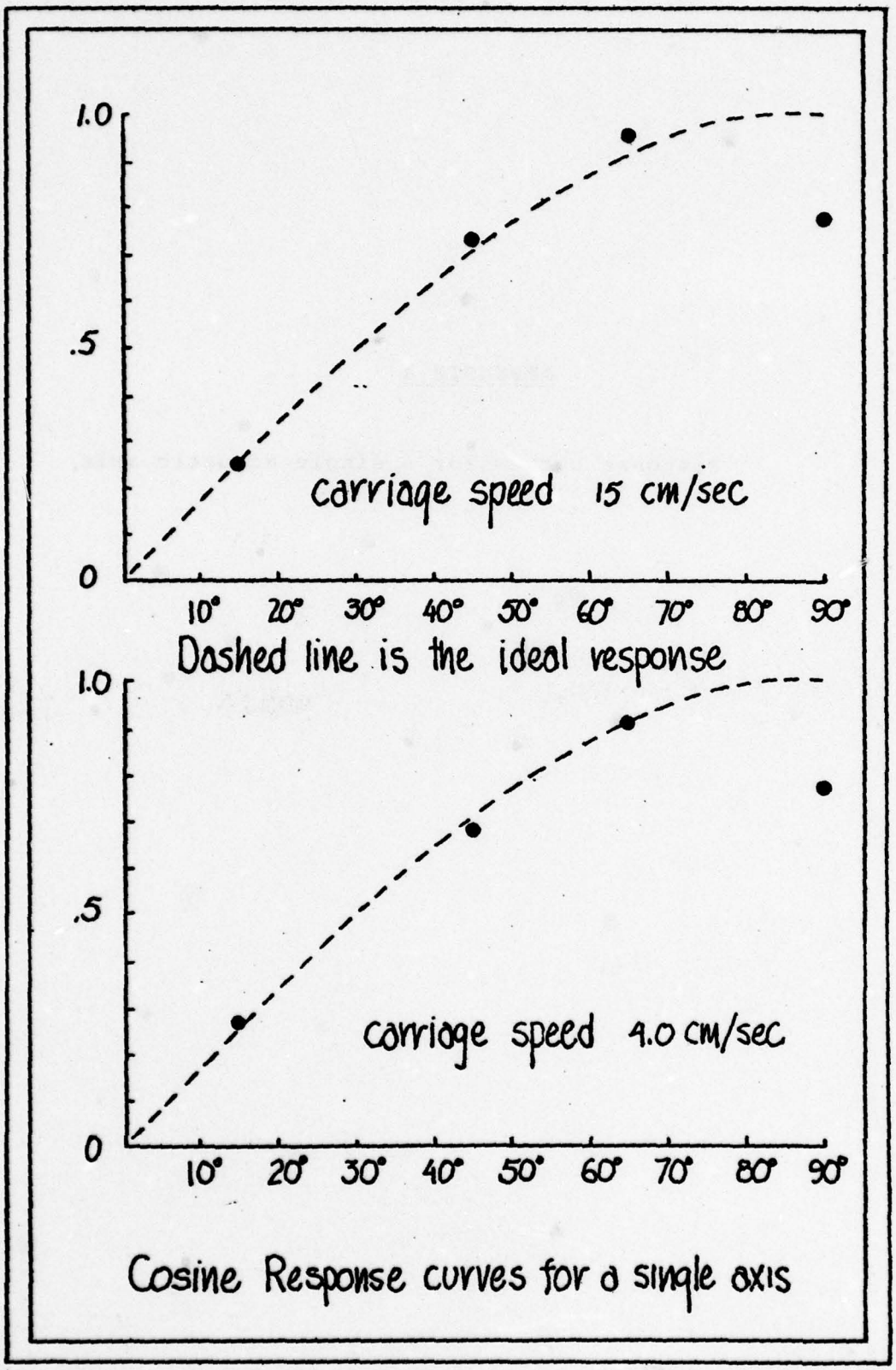

Cosine Response curves for a single axis

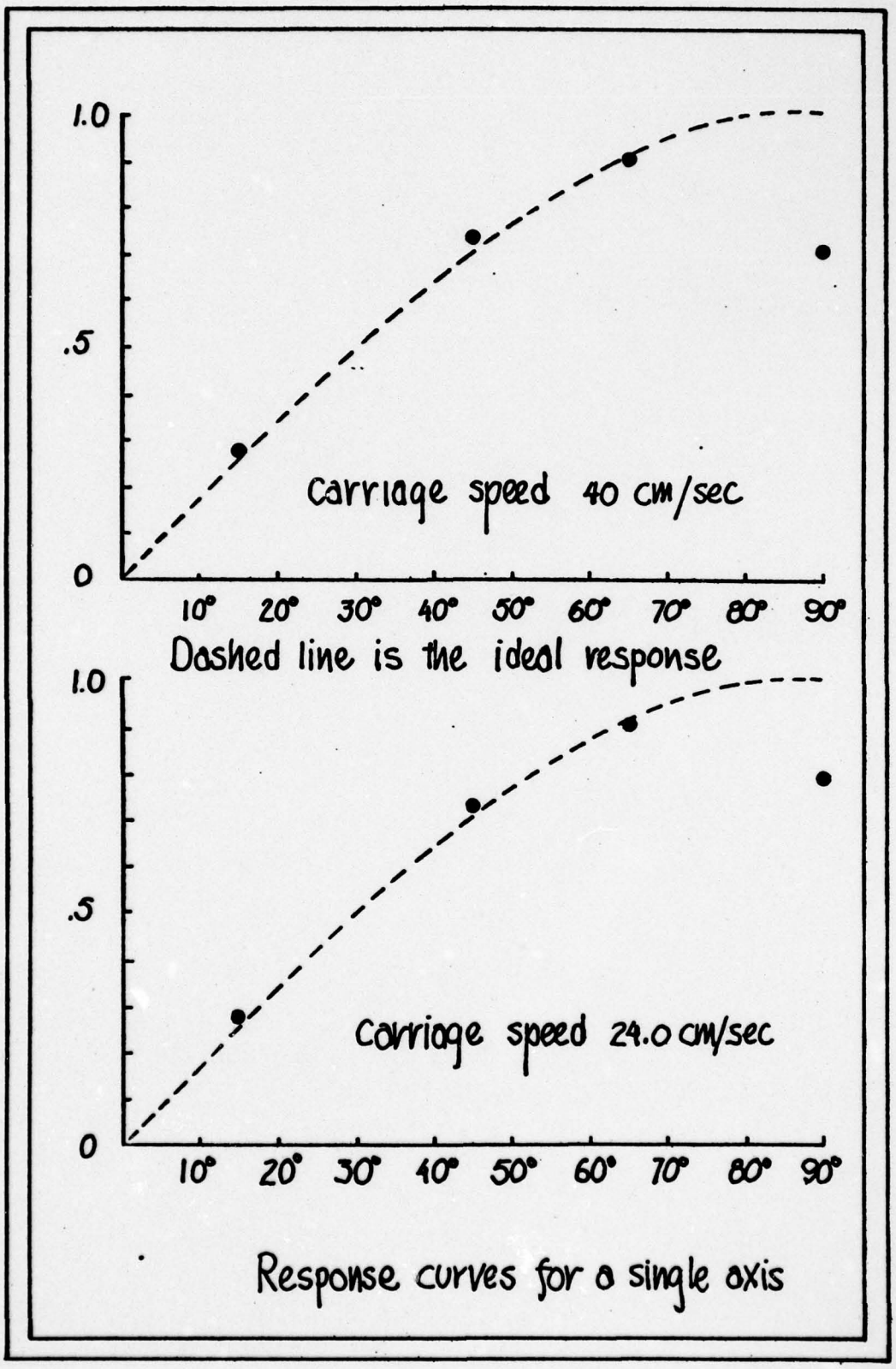

Response curves for a single axis

APPENDIX B

BASS Schematics

B.1 Transmit Board

B.2 Receiver Board

B.3 MUX Board

B.4 Selection Board

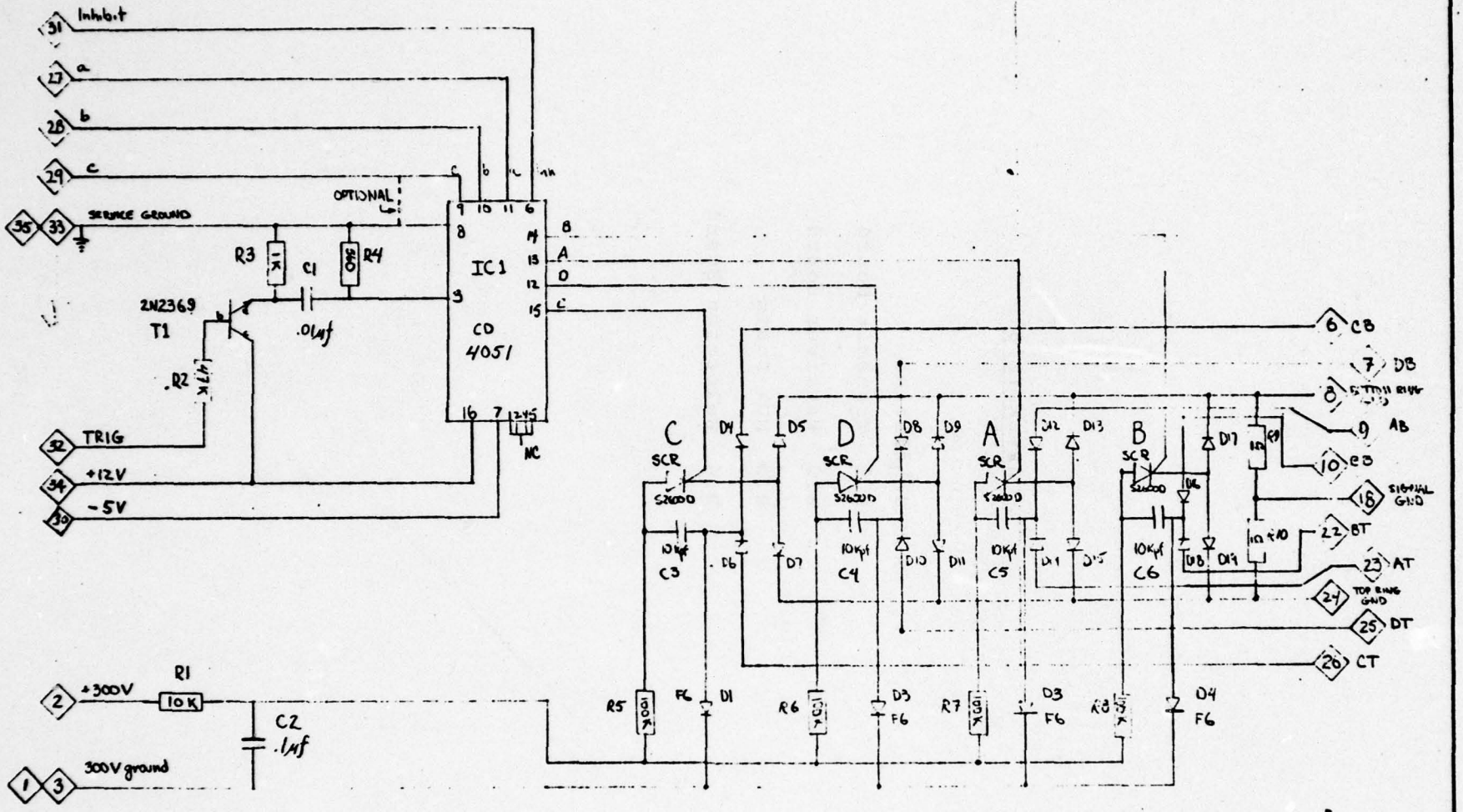

WOODS HOLE OCEANOGRAPHIC INSTITUTION WOODS HOLE, MASS. 02543	TITLE BASS XMTR 001
PROJ. BASS BY JCT	
SHEET ____ OF ____ DATE 25 FEB	

APPENDIX C

Proof that the travel time difference is independent of acoustic path

(Williams, personal communication)

Due to refraction by velocity shear, the acoustic path between the transducers is not in gereral the geometric path. However, the reciprocal acoustic path is the same so the line integral to follow is the same for the two directions with only the sign of dl and the limits of integration reversed.

$$t_1 = \int_A^B \frac{d\vec{\ell}}{\left(c - \frac{\vec{v}\cdot d\vec{\ell}}{|d\vec{\ell}|}\right)}$$

$$t_2 = \int_B^A \frac{d\vec{\ell}}{c - \frac{\vec{v}\cdot d\vec{\ell}}{|d\vec{\ell}|}} = \int_A^B \frac{d\vec{\ell}}{c + \frac{\vec{v}\cdot d\vec{\ell}}{|d\vec{\ell}|}}$$

$$t_1 - t_2 = \int_A^B \left[\frac{1}{\left(c - \frac{\vec{v}\cdot d\vec{\ell}}{|d\vec{\ell}|}\right.} - \frac{1}{c + \frac{\vec{v}\cdot d\vec{\ell}}{|d\vec{\ell}|}}\right] d\vec{\ell}$$

$$= \int_A^B \left[\frac{\left(c + \frac{\vec{v}\cdot d\vec{\ell}}{|d\vec{\ell}|}\right) - \left(c - \frac{\vec{v}\cdot d\vec{\ell}}{|d\vec{\ell}|}\right.}{c^2 - \left(\frac{\vec{v}\cdot d\vec{\ell}}{d\vec{\ell}}\right)^2}\right] d\vec{\ell}$$

$$\delta t = t_1 - t_2 = \int_A^B \left[\frac{2\,\frac{\vec{v}\cdot d\vec{\ell}}{d\vec{\ell}}}{c^2 - \left(\frac{\vec{v}\cdot d\vec{\ell}}{|d\vec{\ell}|}\right)^2}\right] dl$$

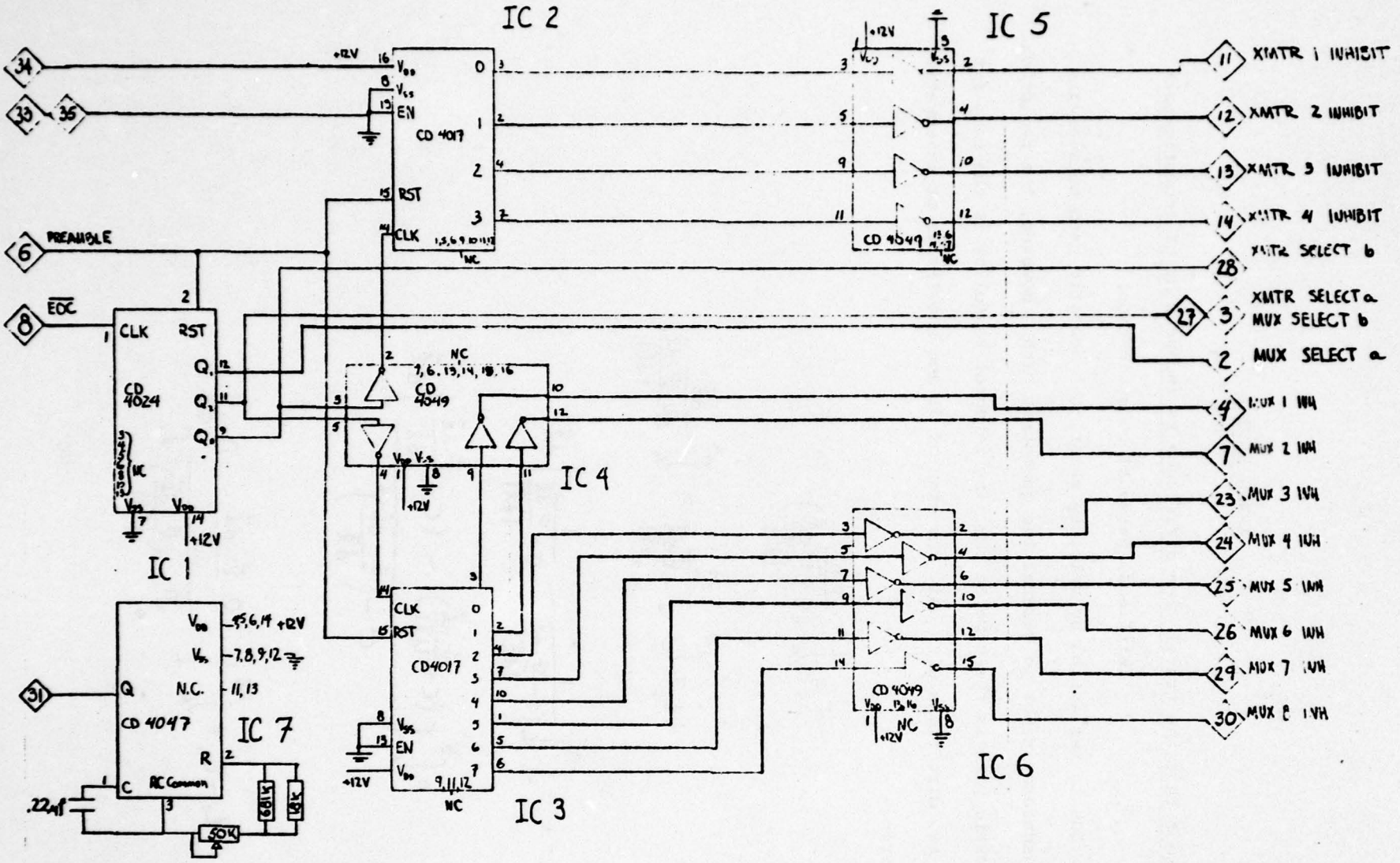

WOODS HOLE OCEANOGRAPHIC INSTITUTION WOODS HOLE, MASS. 02543	TITLE SELECTION BOARD
PROJ. PMS BY JST	
SHEET ____ OF ____ DATE 26 Feb 77	

177

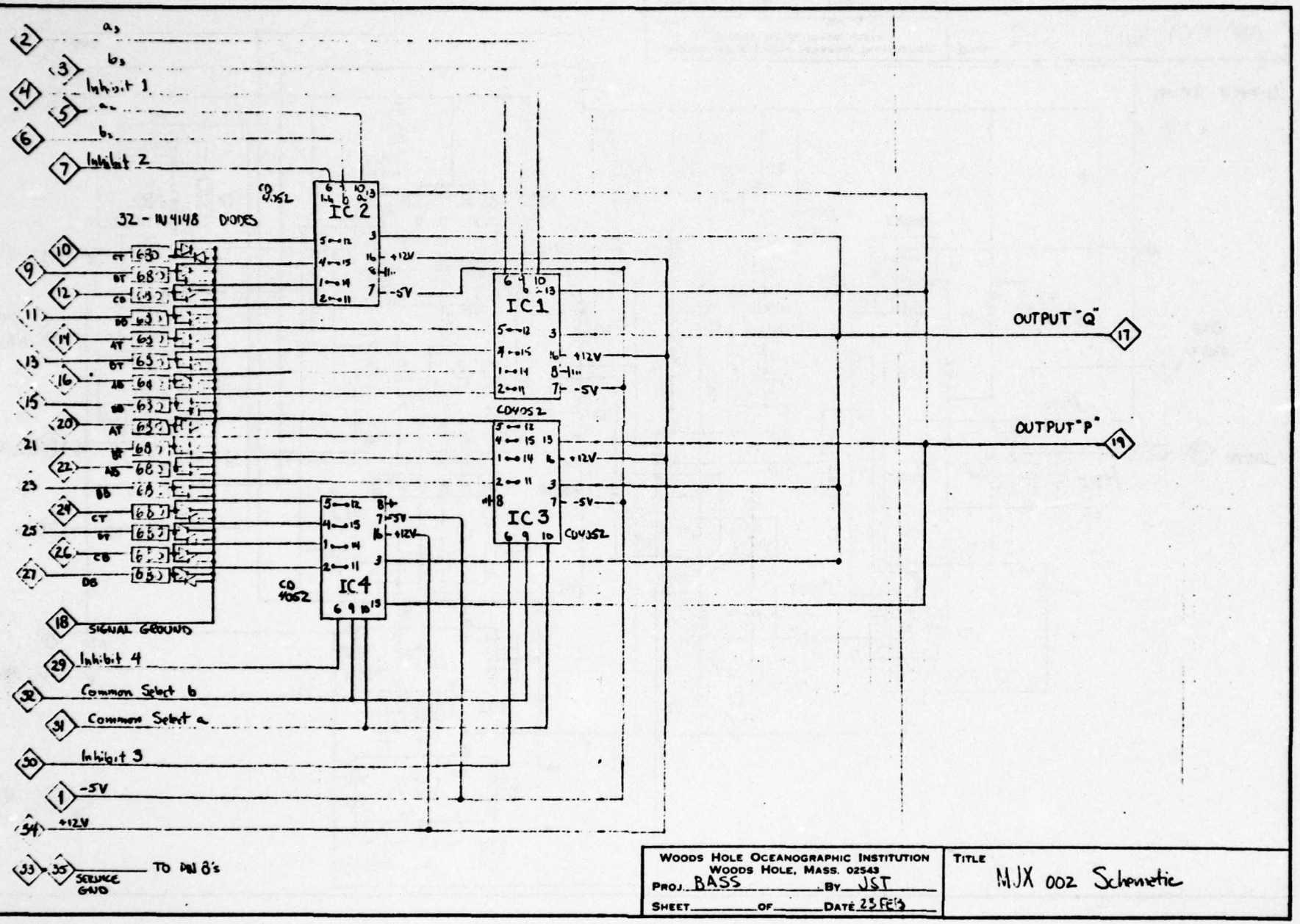

WOODS HOLE OCEANOGRAPHIC INSTITUTION
WOODS HOLE, MASS. 02543
PROJ. BASS BY JST
SHEET OF DATE 23 Feb

TITLE
MJX 002 Schematic

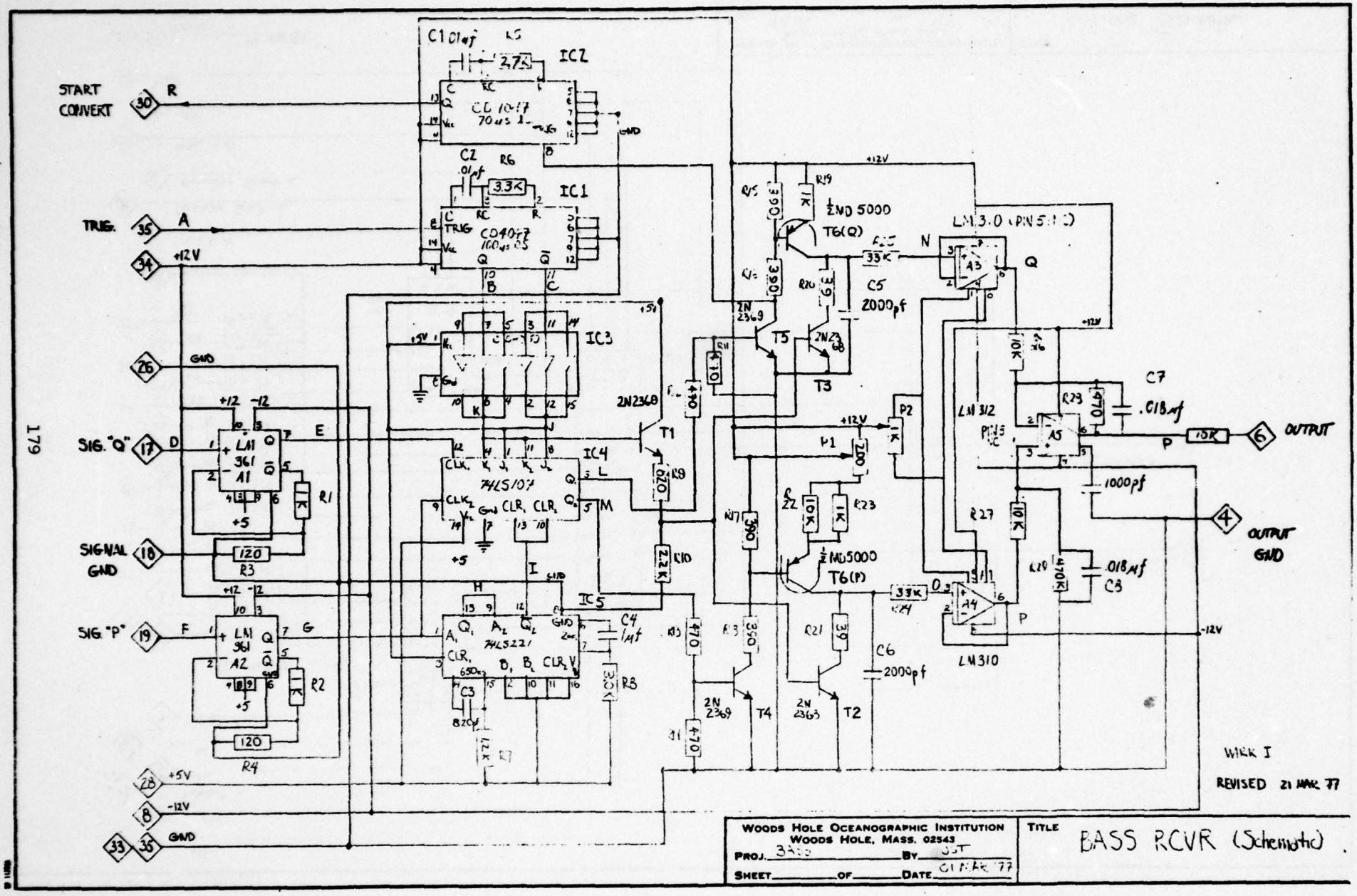
START CONVERT
TRIG.
SIG. "Q"
SIGNAL GND
SIG. "P"
IC1
IC2
IC3
IC4
IC5
CD4047
74LS107
74LS221
LM361
LM3.0 (PIN 5 N.C.)
LM312
LM310
2N2369
2N2368
2N2363
MD5000
OUTPUT
OUTPUT GND
+12V
-12V
+5V
GND
BASS RCVR (Schematic)
WOODS HOLE OCEANOGRAPHIC INSTITUTION
WOODS HOLE, MASS. 02543
REVISED 21 MAR 77

So far, this is exact and path independent. Actually only a discrete number of paths can have rays interconnecting the transducers (a requirement of d'Alembert's principle that for a ray to exist, the travel time as a function of path perturbation must be a local minimum) as long as the velocity structure is not pathological. The fastest of these paths is the one that concerns us.

It is assumed next, that the fastest path is the same in both directions which is reasonable except for nearly isochronal but widely displaced paths. Thus the last equation above is the one describing the measured time difference in Bass for the first arrival path.

Now that a single path has been selected, an approximation must be made to simplify the expression.

$$\text{Assume } \left(\frac{\vec{v}\cdot d\vec{\ell}}{|d\vec{\ell}|}\right)^2 << c^2$$

$\frac{\vec{v}\cdot d\vec{\ell}}{|d\vec{\ell}|} \le \frac{|\vec{v}|\cdot|d\vec{\ell}|}{|d\vec{\ell}|} = |\vec{v}|$ So $\frac{v^2}{c^2}$ is an upper bound on the error in δt introduced by replacing $\frac{1}{c^2 - \left(\frac{\vec{v}\cdot d\vec{\ell}}{|d\vec{\ell}|}\right)^2}$ by c^2

With $v = 1\,m/sec$ and $c = 1500\,m/sec$ $\quad \frac{v^2}{c^2} = 4.4\times10^{-7}$

$$\delta t = \int_A^B \frac{2\,\frac{\vec{v}\cdot d\vec{\ell}}{|d\vec{\ell}|}}{c^2}\,d\ell = \int_A^B \frac{2\vec{v}\cdot d\ell}{c^2}$$

This is now manageable and represents an integral along the acoustic path of the velocity component in the direction of the ray.

BIBLIOGRAPHY

Bohlen, W.F. (1977). Shear stress and sediment transport in unsteady turbulent flows. Estuarine Processes., vol. II, 109-123.

Bowden, K.F. (1962). Measurements of turbulence near the sea bed in a tidal current. J. Geophys. Res., vol. 67, 3182-3186.

Bowden, K.F., and L.A. Fairbairn (1952). Further observations of turbulent fluctuations in a tidal current. Royal Society of London, Phil. Trans. Series A., vol. 244, 335-356.

Bowden, K.F., and L.A. Fairbairn (1956). Measurements of turbulent fluctuations and Reynolds stresses in a tidal current. Proc. Royal Society of London, Series A., vol. 237, 422-438.

Bowden, K.F., L.A. Fairbairn, and P. Hughes (1959). The distribution of shearing stresses in a tidal current. Geophys. J., vol. 2, 288-303.

Bowden, K.F., and M.R. Howe (1963). Observations of turbulence in a tidal current. J. Fluid Mech., vol. 17, 271-284.

Butman (1977) personal communication.

Channon, R.D., and D. Hamilton (1971). Sea bottom velocity profiles on the continental shelf south west of England. Nature, vol. 231, 383-385.

Charnock, H. (1959). Tidal friction from currents near the sea bed. Geophys. J. of the Royal Astronomical Soc., vol. 2, 215-221.

Clauser, F.H. (1956). The turbulent boundary layer. In Advances in Applied Mechanics (H.L. Dryden and T. von Karman, eds.), vol. 4, Academic Press, New York, 1-51.

Corino, E.R., and R.S. Brodkey (1969). A visual investigation of the wall region in turbulent flow. J. Fluid Mech., vol. 37, 1-30.

Daily, J.W., and D.R. Harleman (1966). Fluid Dynamics. Addison-Wesley Publishing Co., Inc., Reading, Massachusetts.

Deacon, E.L. (1968). The levelling error in Reynolds stress measurement. Bull. Amer. Meteor. Soc., vol. 49, 836.

Dyer, K.R. (1970). Current velocity profiles in a tidal channel. Geophys. J. of the Royal Astronomical Soc., vol. 22, 153-161.

Everdale, F.G. (1976). The near bottom turbulent velocity structure; variation over a tidal cycle at a site in eastern Long Island Sound. M.S. Thesis, Univ. of Connecticut, 80 pp.

Francis, J.R.D., H. Stommel, H.G. Farmer, and D. Parson, Jr. (1953). Observations of turbulent mixing processes in a tidal estuary. Woods Hole Oceanographic Institution Technical Report, Ref. No. 53-22.

Frey, H.R., and G.J. McNally (1973). Limitations of conical hot platinum film probes as oceanographic flow sensors. J. Geophys. Res., vol. 78, 1449-1461.

Gordon, C.M. (1974). Intermittent momentum transport in a geophysical boundary layer. Nature, vol. 248, 393-394.

Gordon, C.M. (1975a). Sediment entrainment and suspension in a turbulent tidal flow. Mar. Geol., vol. 18, M57-M64.

Gordon, C.M. (1975b). Period between bursts at high Reynolds number. Phys. Fluids, vol. 18, 141-143.

Gordon, C.M., and C.F. Dohne (1973). Some observations of turbulent flow in a tidal estuary. J. Geophys. Res., vol. 78, 1971-1978.

Gordon, C.M., and J. Witting (1977). Turbulent structure in a benthic boundary layer. In Bottom Turbulence: Proceedings of the 8th International Liège Colloquium on Ocean Hydrodynamics (ed. J.C.J. Nihoul). Elsevier Scientific Publishing Co., Amsterdam, 59-81.

Grant, H.L. (1958). The large eddies of turbulent motion. J. Fluid Mech., vol. 4, 149-190.

Grant, W.F., and O.S. Madsen (1977). NOAA Tech. Report (in press.

Grass, A.J. (1971). Structural features of turbulent flow over smooth and rough boundaries. J. Fluid Mech., vol. 50, part 2, 233-255.

Gytre, T. (1975). Ultrasonic measurements of ocean currents down to 1 mm/sec. Conference proceeding #32 of the IERE Conference on Instrumentation in Oceanography, 23-25 September 1975, University College N. Wales, Bangor, U.K., 69-80.

Hartlett, J.C., and L.D. Kulm (1972). Some observations of near-bottom currents in deep sea channels. J. Geophys. Res., vol. 77, 499-504.

Heathershaw, A.D. (1974). "Bursting" phenomena in the sea. Nature, vol. 248, 394-395.

Heathershaw, A.D. (1976). Measurements of turbulence in the Irish Sea benthic boundary layer. In The Benthic Boundary Layer (ed. I.N. McCave). Plenum Press, New York, 11-31.

Heathershaw, A.D., and J.H. Simpson (1978). The sampling variability of the Reynolds stress and its relation to boundary shear stress and drag coefficient measurements. Estuarine and Coastal Mar. Sci., vol. 6, 263-274.

Issacs, J.D., J.L. Reid, Jr., G.B. Schick, and R.A. Schwartzlose (1966). Near-bottom currents measured in four kilometers depth off the Baja California coast. J. Geophys. Res., vol. 71, 4297-4304.

Kaimal, J.C., and D.A. Haugen (1969). Some errors in the measurement of Reynolds stress. J. Appl. Meteor., vol. 8, 460-462.

Kajiura, K. (1964). On the bottom friction in an oscillating current. Bull. Earthquake Res. Inst., vol. 42, 147-174.

Kim, H.T., S.J. Kline, and W.C. Reynolds (1971). The production of turbulence near a smooth wall in a turbulent boundary layer. J. Fluid Mech., vol. 50, part 1, 133-160.

Kline, S.J., W.C. Reynolds, F.A. Schraub, and P.W. Rundstadler (1967). The structure of turbulent boundary layers. J. Fluid Mech., vol. 30, 741-773.

Knauss, J.A. (1965). A technique for measuring deep ocean currents close to the bottom with an unattached current meter and some preliminary results. J. Mar. Res., vol. 23, 237-245.

Kraus, E.B. (1968). What do we not know about the sea surface wind stress. Bull. Amer. Meteor. Soc., vol. 49, 247-253

Korgen, B.J., G. Bodvarsson, and L.D. Kulm (1970). Current speeds near the ocean floor west of Oregon. Deep-Sea Res., vol. 17, 353-357.

Landau, M.T. (1975). Wave breakdown and turbulence. J. Appl. Math., vol. 28, 735-756.

Lesser, R.M. (1951). Some observations of the velocity profile near the sea-floor. Trans. Amer. Geophys. Union, vol. 32, 207-211.

McCave, I.N. (1971). Some boundary-layer characteristics of tidal currents bearing sand in suspension. Memoires Société Royale des Sciences de Liège. 6e série, tome VI, 107-126.

Miyake, M., M. Donelan, G. McBean, C. Paulson, F. Badgley, and E. Leavitt (1970). Comparison of turbulent fluxes over water determined by profile and eddy correlation techniques. Quart. J. Roy. Met. Soc., vol. 96, 132-137.

Monin, A.S., and A.M. Obukhov (1954). Basic regularities of turbulent mixing in the atmospheric surface layer. Trudy Akad. Nauk SSSR, Geophys. Inst. No. 24(151) 163-187. (English translations: Library of Congress or Special Libraries Assoc. Nos. R-3899 and 59-15097).

Moody, L.F. (1944). Friction factors for pipe flow. Trans. ASME, vol. 66, 671.

Mosby, H. (1946). Experiments on turbulence and friction near the bottom of the sea. Bergens Museums Årbok, Naturvitensk. rekke, no. 3, 1-6.

Mosby, H. (1949). Experiments on bottom friction. Bergens Museums Årbok, Naturvitensk. rekke, no. 10, 2-12.

Nikuradse, J. (1933). Stromungsgesetze in rauhen Rohren, Ver. Deutsch. Ing., Forschungsheft 361.

Pond, S. (1968). Some effects of buoy motion on measurements of wind speed and stress. J. Geophys. Res., vol. 73, 507-512.

Raudkivi, A.J. (1967). Loose Boundary Hydraulics. Pergamon Press, London. 206-208.

Schlicting, H. (1968). Boundary Layer Theory, McGraw Hill Book Co., New York.

Seitz, R.C. (1971). Results of a field study using the 3-axis Doppler shift current meter. Chesapeake Bay Institute, The Johns Hopkins University, Technical Report 71-6.

Smith, J.D., and S.R. McLean (1977). Boundary layer adjustments to bottom topography and suspended sediment. In Bottom Turbulence: Proc. of the 8th International Liège Colloquium on Ocean Hydrodynamics (ed. J.C.J. Nihoul). Elsevier Scientific Publishing Co., Amsterdam, 123-151.

Sternberg, R.W. (1966). Boundary layer observations in a tidal current. J. Geophys. Res., vol. 71, 2175-2178.

Sternberg, R.W. (1969). Camera and dye-pulser system to measure bottom boundary layer flow in the deep sea. Deep-Sea Res., vol. 16, 549-554.

Sternberg, R.W. (1970). Field measurements of the hydrodynamic roughness of the deep sea boundary. Deep-Sea Res., vol. 17, 415-442.

Sternberg, R.W. (1976). Measurements of boundary layer flow and boundary roughness over Campeche Bank, Yucatan. Mar. Geol., vol. 20, M25-M31.

Stewart, R.W. (1974). The air-sea momentum exchange. Boundary Layer Meteor., vol. 6, 151-167.

Sverdrup, H.U., M.W. Johnson, and R.H. Fleming (1942). The Oceans, Their Physics, Chemistry and General Biology. Prentice-Hall, Englewood Cliffs, New Jersey.

Tennekes, H., and J.L. Lumley (1972). A first course in turbulence. The MIT Press, Cambridge, Massachusetts.

Thorpe, S.A., E.P. Collins, and D.I. Gaunt (1973). An electromagnetic current meter to measure turbulent fluctuations near the ocean floor. Deep-Sea Res., vol. 20, 933-938.

Townsend, A.A. (1958). Turbulent flow in a stably stratified atmosphere. Journal of Fluid Mechanics, volume 3, 361-372.

Vincent, C.E., and J.G. Harvey (1976). Roughness length in the turbulent Ekman Layer above the sea bed. Mar. Geol., vol. 22, M75-M81.

Wallace, J.M., H. Eckelman, and R.S. Brodkey (1972). The wall region in turbulent shear flow. J. Fluid Mech., vol. 54, 39-48.

Weatherly, G.L. (1972). A study of the bottom boundary layer of the Florida current. J. Physical Oceanography, vol. 2, 54-72.

Williams, A.J., 3rd, and J.S. Tochko (1977). An acoustic sensor of velocity for benthic boundary layer studies. In Bottom Turbulence: Proc. of the 8th International Liège Colloquium on Ocean Hydrodynamics (ed. J.C.J. Nihoul). Elsevier Scientific Publishing Co., Amsterdam, 83-97.

Wimbush, M. (1976). The physics of the benthic boundary layer. In The Benthic Boundary Layer (ed. I.N. McCave) Plenum Press, New York, 3-10.

Wimbush, M., and W. Munk (1971). The benthic boundary layer. In The Sea, vol. 4, (ed. A.E. Maxwell). Wiley-Interscience, New York, 731-758.

Wiseman, W.J., Jr. (1968). Doppler shift current meter signals and the drop out problem. Chesapeake Bay Institute, The Johns Hopkins University, Technical Report #41.

Wiseman, W.J., Jr. (1969). On the structure of high frequency turbulence in a tidal estuary. Chesapeake Bay Institute, The Johns Hopkins University, Technical Report #59.

BIOGRAPHICAL NOTE

John Steven Tochko was born on December 12, 1950 in Englewood, New Jersey. He grew up in Palisades Park, New Jersey, and attended St. Peter's Preparatory School in Jersey City. In 1968 he enrolled as a mechanical engineering major at The Cooper Union School of Engineering in New York City. At Cooper, he was a member of the American Society of Mechanical Engineers, and was elected to Tau Beta Pi and Pi Tau Sigma. In his senior year he served as president of Pi Tau Sigma and vice-president of Tau Beta Pi. Upon graduating with honors in 1972, he was awarded the Alumni Association Award in Mechanical Engineering. In June 1972 he entered the MIT-Woods Hole Oceanographic Institution Joint Program in Oceanographic Engineering.

AD-A062 842 WOODS HOLE OCEANOGRAPHIC INSTITUTION MASS F/G 8/3
A STUDY OF THE VELOCITY STRUCTURE IN A MARINE BOUNDARY LAYER - --ETC(U)
DEC 78 J S TOCHKO N00014-74-C-0262
UNCLASSIFIED WHOI-78-90 NL

3 OF 3
AD
A062 842

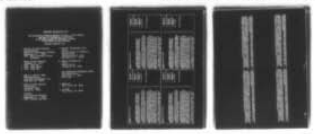

END
DATE
FILMED
2-79
DDC

MANDATORY DISTRIBUTION LIST

FOR UNCLASSIFIED TECHNICAL REPORTS, REPRINTS, & FINAL REPORTS PUBLISHED BY OCEANOGRAPHIC CONTRACTORS OF THE OCEAN SCIENCE AND TECHNOLOGY DIVISION OF THE OFFICE OF NAVAL RESEARCH

(REVISED FEBRUARY 1978)

1 Director of Defense Research and Engineering
Office of the Secretary of Defense
Washington, D.C. 20301
ATTN: Office Assistant Director (Research)

Office of Naval Research
Arlington, VA 22217
1 ATTN: (Code 460)
1 ATTN: (Code 102-OS)
1 ATTN: (Code 200)

1 CDR J. C. Harlett, (USN)
ONR Representative
Woods Hole Oceanographic Inst.
Woods Hole, MA 02543

1 Office of Naval Research
Branch Office
495 Summer Street
Boston, MA 02210

Director
Naval Research Laboratory
Washington, D.C. 20375
6 ATTN: Library, Code 2620

1 National Oceanographic Data Center
National Oceanic & Atmospheric Administration
3300 Whitehaven St., N.W.
Washington, D.C. 20235

12 Defense Documentation Center
Cameron Station
Alexandria, VA 22314

DMA HYDROGRAPHIC/TOPOGRAPHIC CENTER
6500 Brookes Lane
Washington, DC 20315
1 ATTN: SDH

3 NORDA 430
NSTL Station, MS 39529

2 CO NORDA
NSTL Station, MS 39529

Woods Hole Oceanographic Institution
WHOI-78-90

A STUDY OF THE VELOCITY STRUCTURE IN A MARINE BOUNDARY LAYER - INSTRUMENTATION AND OBSERVATIONS by John S. Tochko. 190 pages. December 1978. Prepared for the Office of Naval Research under Contract N00014-74-C-0262; NR 083-004 and for the National Science Foundation under Grant OCE 76-10523.

The design and operation of a unique flow measuring instrument for bottom boundary layer studies in the marine environment is documented. The effectiveness of the instrument in acquiring data with which models of near bottom flows in the ocean can be tested is demonstrated by the results of a field experiment in Vineyard Sound.

The instrument uses four sensors which measure the mean and fluctuating parts of the three components of the velocity vector at four heights above the sea bed. The sensors employ the acoustic travel time difference technique, and are designed to minimize sensor-induced flow disturbances. BASS, an acronym for Benthic Acoustic Stress Sensor, has a resolution of .033 cm/sec per least bit, a range of ±62 cm/sec, noise of .07 cm/sec in 10 sec, and an estimated accuracy of ∓.5 cm/sec, referred to an *in situ* zero point. A complete set of velocity measurements is made every .750 seconds, each measurement being the vector component averaged over 15 cm. The data is internally recorded on digital cassette tape. Eight hours of continuous data can be recorded.

BASS was deployed in a tidal flow in Vineyard Sound at a depth of 10 m where a time series of u, v, and w velocities at 26 cm, 46 cm, 96 cm, and 210 cm above the bottom was recorded. (Cont. on back)

1. Benthic Boundary Layer Flow
2. Acoustic Current Meter
3. Reynolds Stress Measurement

I. Tochko, John S.
II. N00014-74-C-0262; NR 083-004
III. OCE 76-10523

This card is UNCLASSIFIED

Woods Hole Oceanographic Institution
WHOI-78-90

A STUDY OF THE VELOCITY STRUCTURE IN A MARINE BOUNDARY LAYER - INSTRUMENTATION AND OBSERVATIONS by John S. Tochko. 190 pages. December 1978. Prepared for the Office of Naval Research under Contract N00014-74-C-0262; NR 083-004 and for the National Science Foundation under Grant OCE 76-10523.

The design and operation of a unique flow measuring instrument for bottom boundary layer studies in the marine environment is documented. The effectiveness of the instrument in acquiring data with which models of near bottom flows in the ocean can be tested is demonstrated by the results of a field experiment in Vineyard Sound.

The instrument uses four sensors which measure the mean and fluctuating parts of the three components of the velocity vector at four heights above the sea bed. The sensors employ the acoustic travel time difference technique, and are designed to minimize sensor-induced flow disturbances. BASS, an acronym for Benthic Acoustic Stress Sensor, has a resolution of .033 cm/sec per least bit, a range of ±62 cm/sec, noise of .07 cm/sec in 10 sec, and an estimated accuracy of ∓.5 cm/sec, referred to an *in situ* zero point. A complete set of velocity measurements is made every .750 seconds, each measurement being the vector component averaged over 15 cm. The data is internally recorded on digital cassette tape. Eight hours of continuous data can be recorded.

BASS was deployed in a tidal flow in Vineyard Sound at a depth of 10 m where a time series of u, v, and w velocities at 26 cm, 46 cm, 96 cm, and 210 cm above the bottom was recorded. (Cont. on back)

1. Benthic Boundary Layer Flow
2. Acoustic Current Meter
3. Reynolds Stress Measurement

I. Tochko, John S.
II. N00014-74-C-0262; NR 083-004
III. OCE 76-10523

This card is UNCLASSIFIED

Woods Hole Oceanographic Institution
WHOI-78-90

A STUDY OF THE VELOCITY STRUCTURE IN A MARINE BOUNDARY LAYER - INSTRUMENTATION AND OBSERVATIONS by John S. Tochko. 190 pages. December 1978. Prepared for the Office of Naval Research under Contract N00014-74-C-0262; NR 083-004 and for the National Science Foundation under Grant OCE 76-10523.

The design and operation of a unique flow measuring instrument for bottom boundary layer studies in the marine environment is documented. The effectiveness of the instrument in acquiring data with which models of near bottom flows in the ocean can be tested is demonstrated by the results of a field experiment in Vineyard Sound.

The instrument uses four sensors which measure the mean and fluctuating parts of the three components of the velocity vector at four heights above the sea bed. The sensors employ the acoustic travel time difference technique, and are designed to minimize sensor-induced flow disturbances. BASS, an acronym for Benthic Acoustic Stress Sensor, has a resolution of .033 cm/sec per least bit, a range of ±62 cm/sec, noise of .07 cm/sec in 10 sec, and an estimated accuracy of ∓.5 cm/sec, referred to an *in situ* zero point. A complete set of velocity measurements is made every .750 seconds, each measurement being the vector component averaged over 15 cm. The data is internally recorded on digital cassette tape. Eight hours of continuous data can be recorded.

BASS was deployed in a tidal flow in Vineyard Sound at a depth of 10 m where a time series of u, v, and w velocities at 26 cm, 46 cm, 96 cm, and 210 cm above the bottom was recorded. (Cont. on back)

1. Benthic Boundary Layer Flow
2. Acoustic Current Meter
3. Reynolds Stress Measurement

I. Tochko, John S.
II. N00014-74-C-0262; NR 083-004
III. OCE 76-10523

This card is UNCLASSIFIED

Woods Hole Oceanographic Institution
WHOI-78-90

A STUDY OF THE VELOCITY STRUCTURE IN A MARINE BOUNDARY LAYER - INSTRUMENTATION AND OBSERVATIONS by John S. Tochko. 190 pages. December 1978. Prepared for the Office of Naval Research under Contract N00014-74-C-0262; NR 083-004 and for the National Science Foundation under Grant OCE 76-10523.

The design and operation of a unique flow measuring instrument for bottom boundary layer studies in the marine environment is documented. The effectiveness of the instrument in acquiring data with which models of near bottom flows in the ocean can be tested is demonstrated by the results of a field experiment in Vineyard Sound.

The instrument uses four sensors which measure the mean and fluctuating parts of the three components of the velocity vector at four heights above the sea bed. The sensors employ the acoustic travel time difference technique, and are designed to minimize sensor-induced flow disturbances. BASS, an acronym for Benthic Acoustic Stress Sensor, has a resolution of .033 cm/sec per least bit, a range of ±62 cm/sec, noise of .07 cm/sec in 10 sec, and an estimated accuracy of ∓.5 cm/sec, referred to an *in situ* zero point. A complete set of velocity measurements is made every .750 seconds, each measurement being the vector component averaged over 15 cm. The data is internally recorded on digital cassette tape. Eight hours of continuous data can be recorded.

BASS was deployed in a tidal flow in Vineyard Sound at a depth of 10 m where a time series of u, v, and w velocities at 26 cm, 46 cm, 96 cm, and 210 cm above the bottom was recorded. (Cont. on back)

1. Benthic Boundary Layer Flow
2. Acoustic Current Meter
3. Reynolds Stress Measurement

I. Tochko, John S.
II. N00014-74-C-0262; NR 083-004
III. OCE 76-10523

This card is UNCLASSIFIED

The mean velocity was determined by fitting each 6 hour series with a sixth order polynomial and the deviations from the polynomial, the fluctuating velocity components, were correlated to produce Reynolds stress profiles. The stress series shows very few negative stress events while the dominant positive events have an average duration of 5 seconds and exceed 30 dynes/cm^2.

Zero offset was removed from the mean by assuming a log profile at maximum ebb. Deviations from a log profile developed when the current dropped below 40% of maximum, i.e., when the flow could no longer be considered steady. A break in the Reynolds stress profile at 1 m suggested a larger length scale than the 1 cm bottom roughness was present in the flow. A value of u_* was determined by using the quadratic drag law (u_* = 1.56 cm/sec), the log profile method (u_* = 1.60 cm/sec), and the eddy correlation method (u_* = 1.91 cm/sec). Integral length scales of 5 m cross-stream, and 2.5 m vertically were identified by correlation calculations. Two length scales were present in the downstream direction, 5 m within 1 meter of the wall and 8 m further from the wall.

The mean velocity was determined by fitting each 6 hour series with a sixth order polynomial and the deviations from the polynomial, the fluctuating velocity components, were correlated to produce Reynolds stress profiles. The stress series shows very few negative stress events while the dominant positive events have an average duration of 5 seconds and exceed 30 dynes/cm^2.

Zero offset was removed from the mean by assuming a log profile at maximum ebb. Deviations from a log profile developed when the current dropped below 40% of maximum, i.e., when the flow could no longer be considered steady. A break in the Reynolds stress profile at 1 m suggested a larger length scale than the 1 cm bottom roughness was present in the flow. A value of u_* was determined by using the quadratic drag law (u_* = 1.56 cm/sec), the log profile method (u_* = 1.60 cm/sec), and the eddy correlation method (u_* = 1.91 cm/sec). Integral length scales of 5 m cross-stream, and 2.5 m vertically were identified by correlation calculations. Two length scales were present in the downstream direction, 5 m within 1 meter of the wall and 8 m further from the wall.

The mean velocity was determined by fitting each 6 hour series with a sixth order polynomial and the deviations from the polynomial, the fluctuating velocity components, were correlated to produce Reynolds stress profiles. The stress series shows very few negative stress events while the dominant positive events have an average duration of 5 seconds and exceed 30 dynes/cm^2.

Zero offset was removed from the mean by assuming a log profile at maximum ebb. Deviations from a log profile developed when the current dropped below 40% of maximum, i.e., when the flow could no longer be considered steady. A break in the Reynolds stress profile at 1 m suggested a larger length scale than the 1 cm bottom roughness was present in the flow. A value of u_* was determined by using the quadratic drag law (u_* = 1.56 cm/sec), the log profile method (u_* = 1.60 cm/sec), and the eddy correlation method (u_* = 1.91 cm/sec). Integral length scales of 5 m cross-stream, and 2.5 m vertically were identified by correlation calculations. Two length scales were present in the downstream direction, 5 m within 1 meter of the wall and 8 m further from the wall.

The mean velocity was determined by fitting each 6 hour series with a sixth order polynomial and the deviations from the polynomial, the fluctuating velocity components, were correlated to produce Reynolds stress profiles. The stress series shows very few negative stress events while the dominant positive events have an average duration of 5 seconds and exceed 30 dynes/cm^2.

Zero offset was removed from the mean by assuming a log profile at maximum ebb. Deviations from a log profile developed when the current dropped below 40% of maximum, i.e., when the flow could no longer be considered steady. A break in the Reynolds stress profile at 1 m suggested a larger length scale than the 1 cm bottom roughness was present in the flow. A value of u_* was determined by using the quadratic drag law (u_* = 1.56 cm/sec), the log profile method (u_* = 1.60 cm/sec), and the eddy correlation method (u_* = 1.91 cm/sec). Integral length scales of 5 m cross-stream, and 2.5 m vertically were identified by correlation calculations. Two length scales were present in the downstream direction, 5 m within 1 meter of the wall and 8 m further from the wall.